EVOLUTION OF COLLECTIVE BEHAVIOUR AMONG THORIUM NUCLIDES SPANNED BETWEEN THE DRIP LINES

Thesis submitted to the University of Calicut in partial fulfillment of the requirements for the award of the degree of

Doctor of Philosophy in Physics

by

UMMUKULSU E

under the supervision of

Dr. Antony Joseph

DEPARTMENT OF PHYSICS

UNIVERSITY OF CALICUT

AUGUST 2024

CERTIFICATE

This is to certify that the corrections/suggestions recommended by the adjudicators have been incorporated in the thesis entitled **'Evolution of collective behaviour among thorium nuclides spanned between the drip lines'**, submitted by Ms. Ummukulsu E and the content in the thesis and the soft copy are one and the same.

University of Calicut

Date:

Dr. Antony Joseph
Senior Professor(Retd)
(Research Supervisor)

CERTIFICATE

This is to certify that the thesis entitled **'Evolution of collective behaviour among thorium nuclides spanned between the drip lines'**, is a bonafide record of the research work carried out by Mrs. Ummukulsu E under my supervision, at the Department of Physics, University of Calicut. No part of the work reported in this thesis has been presented before for the award of any degree from any institution.

University of Calicut

Date:

Dr. Antony Joseph
Senior Professor(Retd)
(Research Supervisor)

DECLARATION

I hereby declare that this thesis entitled **'Evolution of collective behaviour among thorium nuclides spanned between the drip lines'**, is a bonafide record of the research work carried out by me under the supervision of Dr. Antony Joseph (Senior Professor, Department of Physics, University of Calicut) and that no part of this thesis has been presented before for the award of any other degree or diploma.

University of Calicut — Ummukulsu E

Date:

Acknowledgments

I am immensely grateful for the consistent and invaluable academic and personal support provided by Prof. (Dr) Antony Joseph throughout my research career. His expertise and insights were instrumental in shaping the direction of my research. His expertise, dedication, and insightful feedback have been instrumental in the success of my research project. His encouragement and mentorship have not only enhanced my technical skills but also inspired me to strive for excellence.

I am grateful to Dr. Mohammed Shahin, Head, Department of Physics, University of Calicut for the help and support during my thesis submission. I would like to thank the prior heads of the Physics Department, Prof. C.D Ravikumar and Prof. A. M. Vinodkumar for their prompt advice and activities throughout my research career. I also like to thank all the faculty members, library and office staff in the Calicut University Physics Department for the constant encouragement and support during the entire course of my research study.

I am also extending my gratitude to the Department of Computer Science at the University of Calicut for providing the essential computing facilities to conduct this research.

I think fondly of all my colleagues in Calicut University, past and present, whose companionship energised me during my research career. I would like to specially mention the support from my friends Anjana, Nicemon Thomas, Vishnu, Shaima, Vafiya, Midhun, Swapna, Shana, Akhil, Nived, Jinu, Parvathy, Anjali, Aneena, Hisna, Faheema, Ashifa, Aruna, Hashir, Sravan, Anju, Amina, Baheeja, Farha, Gayathri, Riyas, Hajara, Shan, Nithu Ashok, Sanil and Jisha with whom I spent my quality time. This acknowledgment would not be complete without mentioning those who had helped me through all of my personal and

professional struggles and whom I love more as a family member than a friend.

I do not know how to express my gratitude to my family for the unconditional support throughout this journey. I am really grateful to my mother, who helped shape who I am today and had always stood by me, especially during my difficulties. I recall my husband's support during my entire research career. As a husband and friend, his support and concern for me have always made it possible for me to commit to my profession. The unconditional love from my kids Sheza and Izu and their cheerful faces is my constant source of energy and delight.

I also appreciate the good company, love, and support from my brother, sisters, sister-in-law and all other family members during these days. I also remember all my family members, teachers and friends for their whole hearted support and wishes.

Finally I would like to acknowledge the financial support from CSIR, Govt. of India by way of JRF and SRF, for carrying out this work, without which this work would have been impossible. In conclusion, I extend my gratitude to every person who had provided support and encouragement, contributing to the accomplishment of my goal and the successful completion of my thesis work.

Ummukulsu E

List of publication

International Journals

1. **Shape evolution of thorium isotopes in between the drip-lines**
   Ummukulsu E and Antony Joseph, International Journal of Modern Physics E, 33(05): 2450016 (2024) DOI: 10.1142/S0218301324500162.

2. **Investigation on the structure properties of thorium nuclei spanned between the drip-lines and the prediction of shell closure**
   E. Ummukulsu, Antony Joseph, Eur. Phys. J. Plus 138(12): 1077(2023) https://doi.org/10.1140/epjp/s13360-023-04742-3

3. **Nuclear collective level density and shape of thorium isotopes**
   E. Ummukulsu, Antony Joseph, Indian J Phys 97(7): 2153–2158 (2023) https://doi.org/10.1007/s12648-023-02596-0

4. **Deformation studies on thorium isotopes**
   Erumban Ummukulsu, Antony Joseph, Nuclear and Particle Physics Proceedings 339: 120-123 (2023)

5. **Variation of collective level density parameter around $N = 184$ in even-even actinides**
   E. Ummukulsu, Antony Joseph, Indian J Phys 96: 4301–4306 (2022) https://doi.org/10.1007/s12648-022-02377-1

Oral/Poster presentations in International and National symposia/conferences

1. **Study of two-neutron separation energy and single-particle energies in thorium isotopes**

E. Ummukulsu, Antony Joseph, 67^{th} DAE-BRNS Symposium on Nuclear Physics, SNP-2023, Indian Institute of Technology Indore, ISBN-978-81-954733-9-7 (2023)

2. **Isovector dipole resonance in thorium isotopes**

   E. Ummukulsu, Antony Joseph, 67^{th} DAE-BRNS Symposium on Nuclear Physics, SNP-2023, Indian Institute of Technology Indore, ISBN-978-81-954733-9-7 (2023)

3. **Deformation studies on thorium isotopes**

   E. Ummukulsu, Antony Joseph, 23rd National Symposium on Radiation Physics,University of Mysore Manasagangotri, Mysuru, (2023)

4. **Radioisotope production from thorium**

   E. Ummukulsu, Antony Joseph, DST-PURSE Satellite Symposium, Bharatiar university, Coimbatore, (2022)

5. **Shape evolution of thorium-228, 230 and 232**

   E. Ummukulsu, Antony Joseph, 66^{th} DAE Symp. on Nucl. Phys. Guwahati, Assam, ISBN-978-81-959225-1-2 (2022)

6. **Charge Radii of Thorium Nuclei Lying Between the Drip Lines**

   E. Ummukulsu, Antony Joseph, 34^{th} Kerala Science Congress, Thiruvananthapuram, (2022)

7. **Radii of Thorium Nuclides Lying in Between the Drip Lines**

   E. Ummukulsu, Antony Joseph, Online International Conference on Recent Trends in Nuclear Physics, 9(2):209-213, ISSN-2321-9289 (2022)

8. **Study of Quadrupole Deformation of Thorium Nuclides**

   E. Ummukulsu, Antony Joseph, Amalit - 2022 Conference Proceedings,

Amal College of Advanced Studies, Nilambur, ISBN-978-81-950313-5-1 (2022)

9. **Medical isotope production by charged particle irradiation of natural thorium**

   E. Ummukulsu, Antony Joseph, 65^{th} DAE Symp. on Nucl. Phys., DAE Convention Centre, Anushakti Nagar, Mumbai, ISBN-818372084-6 (2021)

10. **Systematic study on level density parameter of even-even actinides**

    E. Ummukulsu, Antony Joseph, 32^{nd} Kerala Science Congress, Yuvakshethra Institute of Management Studies, Palakkad, (2020)

11. **Comparison of nuclear level density parameter with different mass tables**

    E. Ummukulsu, Antony Joseph, International Conference on Theoretical and Experimental Physics, Farook college, Kozhikkode, ISBN-978-81-935852-4-5 (2020)

12. **Effective and collective level ensity parameter for thorium isotopes**

    E. Ummukulsu, Antony Joseph, 64^{th} DAE Symp. on Nucl. Phys., Lucknow, ISBN-818372083-8 (2019)

13. **Level density parameters of thorim isotopes spanned between drip lines**

    Proceedings of the National Seminar on new horizons in theoretical and experimental physics, S.A.R.B.T.M Govt.College, Koyilandy ISBN-978-93-5391-753-1 (2019)

Contents

List of Figures

List of Tables

Preface

The study of atomic nuclei is important in the context of a wide variety of applications, in particular, nuclear energy, nuclear medicine, trace element analysis etc. Also, it is relevant in the context of astrophysical applications, stellar evolution, nucleosynthesis and in nuclear reactions. Over the years, the structure properties of nuclei had gained considerable attention in nuclear physics. The structure of nuclei give information on the behaviour of nuclei. After the discovery of nucleus and its constituent particles, tremendous developments had taken place in this field. It is such a vast area of research that there are still plenty of facts that are unknown to us. In the last few decades, many new results have come out in structure studies, related to its theoretical and experimental aspects. Nowadays, several theoretical approaches are available in the literature, to explain the static properties and dynamic behaviour of atomic nuclei. Single particle excitation and collective excitation are the possible excitation modes in a nucleus. The main objectives of this thesis work is to investigate the structure properties of thorium nuclei lying on and off the valley of β-stability. The nuclei far away from the line of β-stability are unstable, and coupling between the bound and continuum states affect the multipole response of the nuclear systems and different modes of excitation may be generated. Thus, quantitative description of nuclear ground and excited state properties are necessary in the case of thorium isotopes.

In order to analyse the complete behaviour of a nucleus, based on experimental results, different theoretical models are necessary. A theoretical model describes the structure of a nucleus based on a reasonable analogy that is related to our previous knowledge and enable us to ascribe new properties. Different theoretical models like liquid-drop model, shell model, collective model, Nilsson model etc. and approaches like mean-field theory are important in structure

studies. Thorium nuclei are of special interest, because of their various practical applications. They have use in various stages of nuclear fuel reactors, and in the production of radioisotopes of medical interest such as ^{99}Mo,^{115}Cd and ^{111}I. These isotopes can be obtained from the fission of thorium isotopes by using protons and deuterons as projectiles. Thorium nuclei appear in various stages of nucleosynthesis. Thorium is abundant in metal-poor stars and are synthesized through the r-process. The present study is expected to provide us with the information necessary to identify the trends in the physical properties of thorium nuclei, lying from proton drip-line to neutron drip-line and also to check for the emergence of new magic numbers. It provides new data for testing nuclear models in the context of nuclear astrophysics. As the first part of this work, we have estimated the nuclear level density parameters of thorium nuclei in the mass range 204-280. The calculations were performed by employing the Gilbert-Cameron model. Specifically, we computed the level density parameters under two conditions, one, considering the collective enhancement effect, which accounts for the rotational and vibrational effects of nuclei, and the other without incorporating this enhancement. The results of these calculations give information on the variation of both the collective and effective level density parameters in relation to the neutron number. The collective enhancement factor of thorium isotopes around neutron numbers N=126 (^{216}Th) and 184 (^{274}Th) are of special interest. The collective enhancement factor for ^{216}Th and ^{274}Th are low when compared to those for the nearby isotopes. This may be due to the shell closure around neutron number N=126 and 184. The collective enhancement effect is high at lower excitation energies and low at higher excitation energies. The rotational and vibrational effects are shown by nuclei at the excitation energies between 0 and 50 MeV. For comparing the behavior, we have also calculated the collective level density parameters of few other selected even-even actinides, lying around

the neutron number N=184. The level density parameters have been systematically estimated for the isotopes of Th, U, Pu, Cm, Cf, Fm and No. The nuclear level densities of ^{274}Th, ^{276}U, ^{278}Pu, ^{280}Cm, ^{282}Cf, ^{280}Fm and ^{282}No were found to be minimum in the respective isotopic chains. The shell correction energy of these nuclei are low as compared to their nearby nuclei and the collective effect becomes lowered at magic configuration, which leads to a reduction in the level density. The dip in the value of the level density parameter may be attributed to the shape transition of nuclei from deformed to spherical.

The nuclear structure properties of thorium nuclei lying on and in between the drip-lines were investigated in the framework of the relativistic mean-field theory by applying the density dependent meson exchange and point-coupling models. The ground state parameters like binding energy, charge radii, two-neutron separation energy and shell gap, rms radii and its isotopic shift, chemical potential, quadrupole deformation, density distribution and single-particle energy were estimated. These values were then compared with the available experimental and theoretical data and were found to be in good agreement. Broken linearities were observed at around the neutron numbers N=126, 138 and 184 in the plots of various evaluated values against neutron number and single-particle energy gaps were determined at around these neutron numbers. Large deviation and shell gaps were observed at around the neutron numbers N=126 and 184. Hence, these numbers are neutron magic numbers and the corresponding thorium nuclei are more stable than their neighbours. A small deviation and shell gap were observed at around N=138, and hence we conclude that this neutron number is semi-magic and the associated nucleus is relatively stable. Most of the thorium nuclei are of prolate shape. However, they are spherical at N=126 and 184.

The ground state deformation of thorium nuclei lying in between the drip lines were described in terms of the axially symmetric deformation parameter

β_2 and triaxial deformation parameter γ. The nuclear shape evolution of thorium isotopes ranging from ^{204}Th to ^{280}Th was investigated using the relativistic mean-field theory. The binding energy of thorium isotopes as a function of the deformation parameter β_2 were plotted and the minima were identified. The study on shape evolution with triaxial deformation confirms that majority of thorium isotopes exhibit a prolate shape, while ^{216}Th and ^{274}Th are characterized by spherical shapes. A slight triaxial behaviour was observed in ^{220}Th and ^{268}Th for the values of $\beta_2 = 0.05$ and $\gamma = 10°$. This triaxial behavior was observed within the region associated with shape phase transition.

The excitation of atomic nuclei offers valuable insights into their structure. The Random Phase Approximation (RPA) stands as the foremost theory for investigating the dynamics of nuclei. Giant resonance is the prime example of the collective oscillation of nucleons. It is the collective oscillation of nucleons which characterizes the phase of motion of the nucleons. In giant dipole resonance, a dual component structure is observed in deformed nuclei, and this splitting arise from the distinct frequencies of oscillation along the major and minor axes of deformation. In axially deformed thorium nuclei, the isovector giant dipole resonance display two components with K=0,1, where K is the projection of total angular momentum J=1 on the symmetry axis. There is no energy separation between the two modes of oscillation in ^{216}Th and ^{274}Th, due to its spherical symmetry. This study also confirms the possibility of extra stability of ^{216}Th (N=126) and ^{274}Th (N=184) in the isotopic chain of thorium.

The thesis contains six chapters, The general introduction, literature survey, motivation and objectives of the thesis work are included in chapter 1. The introduction part includes different theoretical models currently in use for nuclear structure studies. Chapter 2 gives a detailed description of the calculations of nuclear level density of the selected thorium isotopes and of other nearby actinide

elements. Chapter 3 is devoted to the description of the mean-field theory and the studies on the ground state properties of thorium nuclei based on it. The shape evolution of thorium is included in chapter 4, with a detailed account of the theoretical model and schematic representations. Chapter 5 contains the details of the study on the dipole strength distribution of thorium nuclei, based on the random phase approximation. Chapter 6 summarises the results and presents the future perspectives.

Chapter 1

Introduction

The atomic nucleus is a system of particles, consisting of protons and neutrons, collectively known as nucleons. The interaction between nucleons is responsible for the binding of nuclei. Neutrons and protons are virtually identical but differ in their electric charge. They attract each other through strong nuclear force. They have spin and are fermions obeying Pauli's exclusion principle.

In the world of subatomic physics, J.J Thomson explored the structure of atoms and suggested that equal number of positively and negatively charged particles are uniformly distributed in a spherical volume and he had estimated the radius of atoms. In 1911, Rutherford performed the α-scattering experiment and found that the mass of an atom is concentrated at its centre (which has positive charge [1]). The centre of the atom was called nucleus. Later, in 1932, Chadwick discovered that the nucleus consists of neutrons also. In 1935, Yukawa [2, 3] put forwarded that the force between the nucleons emerge from meson exchange and this discovery introduced the notion of field quantum as the mediator of interacting forces. With the establishment of Quantum Chromodynamics (QCD), the Yukawa picture was found to be more appropriate. The behaviour of nucleus is determined by a fundamental force which is responsible for the interaction between nucleons. In turn, this nuclear force arises from the strong

interaction between quarks, where gluons play the role of the field quanta.

The study of nuclei is important in many respects, especially due to the wide variety of its applications, including those in nuclear energy, nuclear medicine, in maintaining health in living organisms, including human beings by keeping the trace level of essential elements, etc. More over, it is important in astrophysical scenarios such as stellar evolution, nucleosynthesis and also in understanding nuclear reactions.

The structure properties of nuclei draw considerable attention in nuclear physics. The structure of nuclei give information on the behaviour of nuclei. Even after attaining considerable progress in this direction, many information on the structure of nuclei are still unknown. Over the last several decades, many developments had taken place in nuclear structure studies, both on its theoretical and experimental aspects.

1.1 Nuclear models

In order to understand the complete behaviour of a nucleus, based on experimental results, different theoretical models are necessary. A theoretical model, describes the structure of a nucleus based on a reasonable analogy that is related to our previous knowledge and enables to predict the properties. The following section briefly describes various nuclear models, relevant to the structure studies.

1.1.1 Liquid-drop model

The Russian scientist George Gamov proposed the first nuclear model, the liquid drop model in 1929. According to this model, an atomic nucleus is regarded as a drop of Fermi liquid. To a certain level of accuracy, it could describe the binding energy of nuclei. However, it cannot explain the discontinuity in neutron

separation energy. According to this model, the short-range nuclear force that binds the nucleons together, gives it a spherical shape. The model proposed that the density of a nucleus is constant and the nucleus is incompressible. The nuclear force is identical for every nucleon and is saturated. Neils Bohr added more insight on to the liquid drop model from the studies on nuclear fission of heavy nuclei. Nuclear deformation, ground state mass, fission barrier, fission and fusion reactions etc. can also be explained by the liquid drop model.

Based on the liquid drop model, Carl Friedrich Weizsäcker and Hans Albrecht Bethe developed a formula for finding the nuclear binding energy. This binding energy formula is also known as the semi-emperical mass formula [4, 5]. It is said to be semi-empirical because the various fitting parameters or coefficients in it are derived from the experimental results. If Z is the number of protons and N is the number of neutrons in an atomic nucleus, the binding energy can then be obained as,

$$E_B = a_V A - a_S A^{\frac{2}{3}} - a_C \frac{Z^2}{A^{\frac{1}{3}}} - a_A \frac{N-Z}{A} - \delta(A,Z) \tag{1.1}$$

where $A = N + Z$ is the mass number and a_V, a_S, a_C, a_A are the coefficients corresponding to volume energy, surface energy, electrostatic energy (Coulomb energy) and asymmetry energy, respectively. The volume energy is the main part of the binding energy. The surface energy is due to the surface tension. The Coulomb energy arises from the repulsive force between charged particles and the symmetry energy is the contribution due to the symmetry property of the

nuclear force. Also, $\delta(A, Z)$ is the strength of the pairing effect.

$$\delta(A,Z) = \begin{cases} +a_p A^{-\frac{1}{2}} \\ 0 \\ -a_p A^{-\frac{1}{2}} \end{cases}$$

with a_p being pairing term. The observed increase in the binding energy of even-even nuclei, when compared to even-odd or odd-even nuclei and the decrease of binding energy for odd-odd nuclei can be explained using this formula. The liquid drop model does not account for why certain nuclei exhibit additional stability, nuclear magnetic moments, the spin of the excited states of nuclei etc. But still, as mentioned earlier, this model can predict nuclear mass, binding energy of nuclei, α- and β-particle emission in radioactivity, many features of nuclear fission process etc.

1.1.2 Shell model

The inadequacies of the liquid drop model necessitated the formulation of a better model, the nuclear shell model [6]. Maria-Goeppet Mayer and Hans Jens [7] developed this model in 1949. They introduced the concept of magic numbers and attributed the discontinuity in neutron separation energy to the shell closure. Subsequently, the neutron or proton numbers of 2, 8, 20, 28, 50, 82 and 126 were predicted to be magic numbers and was made use of by Neils Bohr to explain nuclear fission.

The shell model or independent particle model assumes that the nucleons are moving independently in an average potential and they interact by strong interaction. This model is based on Pauli's exclusion principle. The energy states of nucleons are filled from lower to higher, by adding nucleons to the

system. There are separate energy states for protons and neutrons and nucleons occupy each energy state with definite angular momentum.

In nuclear shell model, the nucleons are assumed to be in a potential well. The Hamiltonian describes the energy of the system, which for a potential V is,

$$H = \frac{-\hbar^2}{2m}\nabla^2 + V(r_i) \tag{1.2}$$

If the Hamiltonian operates on the wave function, the Schrodinger equation gives the allowed energy levels of the nucleons.

$$\frac{-\hbar^2}{2m}\nabla^2 + V(r_i)\psi(r) = E_n\psi(r) \tag{1.3}$$

where $\psi(r)$ gives the eigen function and E_n the corresponding energy eigen values. The potential gives the specific solution for the equation 1.3.

If m is the mass of a nucleon, ω is the angular frequency of oscillation and the potential is of three-dimensional harmonic oscillator type, $V(r) = \frac{1}{2}m\omega^2 r^2$, then it gives the eigen energy,

$$E_n = \hbar\omega_0(n + \frac{3}{2}) \tag{1.4}$$

where ω_0 is the angular frequency of oscillation in the ground state and n is the principal quantum number.

If the choice of the potential is Wood-Saxon type,

$$V(r) = -\frac{V_0}{1 + \exp\left[\frac{r-R}{a}\right]} \tag{1.5}$$

where $a = 0.65fm$, then R gives the radius of the nucleus. But these two potentials failed to predict the neutron magic number after 20. To improve the nuclear shell model, the potential was modified by including the effect of

spin-orbit coupling.

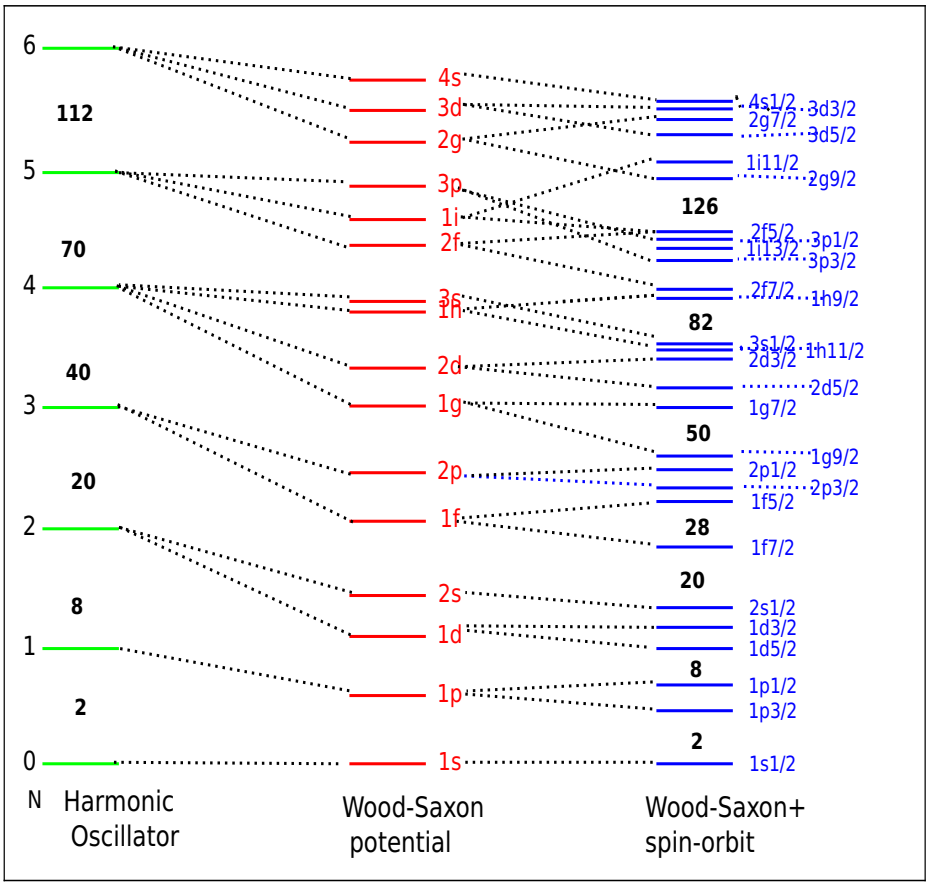

Figure 1.1: The energy levels obtained by different potentials in shell model. The energy levels arising from harmonic oscillator potential (left), Wood-Saxon potential (middle) and spin-orbit interaction included in the Wood-Saxon potential (right).

Then the modified Wood-Saxon potential is,

$$V(r) = -\frac{V_0}{1+\exp\left[\frac{r-R}{a}\right]} + V_{SO}(r)(l.s) \tag{1.6}$$

It gives the interaction between the orbital angular momentum and spin angular momentum of a nucleon. This potential successfully predicted the magic numbers and it could explain the gap between the energy levels. The nuclei having magic number of protons or neutrons or both show extra stability and are more abundant than others. The shell model could successfully predict the

spin of a good number of nuclei, the electric quadrupole moments of odd-odd nucleui and their energy levels [8, 9]. However, it failed to explain some other properties of nuclei such as magnetic moments, nuclear shape, nuclear excitations etc. Figure 1.1 represents the energy levels obtained by different potentials in shell model. The energy levels arise from harmonic oscillator potential (left), Wood-Saxon potential (middle) and spin-orbit interaction included in the Wood-Saxon potential (right). Inclusion of the Spin-orbit interaction in the Wood-Saxon potential predict the existence of magic numbers 2, 8, 20, 28, 50, 82 and 126.

1.1.3 Collective model

The shell model successfully describes nuclei having closed shell and nearly closed shell. As we move away from the closed shell configuration, large quadrupole moments are observed. This effect is due to the motion of nucleons inside the nucleus. To understand the behaviour of such nuclei far from closed shell, Bohr and Mottelson [10–13] introduced the collective model. It is the unified version of the shell model and the liquid drop model. The collective model describes the rotational and vibrational motions of nuclei. The rotational and vibrational effects are exhibited by many deformed nuclei. The single-particle and collective behaviour can be incorperated into a nucleus. The collective excitation of nucleus comes in as a result of the rotational and vibrational motions. The rotational excitation does not change the intrinsic structure of nuclei, but vibrational excitations bring in vibrations of nuclei about their equillibrium shapes. Spherical nuclei show vibrational spectra and the energy is the same as their intrinsic excitations. The deformed nuclei show rotational spectra and the collective excitation leads to static and dynamic quadrupole moments of the nucleus. This unified model can describe the excitation spectra, transfer reaction cross-sections,

electromagnetic transition rates etc.

According to the collective model, the length of a radius vector pointing from the origin to the nuclear surface $R(\theta, \phi, t)$ is [14],

$$R(\theta, \phi, t) = R_{av}[1 + \sum_{\lambda=0}^{\infty} \sum_{\mu=-\lambda}^{\lambda} \alpha^*_{\lambda,\mu}(t) Y_{\lambda,\mu}(\theta, \phi)] \tag{1.7}$$

where R_{av} is the radius of the spherical nucleus, $\alpha^*_{\lambda,\mu}$ is the deformation variable in terms of the spherical harmonics $Y_{\lambda,\mu}(\theta, \phi)$ and λ is the multipolarity of the shape oscillation. The nuclear shape is invariant under rotation about a symmetry axis, so that,

$$\alpha_{\lambda,\mu} = \alpha_{\lambda,-\mu} \tag{1.8}$$

For axially symmetry case, $\mu = 0$, and the resulting parameter $\alpha_{\lambda,0}$ is equal to β_λ. $\lambda = 0$ stands for the monopole mode and $\lambda = 1$, the dipole mode. The quadrupole deformations ($\lambda = 2$) give rise to important deformation parameters relevant to nuclear structure. The five coefficients of $\alpha_{\lambda,\mu}$ are reduced to the real independent deformation parameters $a_{2,0}$ and $a_{2,2} = a_{2,-2}$.

These parameters can be expressed in terms of the quadrupole deformation parameter β_2 and triaxial deformation parameter γ [15] as,

$$a_{2,0} = \beta_2 cos\gamma \tag{1.9}$$

$$a_{2,2} - \frac{1}{\sqrt{2}} \beta_2 sin\gamma \tag{1.10}$$

Figure 1.2 shows the schematic representation of the surface of a vibrating

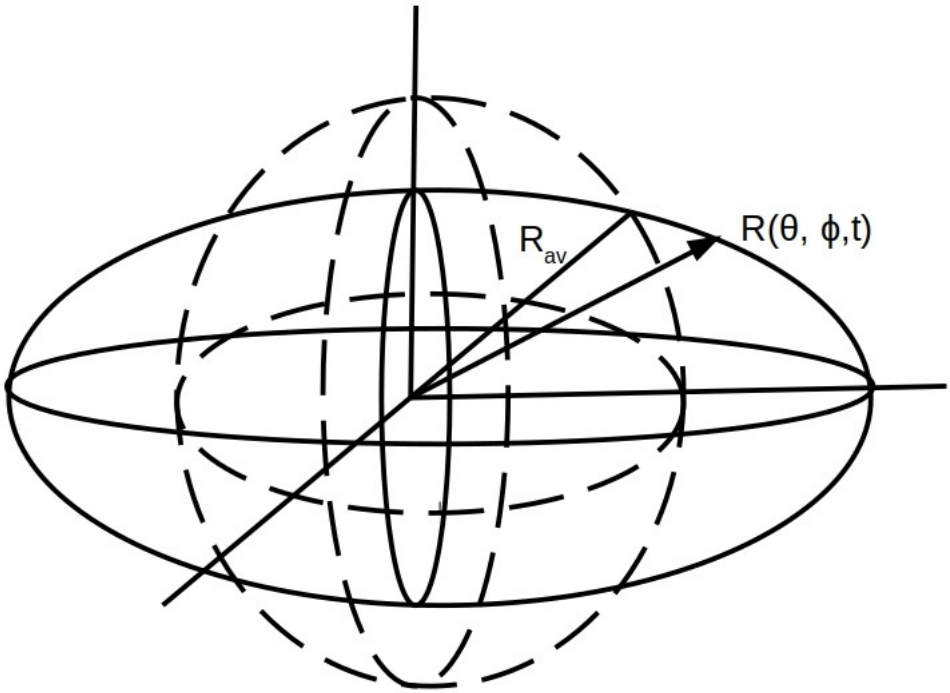

Figure 1.2: Surface of a vibrating nucleus with equilibrium shape.

nucleus with equillibrium shape. The behaviour of the nucleus is explained by assuming the motion of the nucleons outside the core getting combined with the paired nucleons inside the core. This model can explain nuclear shapes, electric and magnetic behaviour and energy spectra corresponding to collective excitations.

1.1.4 Nilsson model

As a result of the collective behaviour, many of the nuclei are spherically deformed. Nuclei with mass number $A > 220$ are permanently deformed. The existence of nuclei having large deformation cannot be explained by spherical shell model. Under such situations, a deformed shell model is necessary. The single-particle spectrum of deformed nuclei shows large gaps than that of spherical nuclei. This gaps can be explained in terms of the single-particle motion in a deformed mean-field potential. This idea was put forwarded by Nilsson [12]

and hence this model is known as Nilsson model. The deformed shell model or Nilsson model is dealing with deformed nuclei. The deformed potential $V(r)$ is [12],

$$V(r) = \frac{1}{2}m(\omega_{\perp}^2(x^2+y^2)+\omega_z^2 z^2) + Cl.s + Dl^2 \tag{1.11}$$

This equation is related to the deformation parameter δ through,

$$\omega_z = \omega_0(\delta)\sqrt{1+\frac{2}{3}\delta} \tag{1.12}$$

and

$$\omega_{\perp} = \omega_0(\delta)\sqrt{1-\frac{4}{3}\delta} \tag{1.13}$$

The deformation δ is related to the deformation parameter β through,

$$\delta = \frac{3}{2}\sqrt{\frac{5}{4\pi}}\beta \tag{1.14}$$

. Then, the Nilsson Hamiltonian can be written as,

$$H = \frac{-\hbar^2}{2m}\nabla^2 + \frac{1}{2}m\omega_0^2 r^2 Y_{20}(\theta,\phi) - Cl.s + Dl^2 \tag{1.15}$$

The energy from the eigenstate equation is,

$$E = \hbar\omega[(N+\frac{3}{2}) + \frac{3}{4}\sqrt{\frac{5}{\pi}}\beta_2(\frac{N}{3}-n_z)] \tag{1.16}$$

Each single-particle energy level is represented by the asymptotic quantum numbers $\Omega^{\pi}[Nn_z\Lambda]$, where $\Omega = \Lambda + \Sigma$ and N is the principal quantum number. n_z is the projection on symmetry axis, $n_z = 0, 1, 2...N$. Λ, Σ and Ω are the

projection of the orbital angular momentum, spin angular momentum and the total angular momentum. The schematic representation of the Nilsson diagram is given in Figure 1.3. In Nilsson diagram, the energies of the valence orbitals are drawn as a function of the deformation parameter β_2. The Nilsson model provides information on single-particle behaviour of nuclei in deformed state. The Nilsson model can explain the nuclear properties such as energy level, shape, shell structure etc. However it does not provide information on some aspects of nuclear physics such as nuclear interactions,nuclear excitations, superdeformation and hyperdeformation.

1.1.5 Mean-field theory

The mean-field theory or the mean-field model was developed to study many-body systems. This model successfully describes spherical nuclei, deformed nuclei, closed shell nuclei and nuclei away from the line of β-stability. The properties of nuclei can be analysed by taking into account the relativistic and the non-relativistic aspects. In both contexts, the mean-field theory is reasonably successful. In this model, the many-body problem is converted into a one-body problem. The Skyrme and Gogny type effective forces of interaction can be used in non-relativistic mean-field theory [17–19]. The Skyrme interaction is of zero range and the Gogny type of interaction is of finite range. The relativistic mean-field [20–22] has finite range due to meson exchange, and the spin-orbit effect is also imparted. The spin-orbit term comes from the effective force. The relativistic mean-field theory successfully describes nuclear properties such as the saturation mechanism, spin-orbit effect, spin-symmetry etc.

During the last several decades, the relativistic mean-field theory had been widely used for the nuclear structure studies. It is applicable to all nuclei in the nuclear chart [22–24]. In 1951, the relativistic mean-field theory was explained

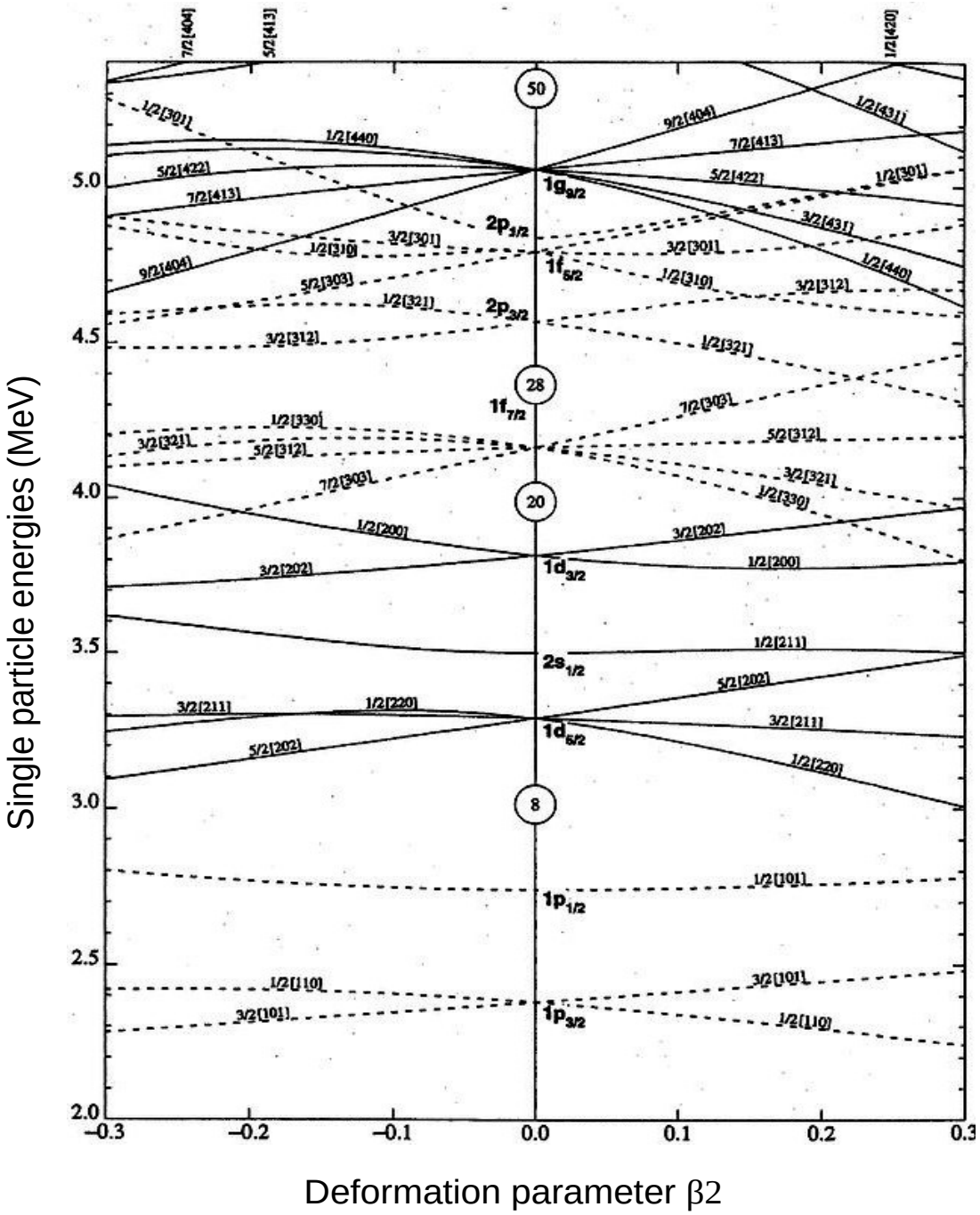

Figure 1.3: Nilsson diagram, the energies of valence orbitals as a function of deformation parameter β_2. (The positive parity states are represented by solid lines and negative parity states by dashed lines. This figure was taken from [16])

by Schiff [25]. According to Schiff's concept, the linear and nonlinear interaction fields can be used here. The linear interaction of scalar field is used to explain the structure properties of nuclei and the nonlinear term helps to explain the saturation in nuclear systems. Johnson and Teller [26] modified the concept of Schiff, which included only the scalar σ meson in nucleon-nucleon interaction. Later Durr [27] proposed the vector fields, which could explain many other structure properties such as spin-orbit interaction, energy dependence of nuclear optical potential. They also suggested that the saturation properties arise from nonlinear coupling of the scalar meson interactions.

The relativistic mean-field model was developed by Walecka [22] in 1974. The relativistic mean-field theory is based on the assumption that, nucleons can be considered as point-like particles and they move independently in the mean-field and the effect of relativity is taken into account. Later, Teller proposed the relativistic density functional theory from Walecka model [22, 26, 28–30]. In this model, sigma (σ), omega (ω) and rho (ρ) mesons were incorporated to describe the nuclear system and included nonlinear interaction in sigma meson. In the relativistic version of the quantum hydrodynamic model, we can consider the spin-orbit interaction, finite range nuclear interaction and the density dependent nuclear interaction. This model gives excellent results in nuclear binding energy, nuclear radii, deformation and other structure properties of spherical and deformed nuclei [31–34]. The nuclear properties were described by the Dirac equation with no-sea approximation. The densities and currents estimated with the negative energy states are neglected. The isoscalar scalar field is used for long range attraction, isoscalar vector field for short range repulsion, the isovector vector field can be considered for the nuclear interaction with isospin-dependence and the electromagnetic interaction for the photon field.

Different approaches were suggested to include the density dependence.

Boguta and Bodmer [35] first introduced the density dependence via nonlinear interaction between scalar mesons. Later, Brookmann and Toki [36] proposed the density dependence explicitly through the coupling constants. Finally, the finite range interaction was also included in the relativistic mean-field theory by point coupling functional. This was introduced by Buervenich and Madland [37].

1.1.6 Random phase approximation (RPA)

The excitation of nuclei leads to many interesting phenomena. The study of collective excitation is an active area of research in nuclear physics. The excitation of deformed nuclei can be studied using Random Phase Approximation (RPA) [24, 38–41]. This excitation is intrinsic and do not have angular momentum. This approximation limits the amplitude of motion to be small and is equivalent to the time-dependent Hartree-Fock theory. For closed shell nuclei, random phase approximation can be used, while for open shell nuclei, the quasiparticle random phase approximation (QRPA) is suitable. Two different mathematical approaches are used in RPA. One is the response-function formalism and the other is the matrix formalism. In the response-function formalism, the excitation is studied in a large space of configuration and this interaction is limited to zero-range. This formalism is used for the excitation into continuum. This method is extensively used to study the collective electron excitation in spherical atomic clusters. This theory was developed by David Bohm and David Pine [24, 38] in 1950s to describe the collective oscillation of electron gas .

Nuclei lying near to the neutron drip line show diffused neutron density and this affects the collective vibrations of such nuclei. The electric dipole, quadrupole and other modes of excitations may appear in nuclei lying in the vicinity of the drip lines. The ground state and collective properties in such nuclei are characterized by the closeness of the Fermi surface to the particle

continuum. For weakly bound nuclei, the quasiparticle configuration space is included for the transition to low-lying nuclear states, the states with both nucleons in the discrete level, one nucleon in the bound state and the other one in continuum and the state with both nucleons in continuum. So, the collective low lying excitation of weakly bound nucleus is described in terms of the quasiparticle random phase approximation, based on the relativistic mean-field theory and the Hartree-Fock Bogoliubov framework. This method gives the best theoretical results for nuclei far away from the valley of $\beta-$stability. It successfully describes the multipole response and low-lying collective states.

1.2 Review of Literature

The treatment of collective modes in nuclei is well documented in literature, starting from its discovery [42] upto the recent discussions. Klaus Morawetz [43] investigated the collective excitations in asymmetric nuclear matter [44, 45] by numerical simulation of the Vlasov equation and by comparison with the linear response theory.

Blin-Stoyle in 1957 [46] suggested that the energies of rotational levels in nuclei indicate the effective mass of a nucleon in a nucleus and is approximately one-half of the actual mass. In the year 1980, Hess [47] presented a general collective model that includes all possible cases, like vibrational, rotational and γ unstable nuclei. Collective properties are illustrated by the Potential-Energy-Surfaces (PES), describing all the deformation effects of a nucleus. This model is applied to the case of ^{238}U, where very high-spin states are known from experiments.

Alberico in 1982 [48], studied the longitudinal collective vibrations of infinite nuclear matter in the long wavelength limit. He solved the theory for a selection of Skyrme interactions and considered the properties of the ground state of

several systems.

Yacobus Yulianto [49] performed the investigation of nuclear ground state properties of ^{208}Pb by using the Skyrme-Extended-Thomas-Fermi Approach (SETFA) method with SLY4 set of parameters. The energy optimization calculation was performed using the SETFA code. The SETFA results were in good agreement with the related experimental results, and also with the results of the HFBRAD and HFODD- HFBTHO codes. It was indicated that Skyrme-Extended-Thomas-Fermi method can be used to explain the nuclear ground state properties, especially of the even-even stable nuclides.

Engel [50] used the Skyrme-Hartree-Fock method, allowing all symmetries to be broken, to calculate the time-reversal-violating nuclear Schiff moment in the octupole-deformed nucleus ^{225}Ra. His work includes self-consistency and polarization of the core by the last nucleon. They confirmed that the Schiff moment is large compared to those of the reflection-symmetric nuclei. Nikola [51] studied the bulk deformation properties of many nuclides using the Skyrme nuclear energy density functionals. He applied the nuclear density functional theory to assess the role of the surface symmetry energy in nuclei.

In 2018, Ghafouri and Sadeghi [52] computed the total binding energy, charge radius, densities, separation energies, pairing gaps and potential energy surfaces for neutrons and protons in various nuclides and compared them with experimental data and the results of the spherical codes. They solved the Skyrme-Hartree-Fock-Bogoliubov equations in the spatial coordinates with spherical symmetry for tin isotopes such as ^{112}Sn.

Laser spectroscopy measurements had been carried out on the neutron-rich tin isotopes by Le Blanc and Cabaret [53]. From their studies, the nuclear moments and the mean square charge radius variations were extracted . The neutron single-particle states in the odd isotopes of tin were identified by (d,p)

angular distribution studies. The cross sections for exciting these states by (d,p) and (d,t) reactions were also measured [54].

Daya Ram [55] studied the axial, non-axial and octupole deformations in thorium isotopic mass chain by using the axial Projected Shell Model (PSM) and the non-axial Cranked Hartree Bogoliubov (CHB) frameworks. From the estimated octupole moments they could infer that the octupole collectivity decreases as one moves from ^{226}Th to ^{230}Th.

The rotational and vibrational energies and the electric transition probability B(E2) of the even–even $^{228–232}$Th isotopes were studied empirically in the framework of a nuclear phenomenological approach by using the SU(3) dynamical symmetries of the Interacting Boson Model by Doma and El-Gendy in 2018 [56].

In another study, Eyyub et al. [57] calculated the nuclear properties of ^{232}Th. They have calculated the nuclear binding energy, rms charge radii, rms radii, neutron and proton density and electromagnetic multipole moments of nuclei, which are used in nuclear reactor. ^{232}Th, ^{238}U, ^{207}Pb, ^{209}Bi and ^{184}W were considered for their study. The Hartree-Fock method with Skyrme interaction was used for studying the structure properties. They have studied different ground state properties with various Skyrme parameterizations and compared their results with experimental data. Li et al. [58] in 2013 studied the evolution of quadrupole and octupole shape of thorium isotopes by density dependent mean-field theory. They predicted the possibilities for the occurrance of shape phase transition in thorium nuclei between spherical and quadrupole deformed prolate shapes and in between nonoctupole and octupole deformed shapes, with varying neutron number. They suggested that ^{224}Th is near to the critical point of double phase transition. Axially symmetric potential energy surface in $\beta_2 - \beta_4$ plain were analyzed and identified rapid shape transition between N=130 and

N=138 from nonoctupole to octupole deformation.

In 2018, Marid et al [59] proposed the relationship between deformed shape and radioactivity in thorium series. They concluded that the radioactive elements can have deformed shape. Much of the earlier research works were focussed mainly on the decay properties of thorium. In another investigation, Das [60] et al. studied the structure and decay properties of thorium isotopes with temperature dependent effective relativistic mean-field theory, with different force parameters. Cluster emission properties of even-even actinides were studied by Warda et al. [61], by using the Hartree-Fock Bogoliubov theory with phenomenological Gogny interaction. They have performed detailed analysis of the scission point. A well developed third minima was predicted by the self-consistent model to impact the fission pathway in thorium isotopes [19, 20, 62–66]. McDonnell et al. [67] in 2013 investigated and interpreted the presence of the third minima configuration. They have studied the isentropic potential energy surface of even-even thorium isotopes at different excitation energies. They predicted a shallow or third minima in the potential energy surface of ^{232}Th and a third minima appeared at neutron number N=136 and N=138. The thermal reduction in pairing, enhancement of shell effect and small excitation energies help to develop the third minima.

1.3 Motivation

In one of our earlier studies [68], we have investigated the level density of thorium nuclei that exist on and off the line of β-stability. These evaluated data including the level density parameters are useful in understanding the mechanism of nuclear reactions taking place under extreme conditions. Accordingly, we have estimated the cross sections for (n,p) and (n,α) reactions for all the thorium isotopes in a selected mass range . In that work, we have noticed some peculiar behaviour in

the values of the level density parameters and other associated data values, at certain neutron numbers. From the literature we have noticed that no systematic studies on the ground state and dynamic properties of thorium isotopes lying between the drip lines have been undertaken. This prompted us to carry out an indepth study of various properties of thorium nuclei lying between the drip lines.

The nuclear landscape is illustrated in Figure 1.4, which is a chart of nuclides with neutron number along the X-axis and proton number along the Y-axis. The black squares represent stable nuclei. These nuclei are stable against beta decay, and are part of the beta stability line. As we travel away from this valley of stability, the nuclei become more and more unstable. At points far enough away from the region of stability, some of the nucleons are completely unbound. The boundaries of nuclear landscape is the proton drip line and neutron drip line. The neutron drip line is the boundary beyond which the addition of more neutrons to a nucleus leads to immediate neutron emission, making the nucleus unstable. The proton drip line is the boundary beyond which the addition of more protons to a nucleus leads to immediate proton emission, making the nucleus unstable. Nuclei beyond the neutron drip line and proton drip line are unbound and decay rapidly. Thorium nuclei are of special interest, because of their various practical applications. They have use in various stages of nuclear fuel reactors. The isotope ^{232}Th is relatively stable and other isotopes decay very slowly through alpha decay. Thorium is not fissile by itself and so it is not directly usable in thermal neutron reactors. However, it can be transmuted inside a reactor to the fissile isotope ^{233}U. ^{232}Th is placed within and around the reactor core, where it absorbs neutron and becomes ^{233}Th. Following two subsequent β-decays it becomes ^{233}U, which is an excellent fissile material. Conversion of thorium-232 to uranium-233 is represented as,

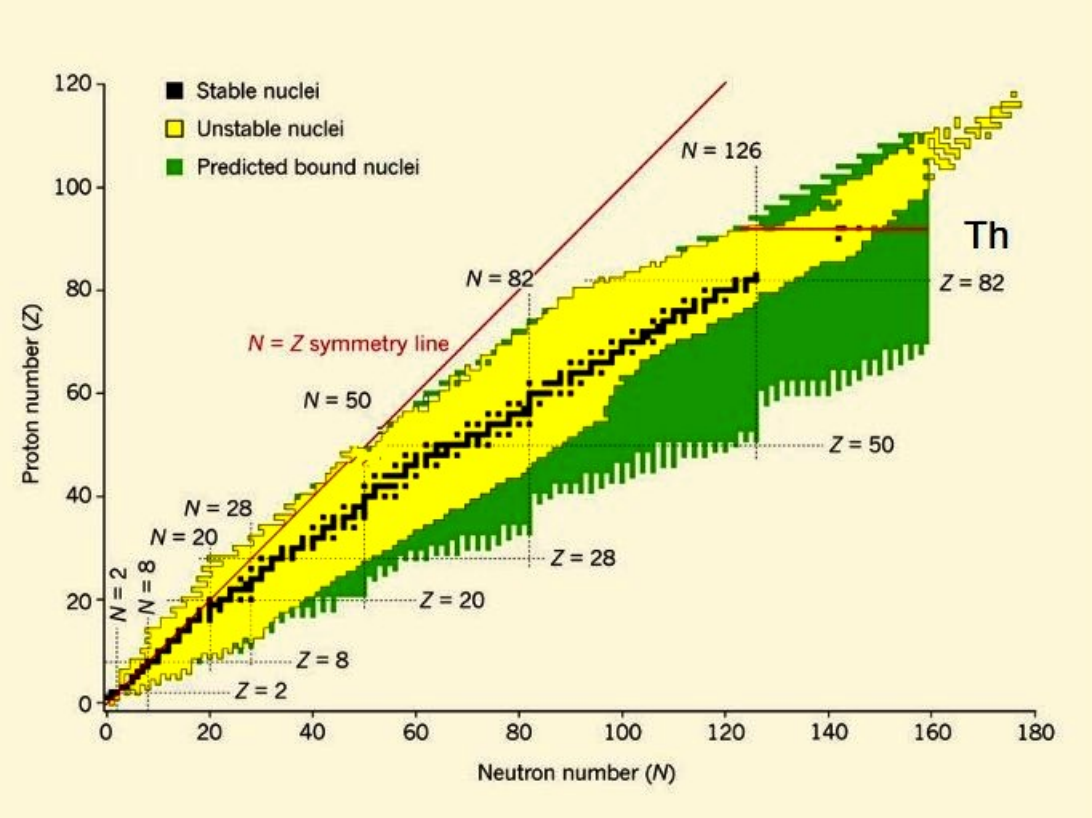

Figure 1.4: The nuclear landscape (`https://inis.iaea.org/collection/NCLCollectionStore/_Public/48/043/48043892.pdf`)

$$\mathrm{n}+{}^{232}_{90}\mathrm{Th} \rightarrow {}^{233}_{90}\mathrm{Th} \xrightarrow{\beta^-} {}^{233}_{91}\mathrm{Pa} \xrightarrow{\beta^-} {}^{233}_{92}\mathrm{U}$$

Another important observation is the possibility of the production of medical isotopes from thorium by irradiating thorium targets with light charged particles like protons and deuterons [69]. Radioisotopes usually used for both the diagnostic and the therapeutic purposes, depend on the radiation emitted by them. Radioisotopes of medical interest ^{99}Mo, ^{115}Cd and ^{111}I are obtained from the fission of thorium, by using protons and deuterons as the projectiles.

Thorium nuclei play significant roles in various stages of nucleosynthesis. Thorium is abundant in metal-poor stars and are synthesized through the r-process [70]. In the case of asymptotic giant-branch stars, thorium is synthesized through the i-process nucleosynthesis [71]. The present study is expected to provide us with the information necessary to identify the trends in the phys-

ical properties of thorium nuclei lying from proton dripline to neutron dripline and also to check for the appearance of new magic numbers. It provides new theoretical data for testing nuclear models in the context of nuclear experiments.

1.4 Objectives of the thesis work

The main objective of this thesis work is to investigate the structure properties of thorium nuclei which are lying on and off the line of β-stability (^{204}Th-^{280}Th). Here we have chosen even-even thorium isotopes, becouse it is more stable than even odd isotopes and for these experimental data are available. The aim of the study can be broadly classified into two, (i) to understand the ground state properties (ii) to understand the dynamic properties of thorium isotopes. For the structure study, the nuclear level density is one of the important factors. The level density of thorium nuclei were estimated by different phenomenological models [68]. The main objectives of thesis work are as follows.

1. To estimate the effective and collective level density parameters of thorium isotopes lying on and off the line of β-stability and identify the variation in the effective and collective level density parameters.

2. Estimate the nuclear level density parameter of other nearby nuclei in actinide series around the neutron number N=184.

3. Investigate the variation of nuclear ground state structure properties like charge radii, binding energy, separation energy, shell gap, chemical potential, deformation parameter, single-particle energy levels with and without deformation parameter and density distribution of thorium isotopes with neutron numbers by using the mean-field theory.

4. Identify the shape evolution of thorium isotopes and check for their shape phase transition. Study the variation of shape in thorium isotopes with triaxial and axial degree of freedom.

5. This thesis also intends to study the collective behaviour of thorium nuclei. Nuclei lying far away from the β-stability line are weakly unbound, and coupling between the bound state and continuum affects the multipole response of the nuclear systems, leading to different modes of excitation.

1.5 Structure of the thesis

The thesis is organised into six chapters. The general introduction, literature survey, motivation and objectives of the thesis work are presented in chapter 1. The introduction part includes different theoretical models currently in use for nuclear structure studies. Chapter 2 gives a detailed description of the calculations of nuclear level density of selected thorium isotopes and of other nearby actinide isotopes. Chapter 3 is devoted to the description of the mean-field theory and the studies on the ground state properties of thorium nuclei based on it. The shape evolution of thorium is included in chapter 4, with detailed account of the theoretical model and schematic representations. Chapter 5 contains the details of the study on the dipole strength distribution of thorium nuclei, based on the random phase approximation. Chapter 6 summarises the results and presents the future perspectives.

Bibliography

[1] H Gegier and Ernest Marsden. On a diffuse reflection of the α-particles. *Proceedings of the Royal Society of London. Series A, Containing Papers of a Mathematical and Physical Character*, 82(557):495–500, 1909.

[2] Hideki Yukawa. On the interaction of elementary particles. i. *Proceedings of the Physico-Mathematical Society of Japan. 3rd Series*, 17:48–57, 1935.

[3] DM Brink and N Sherman. Rough computation of the separation energy of strongly bound nucleons. *Physical Review Letters*, 14(11):393, 1965.

[4] Carl Friedrich von Weizsacker. Besprechung: Grete hermann. die naturphilosophischen grundlagen der quantenmechanik. *Physikalische Zeitschrift*, 37:527–528, 1936.

[5] Hans Albrecht Bethe and Robert Fox Bacher. Nuclear physics a. stationary states of nuclei. *Reviews of Modern Physics*, 8(2):82, 1936.

[6] Maria Goeppert Mayer. On closed shells in nuclei. ii. *Physical Review*, 75(12):1969, 1949.

[7] Otto Haxel, J Hans D Jensen, and Hans E Suess. On the" magic numbers" in nuclear structure. *Physical Review*, 75(11):1766, 1949.

[8] MG Mayer and JHD Jensen. *Elementary Theory of Nuclear Shell Structure,*. Wiley, New York, 1955.

[9] Eugene Feenberg and Bernard T Feld. *Shell theory of the nucleus*. American Institute of Physics, Springer, 1955.

[10] J Lindhard, M Scharff, and HE Schiott. Mat. fys. medd. dan. vid. selsk. *Mat. Fys. Medd. Dan. Vid. Selsk*, 33(14):1–42, 1963.

[11] Aage Niels Bohr and Benjamin Roy Mottelson. Collective and individual-particle aspects of nuclear structure. *Dan. Mat. Fys. Medd.*, 27(CERN-57-38):1–174, 1953.

[12] Sven Gosta Nilsson and O Prior. Binding states of individual nucleons in strongly deformed nuclei. *Fys. Medd*, 29:1–69, 1955.

[13] Aage Niels Bohr and Ben R Mottelson. *Nuclear Structure (in 2 volumes)*. World Scientific Publishing Company, 1998.

[14] Krane Kenneth, S. *Introductory Nuclear Physics*. John Wiley & Sons, Inc., 1988.

[15] David Lawrence Hill and John Archibald Wheeler. Nuclear constitution and the interpretation of fission phenomena. *Physical Review*, 89(5):1102, 1953.

[16] S Thummerer, W Von Oertzen, B Gebauer, SILVIA MONICA Lenzi, A Gadea, DR Napoli, C Beck, and Marc Rousseau. The population of deformed bands in ^{48}Cr by emission of ^{8}Be from the $^{32}S + ^{24}Mg$ reaction. *Journal of Physics G: Nuclear and Particle Physics*, 27(7):1405, 2001.

[17] THR Skyrme. Cvii. the nuclear surface. *Philosophical Magazine*, 1(11):1043–1054, 1956.

[18] THR Skyrme. The effective nuclear potential. *Nuclear Physics*, 9(4):615–634, 1958.

[19] J Dechargé and D Gogny. Hartree-fock-bogolyubov calculations with the $d1$ effective interaction on spherical nuclei. *Physical Review C*, 21(4):1568, 1980.

[20] LD Miller and Alex ES Green. Relativistic self-consistent meson field theory of spherical nuclei. *Physical Review C*, 5(1):241, 1972.

[21] John Dirk Walecka. A theory of highly condensed matter. *Annals of Physics*, 83(2):491–529, 1974.

[22] Brian D Serot and John Dirk Walecka. Relativistic nuclear many-body theory. *Recent Progress in Many-Body Theories: Volume 3*, pages 49–92, 1992.

[23] Brian D Serot. Quantum hadrodynamics. *Reports on Progress in Physics*, 55(11):1855, 1992.

[24] Peter Ring. Relativistic mean field theory in finite nuclei. *Progress in Particle and Nuclear Physics*, 37:193–263, 1996.

[25] Leonard Isaac Schiff. Nonlinear meson theory of nuclear forces. i. neutral scalar mesons with point-contact repulsion. *Physical Review*, 84(1):1, 1951.

[26] MH Johnson and E Teller. Proton distribution in heavy nuclei. *Physical Review*, 93(2):357, 1954.

[27] Hans-Peter Dürr. Relativistic effects in nuclear forces. *Physical Review*, 103(2):469, 1956.

[28] P-G Reinhard. The relativistic mean-field description of nuclei and nuclear dynamics. *Reports on Progress in Physics*, 52(4):439, 1989.

[29] MH Johnson and Edward Teller. Classical field theory of nuclear forces. *Physical Review*, 98(3):783, 1955.

[30] Hans-Peter Dürr and Edward Teller. Interaction of antiprotons with nuclear fields. *Physical Review*, 101(1):494, 1956.

[31] SK Patra and CR Praharaj. Relativistic mean field study of light medium nuclei away from beta stability. *Physical Review C*, 44(6):2552, 1991.

[32] YK Gambhir, P Ring, and Ann Thimet. Relativistic mean field theory for finite nuclei. *Annals of Physics*, 198(1):132–179, 1990.

[33] M Rufa, P-G Reinhard, JA Maruhn, W Greiner, and MR Strayer. Optimal parametrization for the relativistic mean-field model of the nucleus. *Physical Review C*, 38(1):390, 1988.

[34] MM Sharma, GA Lalazissis, and P Ring. Anomaly in the charge radii of *pb* isotopes. *Physics Letters B*, 317(1-2):9–13, 1993.

[35] J Boguta and AR Bodmer. Relativistic calculation of nuclear matter and the nuclear surface. *Nuclear Physics A*, 292(3):413–428, 1977.

[36] Y Sugahara and H Toki. Relativistic mean-field theory for unstable nuclei with non-linear σ and ω terms. *Nuclear Physics A*, 579(3-4):557–572, 1994.

[37] T Bürvenich, DG Madland, JA Maruhn, and P-G Reinhard. Nuclear ground state observables and qcd scaling in a refined relativistic point coupling model. *Physical Review C*, 65(4):044308, 2002.

[38] Jean-Paul Blaizot and Georges Ripka. *Quantum theory of finite systems*. MIT Press, 1986.

[39] George F Bertsch and Ricardo A Broglia. *Oscillations in finite quantum systems*. Cambridge University Press, 1994.

[40] Pier Francesco Bortignon, Angela Bracco, and Ricardo A Broglia. *Giant Resonances: Nuclear structure at finite temperature*. CRC Press, 2019.

[41] Muhsin N Harakeh and Adriaan Woude. *Giant Resonances: fundamental high-frequency modes of nuclear excitation*, volume 24. Oxford Studies in Nuclear Phys, 2001.

[42] W Bothe and W Gentner. Atomumwandlungen durch γ-strahlen. *Zeitschrift für Physik*, 106:236–248, 1937.

[43] Morawetz Klaus, Fuhrmann Uwe, and Rainer Walke. Collective modes in asymmetric nuclei- thesis. 2018.

[44] U Fuhrmann, K Morawetz, and R Walke. Damping rates of hot giant dipole resonances. *Physical Review C*, 58(3):1473, 1998.

[45] F Catara, EG Lanza, MA Nagarajan, and A Vitturi. Effect of large neutron excess on the dipole response in the region of the giant dipole resonance. *Nuclear Physics A*, 624(3):449–458, 1997.

[46] RJ Blin-Stoyle. Collective nuclear motion and the effective mass of a nucleon. *Nuclear Physics*, 2(2):169–172, 1956.

[47] PO Hess, M Seiwert, J Maruhn, and W Greiner. General collective model and its application to $^{238}_{92}U$. *Zeitschrift für Physik A Atoms and Nuclei*, 296:147–163, 1980.

[48] WM Alberico, A Molinari, R Cenni, and Mikkel B Johnson. On the collective modes of infinite nuclear matter. *Annals of Physics*, 138(1):178–212, 1982.

[49] Yacobus Yulianto and Zaki Su'ud. Skyrme-extended-thomas-fermi approach method in investigation of nuclear ground state properties of ^{208}Pb. *Indonesian Journal of Physics*, 27(1):27–33, 2016.

[50] Jonathan Engel, Michaël Bender, Jacek Dobaczewski, JH De Jesus, and Przemyslaw Olbratowski. Time-reversal violating schiff moment of ^{225}Ra. *Physical Review C*, 68(2):025501, 2003.

[51] N Nikolov, N Schunck, Witold Nazarewicz, M Bender, and Junchen Pei. Surface symmetry energy of nuclear energy density functionals. *Physical Review C*, 83(3):034305, 2011.

[52] M Ghafouri, H Sadeghi, and M Torkiha. Self-consistent description of the shfb equations for ^{112}Sn. *Results in physics*, 8:734–743, 2018.

[53] F Le Blanc, L Cabaret, E Cottereau, JE Crawford, S Essabaa, J Genevey, R Horn, G Huber, J Lassen, JKP Lee, et al. Charge-radius change and nuclear moments in the heavy tin isotopes from laser spectroscopy: Charge radius of ^{132}Sn. *Physical Review C*, 72(3):034305, 2005.

[54] Bernard L Cohen and Robert E Price. Nuclear structure studies in the tin isotopes with (d, p) and (d, t) reactions. *Physical Review*, 121(5):1441, 1961.

[55] Daya Ram, Rani Devi, and SK Khosa. Microscopic study of positive-parity yrast bands of $^{224-234}Th$ isotopes. *Pramana*, 80:953–970, 2013.

[56] SB Doma and HS El-Gendy. A nuclear phenomenological study of the even–even thorium isotopes $^{228-232}Th$. *International Journal of Modern Physics E*, 27(05):1850040, 2018.

[57] Eyyup Tel, Hacı Mehmet Şahin, Abdullah Kaplan, Abdullah Aydin, and Taner Altınok. Investigation of the properties of the nuclei used on the new generation reactor technology systems. *Annals of Nuclear Energy*, 35(2):220–227, 2008.

[58] ZP Li, BY Song, JM Yao, D Vretenar, and J Meng. Simultaneous quadrupole and octupole shape phase transitions in thorium. *Physics Letters B*, 726(4-5):866–869, 2013.

[59] Huda A Marid, Naz T Jarallah, and Hameed M Abduljabbar. Radioactivity effect on the shape of even-even nuclei for uranium and thorium series. *Results in Physics*, 11:406–409, 2018.

[60] M Das, KC Naik, N Biswal, and RN Panda. Structure and decay properties of th isotopes using e-rmft formalism. *Atom Indonesia*, 48(2):115–123, 2022.

[61] M Warda and LM Robledo. Microscopic description of cluster radioactivity in actinide nuclei. *Physical Review C*, 84(4):044608, 2011.

[62] VV Pashkevich. On the asymmetric deformation of fissioning nuclei. *Nuclear Physics A*, 169(2):275–293, 1971.

[63] P Möller. Odd-multipole shape distortions and the fission barriers of elements in the region $84 \leq Z \leq 120$. *Nuclear Physics A*, 192(3):529–580, 1972.

[64] S Ćwiok, W Nazarewicz, JX Saladin, W Płóciennik, and A Johnson. Hyperdeformations and clustering in the actinide nuclei. *Physics Letters B*, 322(4):304–310, 1994.

[65] GM Ter-Akopian, JH Hamilton, Yu Ts Oganessian, AV Daniel, J Kormicki, AV Ramayya, GS Popeko, BRS Babu, Q-H Lu, K Butler-Moore, et al. New spontaneous fission mode for ^{252}Cf: Indication of hyperdeformed $^{144,145,146}Ba$ at scission. *Physical Review Letters*, 77(1):32, 1996.

[66] Ragnar Bengtsson, Ingemar Ragnarsson, Sven Åberg, Anna Gyurkovich, Adam Sobiczewski, and Krzysztof Pomorski. Properties of nuclei at the third-minimum deformation. *Nuclear Physics A*, 473(1):77–110, 1987.

[67] JD McDonnell, Witold Nazarewicz, and JA Sheikh. Third minima in thorium and uranium isotopes in a self-consistent theory. *Physical Review C*, 87(5):054327, 2013.

[68] Erumban Ummukulsu, Nithu Ashok, and Antony Joseph. Study of level density and reaction cross-sections in thorium isotopes. *Modern Physics Letters A*, 34(12):1950091, 2019.

[69] Charlotte Duchemin, Arnaud Guertin, Ferid Haddad, Nathalie Michel, and Vincent Metivier. Production of medical isotopes from a thorium target irradiated by light charged particles up to $70MeV$. *Physics in Medicine & Biology*, 60(3):931, 2015.

[70] Ian U Roederer, Karl-Ludwig Kratz, Anna Frebel, Norbert Christlieb, Bernd Pfeiffer, John J Cowan, and Christopher Sneden. The end of nucleosynthe-

sis: production of lead and thorium in the early galaxy. *The Astrophysical Journal*, 698(2):1963, 2009.

[71] Arthur Choplin, Stephane Goriely, and Lionel Siess. Synthesis of thorium and uranium in asymptotic giant branch stars. *Astronomy & Astrophysics*, 667:L13, 2022.

Chapter 2

Nuclear Level Density

2.1 Introduction

A nucleus is a quantum many-body system, where single-particle and collective motions give rise to the fundamental modes of excitation. The description of single-particle excited states involves nucleons occupying distinct orbits. These orbits are generated from their independent motion in a mean-field potential [1]. In a nucleus, the number of quantum mechanical states increases with rise in excitation energy [2–5]. Nuclear levels display a discrete spectrum for low excitation energies. However, when the excitation energy increases above 1 or 2 MeV, the spacing of these levels reduces, depending on the mass of the nucleus. At low excitation energy, the nuclear levels are well separated and it is possible to determine their properties, both experimentally and theoretically. But, when the excitation energy of the nucleus increases, the density of these levels rapidly become high and it is impossible to describe each level individually. One of the basic statistical properties of these levels is their density. Hence, in statistical models for predicting nuclear reactions, level density (LD) is needed at excitation energies where discrete level information is not available or is incomplete.

As the excitation energy increases, the gap between nuclear levels gradually

diminishes, and the character of the excitations becomes increasingly intricate. The width of these resonances are 10^6 times smaller than what would be anticipated for a single-particle excitation.

The nuclear level density holds a significant position in the realm of nuclear physics. Concurrently, LDs play a crucial role in the statistical model computations of nuclear reaction cross sections. These calculations find applications in diverse fields, ranging from astrophysical studies, where they aid in determining the thermonuclear rates of nucleosynthesis, to the design of fission or fusion reactors. The determination of nuclear level density through experimental study is not so feasible, particularly in applications like nucleosynthesis calculations. In such cases, the reliance on level density obtained from certain theoretical models or extrapolated from nuclei for which experimental data is accessible, becomes necessary. Hence, understanding nuclear level density is crucial in various domains including basic nuclear physics research, nuclear medicine [6], nuclear reactor design, nuclear astrophysics [7] etc., and it provides the essential insight into the nuclear thermodynamics [8].

The significance of level density in the theoretical examination of nuclear reaction observables such as cross sections, spectra, and angular distributions need not have to be over emphasized. This critical factor had extensively been investigated in the past, leading to a diverse array of models. These models span from the microscopic level densities derived through combinatorial methods and Hartree–Fock approaches to the analytical expressions based on phenomenology. It is worth noting that despite the availability of microscopic approaches, the phenomenological and analytical level density formulas still continue to be commonly employed in nuclear reaction calculations.

The emergence of advanced experimental facilities of radioactive ion beams, both for the astrophysical investigations and the next generation research, makes

it possible to have nuclear data in regions far from the valley of stability. This presents a significant challenge for nuclear level density (NLD) models. Certainly, the cross-section predictions predominantly rely on the phenomenological approaches, which often adjust various parameters based on the limited experimental data for nuclei near the valley of β-stability or inferred from systematic trends. While this approach tends to be reliable for nuclei in the proximity to experimentally accessible regions, it becomes questionable when dealing with exotic nuclei. To address these challenges, it would be more preferable to utilize methods that are as fundamental (microscopic) as possible, and grounded in physically robust models. Furthermore, these methods should be applicable systematically to the extensive array of nuclei.

Theory of nuclear level density was initiated by Hans Bethe [9] in 1936, on the basis of the Fermi Gas Model of the nucleus. This is one of the reasons for having large number of studies carried out in the past. Derived from Bethe's Fermi Gas model, numerous analytical expressions have been put forth to characterize not just the exponential rise of the number of energy levels with excitation energy but also to account for the influences of shell structure, pairing effects and collective phenomena [10].

NLD has been studied extensively, using both phenomenological [11] as well as microscopic models. Some of the important concepts of the structure of low lying nuclear levels based on shell effects, pairing correlations and collective phenomenon are taken into account in the microscopic models. However, phenomenological models are more convenient for the analysis of the experimental data. For the simplest system having A particles, with an excitation energy E_x , the most general expression for level density is,

$$\rho(A, E_x) = \frac{dN(A, E_x)}{dE_x} \tag{2.1}$$

which is the derivative of the total number of levels $N(A, E_x)$ of a nucleus with an excitation energy lower than E_x. The level density $\rho(E_x, J,)$ corresponds to the number of nuclear levels per MeV around an excitation energy E_x, for a certain spin J and parity π. The total level density $\rho_{tot}(E_x)$ corresponds to the number of levels per MeV around E_x.

$$\rho^{tot} = \sum_{J} \sum_{\pi} \rho(E_x, J, \pi) \tag{2.2}$$

Since nuclear levels are degenerate in M, the total state density $\omega^{tot}(E_x)$ includes the 2J + 1 states for each level. Hence,

$$\omega^{tot}(E_x) = \sum_{J} \sum_{\pi} (2J+1)\rho(E_x, J, \pi) \tag{2.3}$$

Then,

$$\rho(E_x, J, \pi) = P(E_x, J, \pi) R(E_x, J) \rho^{tot}(E_x) \tag{2.4}$$

where $P(E_x, J, \pi)$ is the parity distribution and $R(E_x, J)$ is the spin distribution [12]. The parity distribution is 1/2, since parity equipartition is assumed for the three phenomenological models, which are considered in the subsequent sections. The general expression for the total state density, as obtained from the methods of statistical mechanics [4] is,

$$\omega^{tot} = \frac{\exp[S(E_x)]}{\sqrt{D(E_x)}} \tag{2.5}$$

where S is the entropy and D is the determinant related to the saddle-point approximation. The appropriate choices for S and D lead to the various analytical level density expressions.

2.2 Theoretical Formalism

2.2.1 Phenomenological level density

The accuracy of the calculated nuclear reaction observables in various reaction channels depends on the level density. As a result, numerous theoretical works have been undertaken to establish a reliable LD, utilizing both the phenomenological [3, 11–13] and microscopic models [14–18]. Microscopic models, which are free from adjustable parameters, are well-suited for predicting LDs of nuclei located away from the stability line. On the other hand, phenomenological models, characterized by analytical formulas and adjustable parameters, remain valuable for computing LDs of nuclei around the stability line in practical applications. Typically, the reliability of the phenomenological models is ensured by incorporating the experimental information such as excitation energies and spin-parity of low-lying discrete states. These models, despite having adjustable parameters, prove useful in calculating LDs for nuclei in proximity to the stability line. Hence the combination of these two theoretical approaches allows for a comprehensive understanding and prediction of nuclear reaction observables across a broad range of scenarios.

All phenomenological expressions of level density at high excitation energies follow the Fermi Gas expression, which mainly depends on the *level density parameter* a. The level density expression for the Fermi Gas Model was proposed by Bethe in 1937 [9]. Two types of phenomenological approaches are there, depending on whether the collective effects are explicitly considered or not. If the collective effects are not explicitly included, we get the effective level density and if they are included, we get the collective level density.

The most frequently used phenomenological models are the Fermi Gas Model [9] and the Gilbert-Cameron [11] Model. The Gilbert-Cameron Model

was proposed to combine the constant temperature model [19] for low excitation energies with the Fermi Gas Model for the high excitation energies. The constant temperature model assumes that the phase transition in nuclei occurs without changing the temperature when a nucleus gains energy. Thus, the temperature is independent of the excitation energy [20]. The Fermi Gas Model assumes that equally spaced single particle states are filled with non-interacting fermions. The other two phenomenological models are the Back-shifted Fermi Gas Model [21] and the Generalized Superfluid Model [12]. In Back-shifted Fermi Gas Model, the pairing energy is treated as an adjustable parameter and the Fermi Gas expression is used to describe the level density. The Generalized Superfluid Model (GSM) takes superconductive pairing correlations into account, according to the Bardeen–Cooper–Schrieffer theory.

Fermi Gas Model

The basis of this model is the assumption that individual particle states forming the excited levels within the nucleus exhibit uniform spacing, and it is the basis for the absence of collective levels. The Fermi Gas level density $\rho_F(E_x, J)$ for a given spin J at excitation energy E_x is given by,

$$\rho_F(E_x, J) = \frac{1}{2}\left[\frac{(2J+1)\exp\left[-\frac{\left(J+\frac{1}{2}\right)^2}{2\sigma^2}\right]}{2\sigma^2}\right]\left[\frac{1}{\sqrt{2\pi}\sigma}\frac{\sqrt{\pi}}{12}\frac{\exp\left[2\sqrt{aU}\right]}{a^{\frac{1}{4}}U^{\frac{5}{4}}}\right] \quad (2.6)$$

Then, the total Fermi gas level density $\rho_F^{tot}(E_x)$ at excitation energy E_x is

$$\rho_F^{tot}(E_x) = \frac{\omega_F^{tot}}{\sqrt{2\pi}\sigma} = \frac{1}{\sqrt{2\pi}\sigma}\frac{\sqrt{\pi}}{12}\frac{\exp\left[2\sqrt{aU}\right]}{a^{\frac{1}{4}}U^{\frac{5}{4}}} \quad (2.7)$$

Here, U is defined as $U = E_x - \Delta$, where Δ is the energy shift, which can be given as,

$$\Delta = \chi \frac{12}{\sqrt{A}} \tag{2.8}$$

with

$$\chi = 0 \text{ for odd-odd nuclei}$$
$$\chi = 1 \text{ for odd-even nuclei, and}$$
$$\chi = 2 \text{ for even-even nuclei.}$$

The energy shift, denoted as Δ, is an empirical parameter, with a value equal to or closely related to the pairing energy in certain models. This inclusion of Δ is aimed at replicating the well-known odd-even effects observed in nuclei. The fundamental concept here is that Δ accommodates the necessity to separate pairs of nucleons before individual components can be excited. In practical terms, Δ serves as a crucial adjustable parameter for reproducing the observable results, and its definition may vary among the discussed models. Equation 2.6 clarifies that here, we will utilize both the actual excitation energy E_x as the primary variable for discrete levels and expressions, and the effective excitation energy U, predominantly for expressions associated with the continuum.

One of the significant quantities appearing in these expressions is a, the level density parameter and it is given as,

$$a(E_x) = \tilde{a} \left[1 + \delta W \frac{1 - \exp\left(-\gamma U\right)}{U} \right] \tag{2.9}$$

with $\tilde{a}$ being the asymptotic level density. Here, δW is the shell correction energy in MeV, which is the difference between the real mass of the nucleus and the mass

according to the spherical liquid drop model.

$$\delta W = M_{exp} - M_{LDM} \tag{2.10}$$

The mass from liquid drop model is,

$$M_{LDM} = NM_n + ZM_H + E_{vol} + E_{sur} + E_{Coul} + \delta \tag{2.11}$$

with

$$M_n = 8.07144 \text{ MeV}$$

$$M_H = 7.28899 \text{ MeV}$$

$$E_{vol} = -c_1 A$$

$$E_{sur} = c_2 A^{\frac{2}{3}}$$

$$E_{Coul} = c_3 \frac{Z^2}{A^{\frac{1}{3}}} - c_4 \frac{Z^2}{A}$$

and

$$c_i = a_i \left[1 - k(\tfrac{N-Z}{A})^2\right], \qquad \text{where } i = 1, 2$$

$$c_3 = 0.717 \text{ MeV}$$

$$c_4 = 1.21129 \text{ MeV}$$

$$\delta = \begin{cases} -\frac{11}{\sqrt{A}} & \text{for even-even nuclei} \\ 0 & \text{for odd-even nuclei} \\ \frac{11}{\sqrt{A}} & \text{for odd-odd nuclei.} \end{cases}$$

The value of the asymptotic level density $\tilde{a}$ is given by,

$$\tilde{a} = \alpha A + \beta A^{\frac{2}{3}} \tag{2.12}$$

Generally $\alpha = 0.0666$ and $\beta = 0.2587$. The level density parameter a depends on the shell damping parameter γ. The shell damping parameter γ [12] is obtained

as,

$$\gamma = \frac{0.459}{A^{\frac{1}{3}}} MeV^{-1} \tag{2.13}$$

The level density parameter depends on the sign of the shell correction energy $\delta W(Z,N)$. It influences the shell effect in the energy range upto the neutron separation energy [22].

The spin cut-off factor σ is another fundamental input parameter to calculate the nuclear level density, which characterizes the width of the distribution of the z-component of angular momentum and is defined as,

$$\sigma^2 = R_\sigma \frac{A^{5/3}}{\tilde{a}} \sqrt{aU} \tag{2.14}$$

with $R_\sigma = 0.01389$.

The level density parameter a is theoretically given by
$a = \frac{\pi^2}{6}(g_\pi + g_\nu)$, with g_π and g_ν representing the spacing of proton and neutron single particle states near the Fermi energy.

Δ, a, and σ are three parameters, which determine the ρ_F and ρ_F^{tot}. a and σ have specific energy dependencies. In Fermi Gas Model, the level density parameter a can be derived from D_0, the average level spacing at the neutron separation energy S_n, which is usually obtained from the available experimental set of s-wave resonance.

$$\frac{1}{D_0} = \sum_{J=|I-\frac{1}{2}|}^{J=|I+\frac{1}{2}|} \rho_F(S_n, J, \pi) \tag{2.15}$$

where I is the spin of the target nuclei.

2.2.2 Constant Temperature Model (CTM)

The constant temperature model [19] reproduces nuclear level density in the low energy range. The number of energy levels in the range upto an intermediate matching energy E_x is given by,

$$N(E_x) = \exp\left(\frac{E_x - E_0}{T}\right) \tag{2.16}$$

and the corresponding level density is,

$$\rho_T = \frac{dN(E_x)}{dE_x} = \frac{1}{T}\exp\left(\frac{E_x - E_0}{T}\right) \tag{2.17}$$

Here, E_0 is the ground state energy.

2.2.3 Gilbert-Cameron Model

Gilbert and Cameron [19] introduced a composite model for the nuclear level density, where the constant nuclear temperature, which describes the nuclear level density at the low excitation energy is coupled to the Fermi Gas Model, which represent the level density ρ_F at high excitation energy. Here the excitation energy is divided into two, a low energy part and a high energy part. In the low energy part, from 0 MeV upto a matching energy E_M, the constant temperature law is applicable. In the high energy part above the matching energy E_M, the Fermi Gas Model applies. Hence for the total level density,

$$\begin{aligned} \rho^{tot}(E_x) &= \rho_T^{tot}(E_x) \qquad \text{if} \qquad E_x \leq E_M \\ &= \rho_F^{tot}(E_x) \qquad \text{if} \qquad E_x \geq E_M \end{aligned} \tag{2.18}$$

Then,

$$\begin{aligned} \rho(E_x, J, \pi) &= \tfrac{1}{2} R_F(E_x, J) \rho_T^{tot}(E_x) \qquad \text{if} \qquad E_x \leq E_M \\ &= \rho_F(E_x, J, \pi) \qquad \text{if} \qquad E_x \geq E_M \end{aligned} \tag{2.19}$$

The expression for ρ_T^{tot} and ρ_F^{tot} have to be matched at the matching energy E_M, where their values and their derivatives are identical. From equation (2.18),

$$T\rho_F^{tot}(E_M) = \exp \frac{(E_M - E_0)}{T} \tag{2.20}$$

$$E_0 = E_M - T \ln(T\rho_F^{tot}(E_M)) \tag{2.21}$$

and

$$\frac{1}{T} = \frac{d \ln(\rho_F^{tot}(E_M))}{dE_x} \tag{2.22}$$

Since there are three unknown parameters T, E_0 and E_M, we need another constraint. This is obtained by demanding that, in the discrete level region, the constant temperature law reproduces the experimental discrete levels. The total level density agrees well with the discrete level sequence, i.e., from a lower discrete level N_L with energy E_L to an upper level N_U with energy E_U. i.e,

$$N_U = N_L + \int_{N_L}^{N_U} \rho_T^{tot}(E_x) dE_x \tag{2.23}$$

and

$$\rho_T^{tot}(E_x) = \frac{1}{T} \exp\left(\frac{E_x - E_0}{T}\right) \tag{2.24}$$

Then,

$$N_U = N_L + \left[\exp(\frac{E_U}{T}) - \exp(\frac{E_L}{T})\right] \exp(-\frac{E_0}{T}) \tag{2.25}$$

Equations 2.22 , 2.24 and 2.25 determine T, E_0 and E_M. The empirical formula for the temperature under the two cases are as given below.

- For the effective model,

$$T = -0.22 + \frac{9.4}{\sqrt{A(1+\gamma\delta W)}} \tag{2.26}$$

- For the collective model,

$$T = -0.25 + \frac{10.2}{\sqrt{A(1+\gamma\delta W)}} \tag{2.27}$$

Also, the empirical formula for the matching energy, for the two cases are as follows.

- For the effective model,

$$E_M = 2.33 + \frac{253}{A} + \Delta^{CTM} \tag{2.28}$$

- For the collective model,

$$E_M = 2.67 + \frac{253}{A} + \Delta^{CTM} \tag{2.29}$$

2.2.4 Back-shifted Fermi Gas Model

In the Back-shifted Fermi Gas model (BFGM) [21], the pairing energy is treated as an adjustable parameter. The total Fermi Gas level density $\rho_F^{tot}(E_x)$ at exci-

tation energy E_x is given as equation 2.6. In this case, the effective excitation energy $U = E_x - \Delta^{BFM}$, where the energy shift Δ^{BFM} is given by,

$$\Delta^{BFM} = \chi \frac{12}{\sqrt{A}} + \delta \tag{2.30}$$

with

$$\chi = -1 \text{ for odd-odd nuclei}$$
$$\chi = 0 \text{ for odd-even nuclei}$$
$$\chi = 1 \text{ for even-even nuclei}$$

and δ is an adjustable parameter to fit with the experimental data. The above equation will diverge when U goes to zero. A solution to this problem has been provided by Gross Jean and Feldmeir [23] and was transformed into a practical form by Demetrious and Goriely [17].

The expression for the total Back-shifted Fermi Gas Model level density is,

$$\rho^{tot}_{BFM}(E_x) = \left[\frac{1}{\rho^{tot}_F(E_x)} + \frac{1}{\rho_0(t)} \right]^{-1} \tag{2.31}$$

where

$$\rho_0(t) = \frac{\exp(1)}{24\sigma} \frac{(a_n + a_p)^2}{\sqrt{a_n a_p}} \exp(4 a_n a_p t^2) \tag{2.32}$$

with $a_n = a_p = \frac{a}{2}$ and te nulear temperature $t = \sqrt{\frac{U}{a}}$.

Then, the level density,

$$\rho_F(E_x, J) = \frac{1}{2} \left[\frac{(2J+1)}{2\sigma^2} \exp\left[-\frac{\left(J + \frac{1}{2}\right)^2}{2\sigma^2} \right] \right] \rho^{tot}_{BFM}(E_x) \tag{2.33}$$

2.2.5 Collective Effects in Level Density

The excited levels of nuclei result from the coherent excitations of the fermions it contains. The Fermi Gas Model is not appropriate to describe such levels. The collective effect with excitation energy plays a role in the estimation of level density. It can be shown that the collective effect in phenomenological level density is achieved by explicitly introducing the collective enhancement factor to the effective level density $\rho_{F,eff}(E_x, J, \pi)$. Then the collective level density $\rho_{F,coll}(E_x, J, \pi)$ is,

$$\rho_{F,coll}(E_x, J, \pi) = K_{rot}(E_x) K_{vib} \rho_{F,eff}(E_x, J, \pi) \tag{2.34}$$

Here, K_{rot} and K_{vib} are the rotational and vibrational enhancement factors. The vibrational enhancement factor is approximated as [24],

$$K_{vib} = \exp\left[\delta S - (\frac{\delta U}{t})\right] \tag{2.35}$$

where δS and δU are the changes in the entropy and excitation energy, respectively.

Then,

$$\delta S = \sum_i (2\lambda + 1)((1 + n_i)\ln(1 + n_i) - n_i \ln n_i) \tag{2.36}$$

and

$$\delta U = \sum_i (2\lambda + 1)\omega_i n_i \tag{2.37}$$

where ω_i are the energies and λ_i are the multipolarities and n_i are the occupation numbers for the vibrational excitations.

The occupation number is written as,

$$n_i = \frac{\exp \frac{-\gamma_i}{2\omega_i}}{\exp \frac{\omega_i}{t} - 1} \tag{2.38}$$

where γ_i, the spreading widths of the vibrational excitations [25], are given as,

$$\gamma_i = 0.0075 A^{\frac{1}{3}} (\omega_i^2 + 4\pi^2 t^2) \tag{2.39}$$

Hence,

$$K_{vib} = exp(0.0555 A^{\frac{2}{3}} T^{\frac{4}{3}}) \tag{2.40}$$

The rotational motion also contributes to the collective level density. Its effect is not much stronger and depends on the deformation.

$$K_{rot} = 0.01389 A^{\frac{5}{3}} (1 + \frac{\beta_2}{3}) \sqrt{\frac{U}{a}} \tag{2.41}$$

Here, β_2 is the ground state quadrupole deformation. Then, the final expression for the collective level density is,

$$\rho_{F,coll}(E_x, J, \pi) = K_{rot}(E_x) K_{vib} \rho_{F,eff}(E_x, J, \pi) \tag{2.42}$$

2.3 Results and Discussion

2.3.1 Nuclear level density parameter

The nuclear level density parameter is an important ingredient for estimating the level density. In this study, we have estimated the nuclear level density parameters of even-even thorium nuclei in the mass range 204-280. The calculations were performed by employing the Gilbert-Cameron Model . Specifically, we computed

the level density parameters under two conditions: one considering the collective enhancement effect, which accounts for the rotational and vibrational effects of nuclei, and the other without incorporating this enhancement.

The results of these calculations provide insights into the variation of both the collective and effective level density parameters in relation to the neutron number . The neutron number is a critical factor influencing the nuclear structure and behavior of nuclei. The nuclear level density parameter is estimated by using equation 2.9. The effective and collective level density parameter is estimated from the level density expression 2.6 and 2.42. To visually represent these variations, we have plotted the effective and collective level density parameters (ELD and CLD) of thorium isotopes with neutron number in Figure 2.1. This graphical representation serves to illustrate how the inclusion or exclusion of the collective enhancement effects influences the level density parameters, shedding light on to the new aspects of nuclear structure within the specified mass range. The figure provides a comprehensive view of how these parameters evolve with changes in neutron number, contributing valuable information to our understanding of thorium nuclei in this particular mass range. Earlier in 1969, Gadoli et al. [26] calculated the level density parameter for ^{230}Th, based on the slow neutron spacing. In 2005, Behkmai et al.[27] also estimated the level density parameter of ^{230}Th. We compared our results with their values. The analysis of the level density parameter in our study reveals a notable trend: a decrease in the parameter at specific neutron numbers,namely at N=126 and N=184. This observation suggests the possibility of neutron magic numbers at these points. Neutron magic numbers are associated with a higher stability and enhanced nuclear binding. The calculated value of the level density parameter for ^{230}Th is in good agreement with the value of Gadoli et al.[26] and Behkmai et al [27]. The variation of both effective and collective level density parameters with neutron

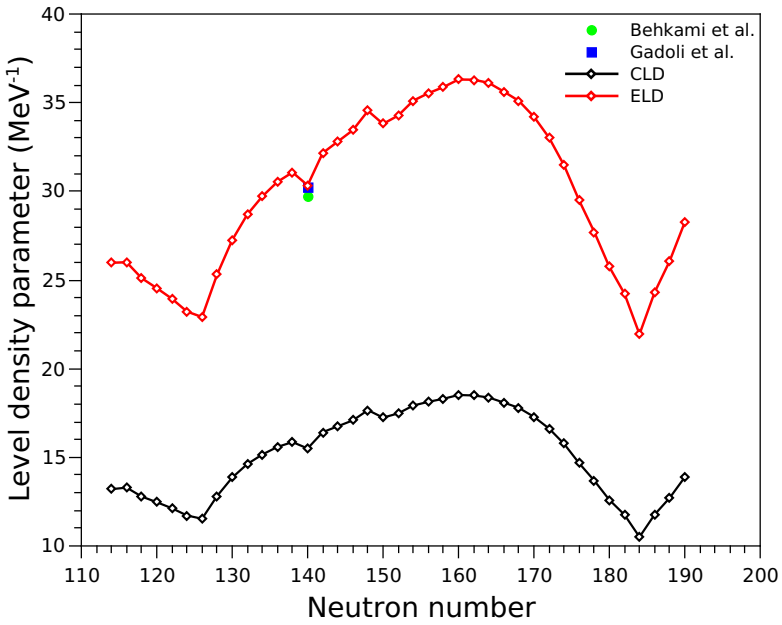

Figure 2.1: Variation of the effective and collective level density parameters with neutron number.

numbers for thorium nuclei reveals a similar behavior. Notably, a subtle dip in the level density parameter is noticeable around the neutron number N=140. Also there is a small hike noticed around N=150 and it may be due to the deformation of thorium isotopes. We also estimated the deformation parameter of thorium isotopes and confirmed in fourth chapter. Most deformed nuclei is $^{240}Th_{150}$. This feature in the plot points to an interesting nuclear structure or behavior around this neutron number. Additionally, the comparison between the collective and effective level density parameters indicates that the collective level density parameter consistently remains smaller than the effective level density parameter across all the neutron numbers considered here. This behaviour can be attributed to the influence of rotational and vibrational effects, which serve to decrease the overall level density. In short, our findings contribute to figure out the behavior of level density parameters in thorium nuclei and suggests the presence of neutron magic numbers and highlight the impact of rotational and vibrational effects on the overall level density. Changes in the level density

parameter also affect the variation in level density.

In Figures 2.2 and 2.3, we have depicted the collective enhancement factors of thorium nuclei in proximity to the neutron numbers N=126 and N=184, corresponding to ^{216}Th and ^{274}Th, respectively. These figures illustrate the variation of the collective enhancement factor with the excitation energy for thorium nuclei with specified neutron numbers.

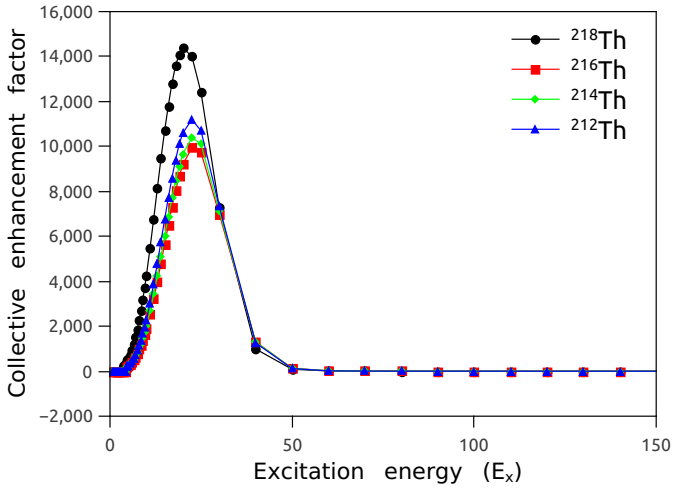

Figure 2.2: Variation of the collective enhancement factor of thorium nuclei around N=126 (^{216}Th) with excitation energy.

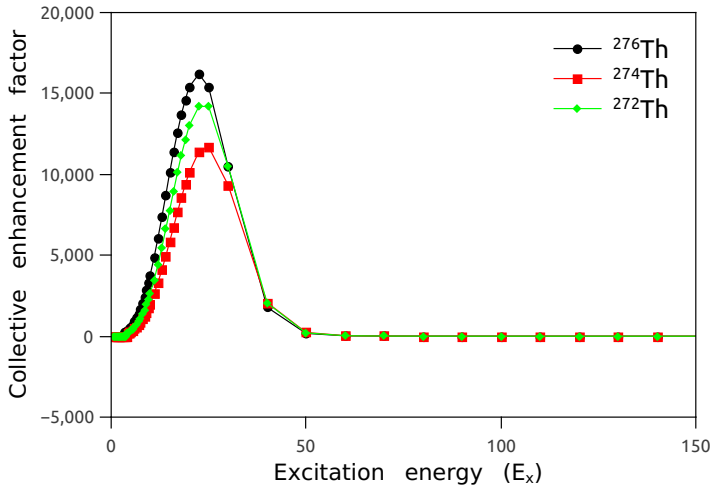

Figure 2.3: Variation of the collective enhancement factor of thorium nuclei around N=184 (^{274}Th) with excitation energy.

Figure 2.2 focuses on neutron number N=126, featuring thorium isotope ^{216}Th. The plot showcases how the collective enhancement factor varies across different excitation energy levels and depicts the behavior of the collective effects in nuclei. Similarly, Figure 2.3 corresponds to neutron number N=184, highlighting the thorium isotope ^{274}Th. This figure presents the collective enhancement factor as a function of excitation energy for ^{274}Th, allowing for a detailed examination of the collective effects near neutron number N=184. These graphical representations serve as valuable visual tools for understanding the interplay between collective enhancement factors and excitation energies in thorium nuclei. The plotted data contributes to a comprehensive exploration of the nuclear structure in these regions, shedding light on to the influence of collective effects on the behavior of thorium nuclei around these neutron magic numbers.

The observed lower values of the collective enhancement factor for ^{216}Th and ^{274}Th in comparison to their neighboring isotopes suggest the need of an explanation linked to the shell closure around neutron numbers N=126 and 184. Shell closures often lead to enhanced nuclear stability, resulting in a diminished impact of collective effects such as rotational and vibrational modes. On examining Figure 2.2, it also becomes apparent that the collective enhancement effect is more pronounced at lower excitation energies and diminishes at higher excitation energies. This trend suggests that the rotational and vibrational effects play a significant role in the lower excitation energy range (0-50 MeV). However, beyond 50 MeV, the collective enhancement effect becomes less prominent or even non-observable. The observed behavior aligns with the expectations in nuclear structure physics, where the collective enhancement effect is particularly relevant at lower excitation energies associated with low-lying states. As excitation energy increases, other nuclear reactions and decay channels may become open, diminishing the effects of collective enhancements.

In summary, the low collective enhancement factors for ^{216}Th and ^{274}Th may indeed be linked to shell closures around neutron numbers N=126 and N=184. The distinct behavior observed in Figure 2.2 and 2.3, with a higher collective enhancement effect at lower excitation energies reflects the significance of rotational and vibrational effects in this energy range. Beyond 50 MeV, the diminishing collective enhancement effect points to a transition to a regime where other nuclear phenomena play more dominant roles.

2.3.2 Variation of the collective level density parameter around N=184 in even-even actinides

The results obtained from the variation of level density parameter with neutron number of thorium isotopes prompted us to carry out this study. Here, we have estimated the nuclear level density parameters of few selected even-even actinides by following the Gilbert Cameron Model and the Back-shifted Fermi Gas Model. Isotopes of U, Pu, Cm, Cf, Fm and No around neutron magic number N=184 were selected selected for the study. In the chart of nuclei they lie nearby to thorium nuclei. Together with this we have considered the results already obtained for thorium isotopes around N=184 (a portion of Figure 2.1).

The level density parameter of $^{268-278}Th$ isotopes, already estimated is re-plotted against neutron number and is given in Fig 2.5. Both GCM and BFGM are showing the same behavior and the level density parameter decreases towards N=184, as already seen in Figure 2.1. The level density parameter for ^{274}Th is found to be the lowest when compared to that of the other even-even isotopes. So, ^{274}Th may be a closed shell nucleus and is more stable than other isotopes. The level density parameter is dependent on the shell correction energy. The variation of shell correction energy of $^{268-278}Th$ with neutron number is plotted in Figure **??**. The shell correction energy of ^{274}Th corresponding to N=184 is

also low as compared to that for other nearby isotopes. As mentioned above we

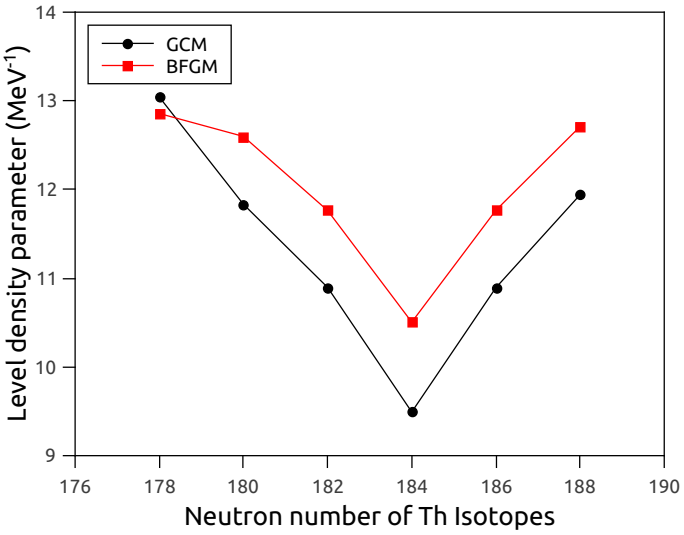

Figure 2.4: Variation of level density parameter of $^{268-278}Th$ with neutron number, by using Gilbert Cameron Model (black) and Back-Shifted Fermi Gas Model (red)

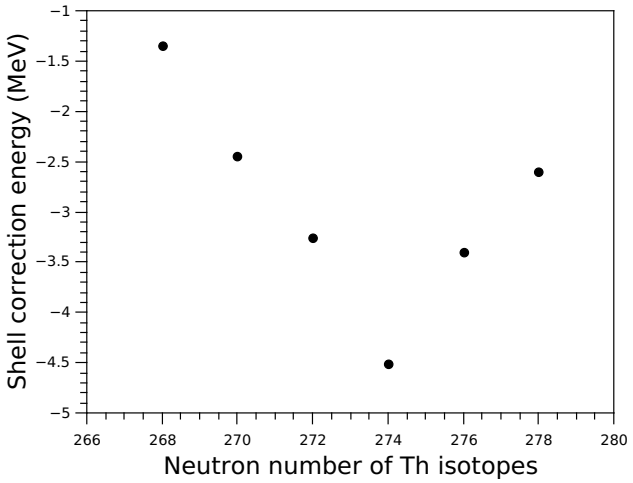

Figure 2.5: Variation of shell correction energy of $^{268-278}Th$ with neutron number

extended these studies to the isotopes of few other even-even actinides around the region of neutron number N=184. $^{270-280}U$, $^{272-282}Pu$, $^{274-284}Cm$, $^{278-288}Cf$, $^{278-288}Fm$ and $^{280-290}No$ were the selected isotopes. The level density parameter of these isotopes were calculated and are plotted in Figure 2.6(a-f).

The level density parameter 2.9 is an important term to find the nuclear

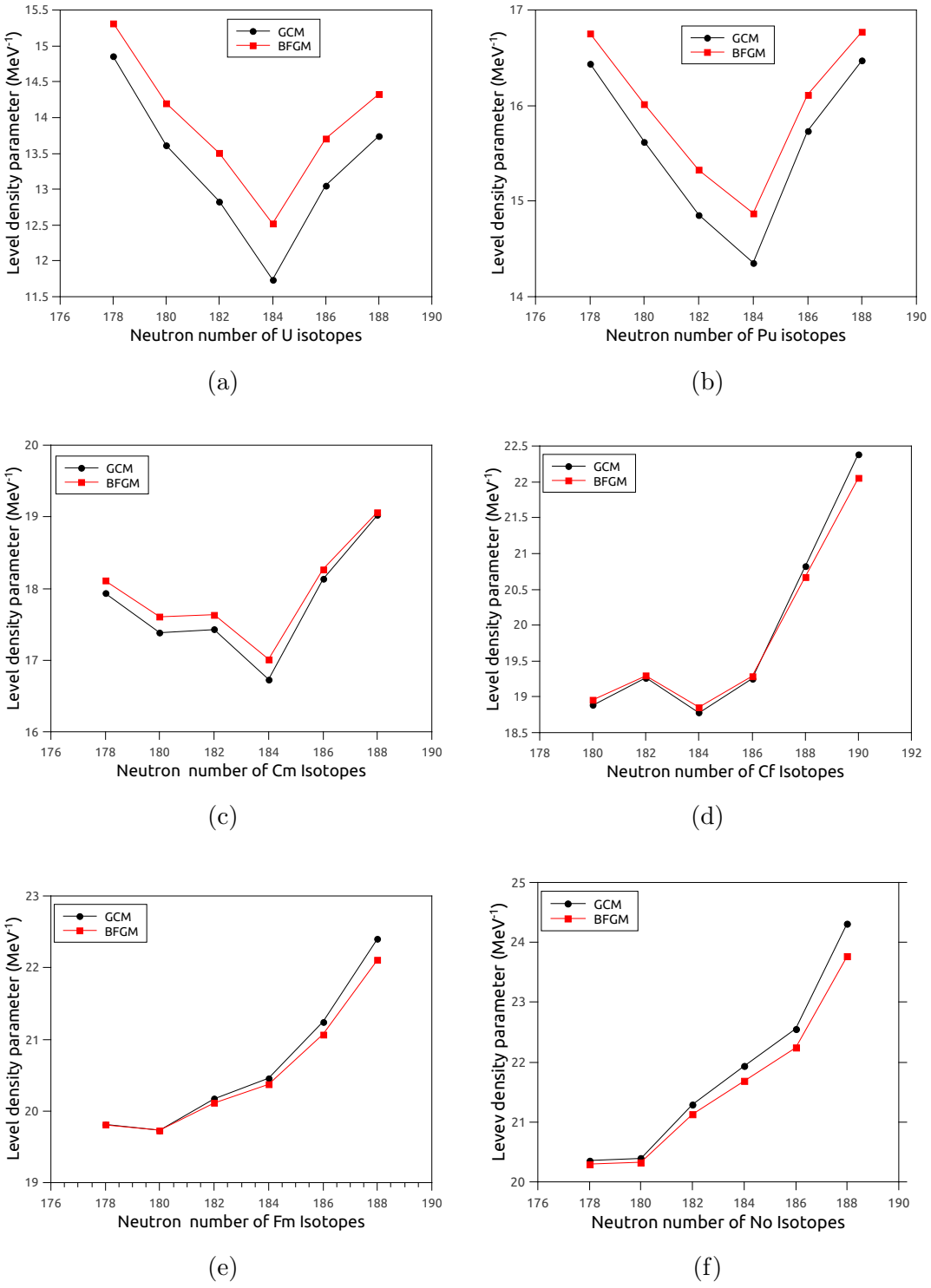

Figure 2.6: Variation of the level density parameters of $^{270-280}U$ (a), $^{272-282}Pu$ (b), $^{274-284}Cm$ (c), $^{278-188}Cf$ (d), $^{278-288}Fm$ (e) and $^{280-290}No$ (f) with neutron number by using the Gilbert Cameron Model (black) and the Back-Shifted Fermi Gas Model (red).

level density 2.6. The nuclear level density is directly proportional to the level density parameter. In the case of U, Pu, Cm and Cf isotopes, the level density parameters are low at N=184 and as a result their nuclear level density will also be low. Hence, these nuclei may be having closed shell and are more stable when compared to other nearby even-even isotopes. All these observations clearly indicate that the level density parameter decreases towards the neutron number N=184 and shows an increase beyond N=184. These observations complement and strongly reconfirm the possibility of having shell closure at N=184. Neutron and proton shell closure in the superheavy region via cluster radioactivity in $^{280-314}116$ isotopes were studied by Biju et al. [28] in 2013. They observed the possibility of shell closure at N=184. However, some variations are observed in the case of Fm and No. For them, there is no sharp dip at N=184, instead, they show a minimum at N=180. We see that ^{280}Fm and ^{282}No are stable with shell closure at N=180. In another study conducted in 2022 Prathapan et al. [29] pointed out the possibility of having a shell closure around N=180 in superheavy nuclei.

2.4 Conclusion

The collective nuclear level density give information on the structure of nuclei. We have calculated the effective and collective level density parameters of even-even thorium nuclei in the mass range 204-280, lying on and off the β-stability line. The level density parameter was found to decrease towards neutron numbers N=126 and 184. The variation of both the effective and collective level density parameters of thorium nuclei shows similar behaviour. The collective level density parameter is lower in value than the effective level density parameter at a specific neutron number. The collective enhancement factor of thorium isotopes around N=126 (^{216}Th) and 184 (^{274}Th) were also evaluated. The collective en-

hancement factor for ^{216}Th and ^{274}Th are low when compared to those for the nearby isotopes. This may be due to the shell closure around neutron number N=126 and 184. The collective enhancement effect is high at lower excitation energies and low at higher excitation energies. The rotational and vibrational effects are shown by nuclei at the excitation energies between 0 and 50 MeV.

As an extension of this study, we have estimated the collective level density parameter for few selected even-even actinides, having neutron number N lying around 184. Accordingly, the level density parameters have been systematically estimated for the isotopes of U, Pu, Cm, Cf, Fm and No. The calculations were performed on the basis of the phenomenological models - the Gilbert Cameron Model (GCM) and the Back-Shifted Fermi Gas Model (BFGM). In the case of U, Pu, Cm and Cf isotopes, the level density parameters are low at N=184 and as a result their nuclear level density are also low. Hence, these nuclei may be having closed shell and are more stable when compared to other nearby even-even isotopes. The shell correction energy of these nuclei are low as compared to the nearby nuclei and the collective effect becomes lowered at magic configurations, which leads to a reduction in the level density.

Bibliography

[1] Otto Haxel, J Hans D Jensen, and Hans E Suess. On the" magic numbers" in nuclear structure. *Physical Review*, 75(11):1766, 1949.

[2] N Quang Hung, N Dinh Dang, and LT Quynh Huong. Simultaneous microscopic description of nuclear level density and radiative strength function. *Physical Review Letters*, 118(2):022502, 2017.

[3] AV Ignatyuk, KK Istekov, and GN Smirenkin. Role of collective effects

in the systematics of nuclear level densities. *Sov. J. Nucl. Phys.(Engl. Transl.);(United States)*, 29(4), 1979.

[4] JR Huizenga and LG Moretto. Nuclear level densities. *Annual Review of Nuclear Science*, 22(1):427–464, 1972.

[5] Hans A Bethe. An attempt to calculate the number of energy levels of a heavy nucleus. *Physical Review*, 50(4):332, 1936.

[6] Hamid Reza Mirzaei, Amirhossein Sahebkar, Rasoul Salehi, Javid Sadri Nahand, Ehsan Karimi, Mahmoud Reza Jaafari, and Hamed Mirzaei. Boron neutron capture therapy: Moving toward targeted cancer therapy. *Journal of cancer research and therapeutics*, 12(2):520–525, 2016.

[7] F-K Thielemann, A Arcones, R Käppeli, M Liebendörfer, T Rauscher, C Winteler, C Fröhlich, I Dillmann, T Fischer, G Martinez-Pinedo, et al. What are the astrophysical sites for the r-process and the production of heavy elements? *Progress in Particle and Nuclear Physics*, 66(2):346–353, 2011.

[8] E Melby, L Bergholt, M Guttormsen, M Hjorth-Jensen, F Ingebretsen, S Messelt, J Rekstad, A Schiller, S Siem, and SW Ødegård. Observation of thermodynamical properties in the ^{162}Dy, ^{166}Er, and ^{172}Yb nuclei. *Physical review letters*, 83(16):3150, 1999.

[9] Hans Albrecht Bethe. Nuclear Physics B. Nuclear Dynamics, Theoretical. *Reviews of Modern Physics*, 9(2):69, 1937.

[10] Roberto Capote, Michel Herman, P Obložinskỳ, PG Young, Stéphane Goriely, T Belgya, AV Ignatyuk, Arjan J Koning, Stéphane Hilaire, Vladimir A Plujko, et al. Ripl–reference input parameter library for cal-

culation of nuclear reactions and nuclear data evaluations. *Nuclear Data Sheets*, 110(12):3107–3214, 2009.

[11] A Gilbert and AGW Cameron. A composite nuclear-level density formula with shell corrections. *Canadian Journal of Physics*, 43(8):1446–1496, 1965.

[12] Arjan J Koning, Stéphane Hilaire, and Stéphane Goriely. Global and local level density models. *Nuclear Physics A*, 810(1-4):13–76, 2008.

[13] Alberto Mengoni and Yutaka Nakajima. Fermi-gas model parametrization of nuclear level density. *Journal of Nuclear Science and Technology*, 31(2):151–162, 1994.

[14] Stéphane Hilaire and Stéphane Goriely. Global microscopic nuclear level densities within the HFB plus combinatorial method for practical applications. *Nuclear Physics A*, 779:63–81, 2006.

[15] S Hilaire, JP Delaroche, and M Girod. Combinatorial nuclear level densities based on the gogny nucleon-nucleon effective interaction. *The European Physical Journal A-Hadrons and Nuclei*, 12(2):169–184, 2001.

[16] Futoshi Minato. Nuclear level densities with microscopic statistical method using a consistent residual interaction. *Journal of nuclear science and technology*, 48(7):984–992, 2011.

[17] Paraskevi Demetriou and Stéphane Goriely. Microscopic nuclear level densities for practical applications. *Nuclear Physics A*, 695(1-4):95–108, 2001.

[18] Stephane Goriely. A new nuclear level density formula including shell and pairing correction in the light of a microscopic model calculation. *Nuclear Physics A*, 605(1):28–60, 1996.

[19] Arnold Gilbert, FS Chen, and Alastair Graham Walter Cameron. Level densities in lighter nuclei. *Canadian Journal of Physics*, 43(7):1248–1258, 1965.

[20] AV Voinov, BM Oginni, SM Grimes, CR Brune, M Guttormsen, AC Larsen, TN Massey, A Schiller, and S Siem. Nuclear excitations at constant temperature. *Physical Review C*, 79(3):031301, 2009.

[21] W Dilg, Wl Schantl, H Vonach, and M Uhl. Level density parameters for the back-shifted fermi gas model in the mass range $40 < a < 250$. *Nuclear Physics A*, 217(2):269–298, 1973.

[22] Dorel Bucurescu and Till von Egidy. Systematics of nuclear level density parameters. *Journal of Physics G: Nuclear and Particle Physics*, 31(10):S1675, 2005.

[23] MK Grossjean and H Feldmeier. Level density of a Fermi gas with pairing interactions. *Nuclear Physics A*, 444(1):113–132, 1985.

[24] AS Iljinov, MV Mebel, N Bianchi, E De Sanctis, C Guaraldo, V Lucherini, V Muccifora, E Polli, AR Reolon, and P Rossi. Phenomenological statistical analysis of level densities, decay widths and lifetimes of excited nuclei. *Nuclear Physics A*, 543(3):517–557, 1992.

[25] AR Junghans, M De Jong, H-G Clerc, AV Ignatyuk, GA Kudyaev, and K-H Schmidt. Projectile-fragment yields as a probe for the collective enhancement in the nuclear level density. *Nuclear Physics A*, 629(3-4):635–655, 1998.

[26] E Gadioli, I Iori, K Molho, and L Zetta. Shell effects on level density in near doubly magic nuclei. *Nuclear Physics A*, 138(2):321–336, 1969.

[27] AN Behkami and M Soltani. Spin cut-off parameter of nuclear level density and effective moment of inertia. *Communications in Theoretical Physics*, 43(4):709, 2005.

[28] RK Biju, MK Preethi Rajan, and KP Santhosh. The predicted doubly magic nuclei in the she. In *Proceedings of the DAE Symp. on Nucl. Phys*, volume 58, page 126, 2013.

[29] K Prathapan, KP Anjali, and RK Biju. Studies on alpha, cluster and halo emissions from $z = 128 - 132$ superheavy nuclei leading to doubly magic $^{310}126$ daughter nuclei. *Indian Journal of Physics*, 96:2949–2961, 2022.

Chapter 3

Structure Properties of Thorium Isotopes

3.1 Introduction

The atomic nucleus is a quantum system, capable of existing in various quantum states, distinguished by attributes such as energies and angular momenta. The state with the lowest energy is termed the ground state, and nuclei typically occupy this state. The characteristics of nuclei, discussed in terms of their ground states, are often referred to as static properties. This stands in contrast to the dynamic aspects of nuclei, which manifest in processes such as nuclear reactions, nuclear excitations, and nuclear decay.

The ground state properties of nuclei can be predicted from several approaches including macroscopic models such as the Bethe-Weizsacker mass formula [1], Finite Range Droplet Model (FRDM) [2] and microscopic models such as the Hartree-Fock (HF) method [3–7], relativistic mean-field theory (RMF)[8, 9] etc. The relativistic mean-field theory provides an accurate description of the ground state and collective excitations of nuclei [10–15].

In the last few years, substantial progress in the experimental research had

yielded valuable information on the structure of nuclei situated far away from the β-stability line. The boundaries of nuclear landscape is mainly governed by the binding energies of nuclei [16, 17]. Numerous questions and phenomena emerge as we extend our explanation for nuclei lying beyond the stability valley towards the neutron and proton drip-lines. To understand the nuclear characteristics, it is essential to employ suitable theoretical frameworks that can offer comprehensive description of the properties exhibited by nuclei. Density Functional Theory (DFT), commonly known as the "self-consistent mean-field method" (SCMF) [18], stands as the sole microscopic approach, currently applicable across the entire nuclear landscape.

The structure properties of nuclei lying far away from the line of β-stability are important in theoretical as well as in experimental studies [19–22]. Different nuclear structure informations like shape staggering [23], shape coexistence [24], neutron skin [25], neutron halo [26] and the existence of neutron magic numbers could be predicted from the ground state properties. Neutron number N=28, 50, 82 and 126 are the well-known magic numbers [27–29]. Several theoretical models are available for studying the nuclear structure properties. Different theoretical approaches such as the Hartree-Fock (HF) [18], Hartree-Fock-Bogoliubov (HFB) [30], relativistic mean-field [31–33], shell model, shell correction approach, α-cluster model etc. are in practice. Each of these gives results that more or less match with the experimental data. The mean-field theory gives the best theoretical results for nuclei distributed far from the line of β-stability, which are deformed and spherical, as well as for neutron deficient and neutron rich nuclei [34]. In recent years, several experimental studies for the determination of nuclear properties were carried out, by using the radioactive ion beams [35] and high sensitive laser spectroscopy [36, 37].

In the present study, we have investigated the nuclear structure properties

like binding energy, charge radii, rms radii and its isotopic shift, two-neutron separation energy and shell gap, chemical potential, quadrupole deformation, density distribution and single-particle energy of thorium (Z=90) nuclei, lying on and off the line of β-stability. This study will help us understand the variation of nuclear properties with neutron number (towards drip-lines) and to predict the shell closure and nuclear stability. Data related to the structure properties are useful for experiments in future and will be helpful in understanding the behaviour of complex nuclei. Thorium is abundant in metal-poor stars and are synthesized through the r-process [38]. In the case of asymptotic giant-branch stars, thorium is synthesized through the i-process nucleosynthesis [39]. The present study is expected to provide us with the information necessary to identify the trends in the physical properties of thorium nuclei lying from proton drip-line to neutron drip-line and also to check for the appearance of new magic numbers, if any. It provides new theoretical data for testing nuclear models in the context of nuclear astrophysics.

3.2 Theoretical Formalism

3.2.1 Mean-field Theory

The nuclear structure studies carried out in the present work is based on the self-consistent relativistic mean-field theory. Nuclear density functional theory, based on the relativistic mean-field approach is used here. Most of the mean-field calculations use phenomenological two-body interactions. In the relativistic mean-field theory, a nucleus is depicted as a configuration of Dirac nucleons that interact with each other by exchanging mesons, all described by an effective Lagrangian. The minimal set of meson fields required for describing both the overall properties and individual single-particle characteristics of a nucleus includes the

isoscalar-scalar σ meson, the isoscalar-vector ω meson, and the isovector-vector ρ meson. In the current relativistic mean-field (Hartree) approximation, the π meson doesn't play a role due to its pseudo-scalar characteristic. The pions do not significantly affect the average behavior of nucleons within a nucleus. However, they become relevant in scenarios involving dynamic processes and in the study of specific nuclear properties like pairing interactions. The Hamiltonian of the Hartree-Fock equation describes nuclear properties. The diagonalization of it gives the required energies.

In relativistic approach, the self-consistent mean-field theory is based on the energy density functional, which gives the information on the nuclear structure. The energy density functional is a functional of the nucleon density matrices, corresponding to the single-particle states. The Meson Exchange (ME) and the Point Coupling (PC) density functionals are used in these calculations.

3.2.2 Meson Exchange Model

In the meson exchange model, the exchange of mesons leads to the finite range interaction with nucleons. Here, the Lagrangian is defined in terms of the Lagrangian density,

$$\mathcal{L} = \mathcal{L}_N + \mathcal{L}_m + \mathcal{L}_{int} \tag{3.1}$$

where $\mathcal{L}_N$ are the Lagrangian of free nucleons and it is taken as,

$$\mathcal{L}_N = \bar{\psi}(i\gamma_\mu \partial^\mu - m)\psi \tag{3.2}$$

with m being the bare mass of a nucleon. $\mathcal{L}_m$ is the Lagrangian of the free meson field and the electromagnetic field.

$$\mathcal{L}_m = \frac{1}{2}\partial_\mu\sigma\partial^\mu\sigma - \frac{1}{2}m_\sigma^2\sigma^2 - \frac{1}{2}\Omega_{\mu\nu}\Omega^{\mu\nu} + \frac{1}{2}m_\omega^2\omega_\mu\omega^\mu - \frac{1}{4}\overrightarrow{R}_{\mu\nu}.\overrightarrow{R}^{\mu\nu} + \frac{1}{2}m_\rho^2\overrightarrow{\rho_\mu}\overrightarrow{\rho}^\mu - \frac{1}{4}F_{\mu\nu}F^{\mu\nu} \quad (3.3)$$

In equations 3.2, ψ represents the Dirac-spinors and in equation 3.3, σ, ω and ρ represent the isoscalar-scalar meson, the isoscalar-vector meson and the isovector-vector meson, respectively. The corresponding masses of these mesons are m_σ, m_ω, and m_ρ and $\Omega_{\mu\nu}$, $\overrightarrow{R}_{\mu\nu}, F^{\mu\nu}$ are the field tensors with,

$$\Omega_{\mu\nu} = \partial_\mu\omega_\nu - \partial_\nu\omega_\mu \quad (3.4)$$

$$\overrightarrow{R}_{\mu\nu} = \partial_\mu\overrightarrow{\rho}_\nu - \partial_\nu\overrightarrow{\rho}_\mu \quad (3.5)$$

and

$$F^{\mu\nu} = \partial_\mu A_\nu - \partial_\nu A_\mu \quad (3.6)$$

The interaction term L_{int} is,

$$L_{int} = -g_\sigma\bar{\psi}\psi\sigma - g_\omega\bar{\psi}\gamma^\mu\psi\omega_\mu - g_\rho\bar{\psi}\overrightarrow{\tau}\gamma^\mu\psi\cdot\overrightarrow{\rho_\mu} - e\bar{\psi}\gamma^\mu\psi A_\mu \quad (3.7)$$

with $g_\sigma, g_\omega, g_\rho$ and e being the coupling constants [40]. From this Lagrangian density, the Hamiltonian density was obtained by the Legendre transformation.

$$\mathcal{H}(\mathbf{r}) = \sum_{i}^{A} \psi_i^+(\boldsymbol{\alpha}\mathbf{p} + \beta m)\psi_i + \frac{1}{2}[(\bigtriangledown\sigma)^2 + m_\sigma^2\sigma^2] - \frac{1}{2}[(\bigtriangledown\omega)^2 + m_\omega^2\omega^2]$$
$$- \frac{1}{2}[(\bigtriangledown\rho)^2 + m_\rho^2\rho^2] - \frac{1}{2}(\bigtriangledown A)^2 + [g_\sigma\rho_s\sigma + g_\omega j_\mu\omega^\mu + g_\rho\overrightarrow{j_\mu}.\overrightarrow{\rho}^\mu + ej_{p\mu}A^\mu] \tag{3.8}$$

Also,

$$\rho_s(\mathbf{r}) = \sum_{i=1}^{A} \bar{\psi}_i(\mathbf{r})\psi_i(\mathbf{r}), \tag{3.9}$$

$$j_\mu(\mathbf{r}) = \sum_{i=1}^{A} \bar{\psi}_i(\mathbf{r})\gamma_\mu\psi_i(\mathbf{r}), \tag{3.10}$$

$$\overrightarrow{j}_\mu(\mathbf{r}) = \sum_{i=1}^{A} \bar{\psi}_i(\mathbf{r})\overrightarrow{\tau}\gamma_\mu\psi_i(\mathbf{r}), \tag{3.11}$$

$$j_{p\mu}(\mathbf{r}) = \sum_{i=1}^{Z} \psi_i^+(\mathbf{r})\gamma_\mu\psi_i(\mathbf{r}) \tag{3.12}$$

Equations 3.9, 3.10, 3.11 and 3.12 represent entities called the isoscalar-scalar density, isoscalar-vector current, isovector-vector current and electromagnetic current, respectively. Here, the summation index runs over the occupied states in the Fermi sea of positive energy. We adjust the model parameters so as to reproduce the experimental data. Thus we take into consideration the contribution from the Dirac sea. By integrating equation (3.8) over the r-space, we

obtain the total energy [40] as a function of the meson fields and Dirac spinors. The total energy is,

$$E_{RMF}[\psi, \bar{\psi}, \sigma, \omega^{\mu}, \rho^{\mu}, A^{\mu}] = \int d^3r \mathcal{H}(\mathbf{r}) \tag{3.13}$$

This basic model, which includes the interaction terms that are only linear in the meson fields, does not offer a precise or quantitative description of complex nuclear systems [41, 42]. Hence, it appears more appropriate to adopt the approach proposed by Brockmann and Toki [43], which involves using density-dependent couplings. In this framework, the coupling constants g_{σ}, g_{ω}, and g_{ρ} are considered to be vertex functions associated with Lorentz-scalar bilinear expressions of nucleon operators [40]. In many applications, the coupling between mesons and nucleons depend on the vector density, which can be expressed as $\rho_v = \sqrt{j_{\mu} j^{\mu}}$ with the nucleon four-current $j^{\mu} = \bar{\psi}\gamma^{\mu}\psi$.

The folllowing single-nucleon Dirac equation 3.14 is obtained by performing a variation of the energy density functional 3.13 with respect to the complex conjugate of the nucleon wave function, denoted as $\bar{\psi}$.

$$\hat{h_D}\psi_i = \varepsilon_i \psi_i \tag{3.14}$$

with the Dirac Hamiltonian

$$\hat{h_D} = \boldsymbol{\alpha} \cdot (\mathbf{p} - \boldsymbol{\Sigma}) + \Sigma_0 + \beta(m + \Sigma_s) \tag{3.15}$$

The nucleon self-energies [44] Σ are defined as,

$$\Sigma_s(\mathbf{r}) = g_{\sigma}\sigma(\mathbf{r}) \tag{3.16}$$

$$\Sigma_\mu(\mathbf{r}) = g_\omega \omega_\mu(\mathbf{r}) + g_\rho \overrightarrow{\tau} \cdot \overrightarrow{\rho}_\mu(\mathbf{r}) + eA_\mu(\mathbf{r}) + \Sigma_\mu^R(\mathbf{r}) \tag{3.17}$$

The vector self-energy incorporates a rearrangement contribution due to the density-dependent nature of the vertex functions g_σ, g_ω, and g_ρ (the dependence of g_σ, g_ω, and g_ρ on the corresponding density gives the rearrangement contribution to the self energy).

$$\Sigma_\mu^R(\mathbf{r}) = \frac{j_\mu}{\rho_\nu}\left(\frac{\partial g_\sigma}{\partial \rho_\nu}\rho_s\sigma + \frac{\partial g_\omega}{\partial \rho_\nu} j_\nu \omega^\nu + \frac{\partial g_\rho}{\partial \rho_\nu}\overrightarrow{j_\nu} \cdot \overrightarrow{\rho}^\nu\right) \tag{3.18}$$

The self energy describes the correction to the mass and energy of a nucleon due to its interactions with mesons within the relativistic framework. The inclusion of the rearrangement self-energy is essential for energy-momentum conservation.

The Helmholtz equations for the meson field 3.19,3.20,3.21, 3.22 were obtained by the variation of the energy density functional with respect to the corresponding meson field,

$$[-\Delta + m_\sigma^2]\sigma = -g_\sigma \rho_s, \tag{3.19}$$

$$[-\Delta + m_\omega^2]\omega^\mu = g_\omega j^\mu, \tag{3.20}$$

$$[-\Delta + m_\rho^2]\rho^\mu = g_\rho \overrightarrow{j}^\mu \tag{3.21}$$

For electromagnetic field, the Poisson equation is

$$-\Delta A^{\mu} = e j_p^{\mu} \tag{3.22}$$

In the ground state solution of an even-even nucleus, the current term and the corresponding spatial components of the meson field vanishes due to the time-reversal invariance. Then, the Dirac equation in the simple form is,

$$\{-i\boldsymbol{\alpha} \bigtriangledown + \beta M^*(\mathbf{r}) + V(\mathbf{r})\}\psi_i(\mathbf{r}) = \varepsilon_i \psi_i(\mathbf{r}). \tag{3.23}$$

Here, the vector potential is $V(\mathbf{r})$ and the effective mass $M^*(\mathbf{r}) = m + g_\sigma \sigma$. The vector potential $V(\mathbf{r})$ is,

$$V(\mathbf{r}) = g_\omega \omega_0 + g_\rho \tau_3 \rho_0 + eA_0 + \Sigma_0^R \tag{3.24}$$

where the rearrangement contribution 3.18 takes the form,

$$\Sigma_0^R = \frac{\partial g_\sigma}{\partial \rho_\nu}\rho_s \sigma + \frac{\partial g_\omega}{\partial \rho_\nu}\rho_\nu \omega_0 + \frac{\partial g_\omega}{\partial \rho_\nu}\rho_{t\nu}\rho_0 \tag{3.25}$$

Here, $\rho_{t\nu}$ is the difference between the proton and the neutron vector densities and it is called the isovector density.

The coupling parameters were obtained in a phenomenological way [44–46]. For σ and ω mesons, the coupling to the nucleon field is parameterized as,

$$g_i(\rho) = g_i(\rho_{sat}) f_i(x) \quad for \quad i = \sigma, \omega \tag{3.26}$$

where

$$f_i(x) = a_i \frac{1 + b_i(x + d_i)^2}{1 + c_i(x + d_i)^2} \tag{3.27}$$

with $x = \frac{\rho}{\rho_{sat}}$, which is the ratio of the baryonic density at a specific position to the saturation density in symmetric case. There are eight parameters present in the equation 3.27, which are not independent. By applying the five constraints $f_i(1) = 1$, $f''_\sigma(1) = f''_\omega(1)$, $f''_i(0) = 0$ Also there are three more additional parameters in the ioscalar channel $g_\sigma(\rho_{sat})$, $g_\omega(\rho_{sat})$ and mass of the σ-meson m_σ. On performing the Dirac-Bruckner [47] calculations on asymmetric nuclear matter, one can suggest that functional form of the density dependence of ρ meson coupling as,

$$g_\rho(\rho) = g_\rho(\rho_{sat})e^{a_\rho(x-1)} \tag{3.28}$$

Here $g_\rho(\rho_{sat})$ and a_ρ are used to parameterize the isovector channel.

3.2.3 Point-coupling Model

The point-coupling model is analogous to the meson-exchange phenomenological model [48–51]. Like the finite-range relativistic density functional approach, the density-dependent point-coupling (DD-PC) functionals involve the use of an effective Lagrangian when performing calculations for the nuclear mean-field. The isoscalar-scalar, isoscalar-vector and isovector-vector four-fermion interactions are included in the effective Lagrangian as,

$$\begin{aligned}\mathcal{L} = {} & \bar{\psi}(i\gamma\cdot\partial - m)\psi - \frac{1}{2}\alpha_S(\rho)(\bar{\psi}\psi)(\bar{\psi}\psi) - \frac{1}{2}\alpha_V(\rho)(\bar{\psi}\gamma^\mu\psi)(\bar{\psi}\gamma_\mu\psi) \\ & - \frac{1}{2}\alpha_{TV}(\rho)(\bar{\psi}\overrightarrow{\tau}\gamma^\mu\psi)(\bar{\psi}\overrightarrow{\tau}\gamma_\mu\psi) - \frac{1}{2}\delta_S(\partial_\nu\bar{\psi}\psi)(\partial^\nu\bar{\psi}\psi) - e\bar{\psi}\gamma\cdot A\frac{1-\tau_3}{2}\psi\end{aligned} \tag{3.29}$$

where α_S, α_V and α_{TV} are the corresponding coupling constants. The free nucleon Lagrangian and the point-coupling interaction terms are also included here. In addition to this, the coupling of proton and electromagnetic fields is also in-

cluded. The derivative term in equation (3.29) arises from the finite-range interactions [32], which give information on the nuclear density distribution. Including the derivative term exclusively in the isoscalar-scalar channel is sufficient for replicating the finite-range effects of the effective interaction. Additionally, these models often treat the mass of the phenomenological σ-meson as an adjustable parameter, while the masses of the ω and ρ mesons are left unconstrained and considered as free values.

The isovector-scalar field, arising from the exchange of δ-mesons, is often omitted in nuclear force calculations because its impact on the nuclear force through one-boson exchange is generally regarded as relatively weak [52].

The corresponding total energy is [40],

$$\begin{aligned} E_{RMF}[\psi,\bar{\psi},A_\mu] &= \int d^3r\mathcal{H}(\mathbf{r}) \\ &= \sum_{i=1}^{A}\int d^3r\psi_i^+(\boldsymbol{\alpha}\cdot\mathbf{p}+\beta m)\psi_i + \frac{1}{2}e\int d^3r j_p^\mu A_\mu + \\ &\qquad \frac{1}{2}\int d^3r[\alpha_S\rho_s^2+\alpha_V j_\mu j^\mu + \alpha_{TV}\overrightarrow{j_\mu}\cdot\overrightarrow{j^\mu}+\delta_S\rho_s\Delta\rho_s] \end{aligned} \tag{3.30}$$

The Dirac equation is obtained by the variation of the energy density functional with respect to the Dirac field,

$$\{-i\boldsymbol{\alpha}\bigtriangledown+\beta M^*(\mathbf{r})+V(\mathbf{r})\}\psi_i(\mathbf{r}) = \varepsilon_i\psi_i(\mathbf{r}). \tag{3.31}$$

where the effective mass $M^* = m + \Sigma_s$ and the nucleon self-energies are,

$$\Sigma_s = \alpha_S\rho_s + \delta_S\Delta\rho_s \tag{3.32}$$

$$\Sigma_\mu = \alpha_V j_\mu + \alpha_{TV} \overrightarrow{\tau} \cdot \overrightarrow{j}_\mu + eA_\mu \tag{3.33}$$

and the corresponding vector potential is,

$$V(\mathbf{r}) = \alpha_V \rho_v + \alpha_{TV} \tau_3 \rho_{t\nu} + eA_0 + \Sigma_0^R \tag{3.34}$$

where Σ_0^R is the rearrangement contribution [40], resulting from the changes in the couplings α_S, α_V, and α_{TV} concerning variations in the nucleon fields within the density operator $\hat{\rho}$.

$$\Sigma_0^R = \frac{\partial \alpha_S}{\partial \rho_\nu}\rho_s^2 + \frac{\partial \alpha_V}{\partial \rho_\nu}\rho_\nu^2 + \frac{\partial \alpha_{TV}}{\partial \rho_\nu}\rho_{t\nu}^2 \tag{3.35}$$

The functional form of the coupling is,

$$\alpha_i(\rho) = a_i + (b_i + c_i x)e^{-d_i x} \quad for \quad i = S, V, TV \tag{3.36}$$

with $x = \frac{\rho}{\rho_{sat}}$, which is the ratio of the baryonic density at a specific position to the saturation density in symmetric matter.

The parameters of DD-ME2 [53] and DD-PC1 [54] interactions are used in the present study are tabulated in Table 3.1. The masses are given in MeV and all other parameters are dimensionless.

The effect of pairing correlation is important for open-shell nuclei and nuclei towards the drip-line. The relativistic energy density functional is dependent on the normal density $\hat{\rho}$ and the pairing density $\hat{\kappa}$ [55].

$$E_{RHB}[\hat{\rho}, \hat{\kappa}] = E_{RMF}[\hat{\rho}] + E_{pair}[\hat{\kappa}] \tag{3.37}$$

Table 3.1: The parameters used in DD-ME2 and DD-PC1 interactions. The masses are given in MeV and all other parameters are dimensionless.

Parameter	DD-ME2	Parameter	DD-PC1
m	939	m	939
m_σ	550.124	a_σ	-10.04616
m_ω	783.000	b_σ	-9.15042
m_ρ	763.00	c_σ	-6.42729
g_σ	10.5396	d_σ	1.37235
g_ω	13.0189	a_ω	5.91946
g_ρ	3.6836	b_ω	8.86370
a_σ	1.3881	b_ρ	1.83595
b_σ	1.0943	d_ρ	0.64025
c_σ	1.7057		
d_σ	0.4421		
a_ω	1.3892		
b_ω	0.9240		
c_ω	1.4620		
d_ω	0.4775		
a_ρ	0.5647		

where $E_{RMF}[\hat{\rho}]$ is the RMF-functional defined in 3.13 and 3.30. $E_{pair}[\hat{\kappa}]$ is defined as,

$$E_{pair}[\hat{\kappa}] = \frac{1}{4}\sum_{n_1 n_1'}\sum_{n_2 n_2'} \kappa *_{n_1 n_1'} <n_1 n_1'|V^{pp}|n_2 n_2'>\kappa_{n_2 n_2'}. \tag{3.38}$$

with $<n_1 n_1'|V^{pp}|n_2 n_2'>$ referring to the elements within a matrix that represent the interactions between pairs of particles due to the two-body pairing force.

3.3 Results and Discussion

The nuclear structure properties such as binding energy, charge radii, two-neutron separation energy, two-neutron shell gap, rms radii and its isotopic shift, chemical potential, the quadrupole deformation, nuclear density distributions and single-particle energy levels of thorium isotopes lying on and in between the proton and neutron drip-lines were determined by applying the mean-field theo-

ries. Even-even thorium isotopes in the mass range 204-280 were selected for this study. The nuclear structure properties were evaluated by using the relativistic density dependent meson exchange (ME) and point-coupling (PC) models, with axially symmetric quadrupole deformations. We have used DD-ME2 [53] and DD-PC1 [32] parameter sets for the entire study and compared the results with the available experimental and theoretical data. The models compute the mean-field solutions for the deformed nuclei. The wave function was expanded on the basis of the axially symmetric harmonic oscillator. In practical situations, the number of harmonic oscillator basis states is truncated to achieve the convergence of the solution. Therefore, we ignore all oscillator quantum numbers for major shells exceeding a certain value, denoted as N_{max}. This maximum value for fermions is represented as N_F, and for bosons, it is denoted as N_B. In the present study, we have considered 12 harmonic oscillator shells for fermions and 20 for bosons. The iterative diagonalization of the Hamiltonian gives the best roots. Here, we have taken into account the pairing correlation.

3.3.1 Binding energy

The binding energy is an important property of nuclei, which helps to predict the validity of nuclear models. Since binding energy is, in general, a measurable entity for stable nuclei, including those of thorium, in the present study, we have calculated the binding energy of even-even thorium nuclei, lying on and in between the drip-lines by using the the relativistic mean-field theory with DD-ME2 3.13 and DD-PC1 3.30 interactions. We have compared our results with the available experimental data [56], Finite-Range Droplet Model (FRDM) [57] values and data from the National Nuclear Data Center (NNDC) [58]. The calculated results and compared data are plotted in Figure 3.1. These calculated results are in good agreement with the available data. The variation of the

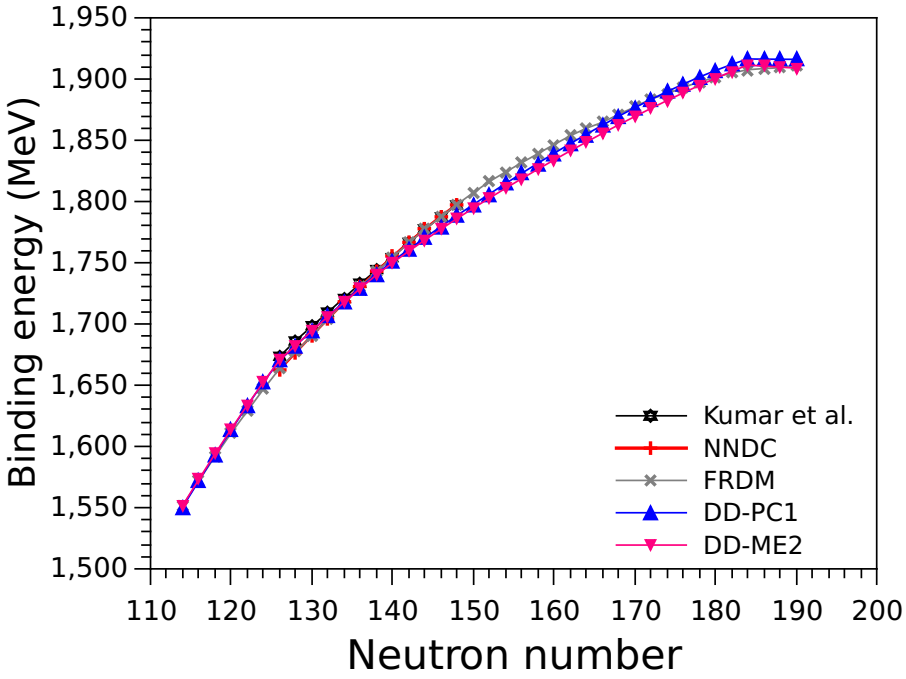

Figure 3.1: Variation of binding energy with neutron number of thorium nuclei lying on and in between the drip lines, by using the density dependent meson exchange interaction DD-ME2 and the density dependent point-coupling interaction DD-PC1.

binding energy with neutron number of thorium nuclei shows an increase from proton drip-line to neutron drip-line and also exhibits broken linearity (slope variation), one at around N=126 with the fraction of 0.4 variation in slope and the other at around N=184 with 0.25 fraction of variation in slope. This broken linearity in binding energy is due to the extra stability of nuclei at around the neutron number N=126 and 184 and they point to the possibility of having shell closure at N=126 and 184.

3.3.2 Charge radii

Nuclear charge radius is another important structure property. So we calculated the charge radii of thorium nuclei and the results were compared with the

available experimental values. The charge radius of a nucleus is,

$$r_c = \sqrt{r_p^2 + 0.64 fm^2} \tag{3.39}$$

Here, r_p is the rms radius of the proton density distribution and 0.64 fm^2 is the finite size of the proton [59]. Figure 3.2 shows the charge radii of thorium nuclei evaluated by using the meson-exchange model and the point-coupling model, under the self consistent relativistic mean-field framework. The experimental data of nuclear charge radii for thorium are available only for a few isotopes [60]. The estimated charge radii were compared with those experimental data.

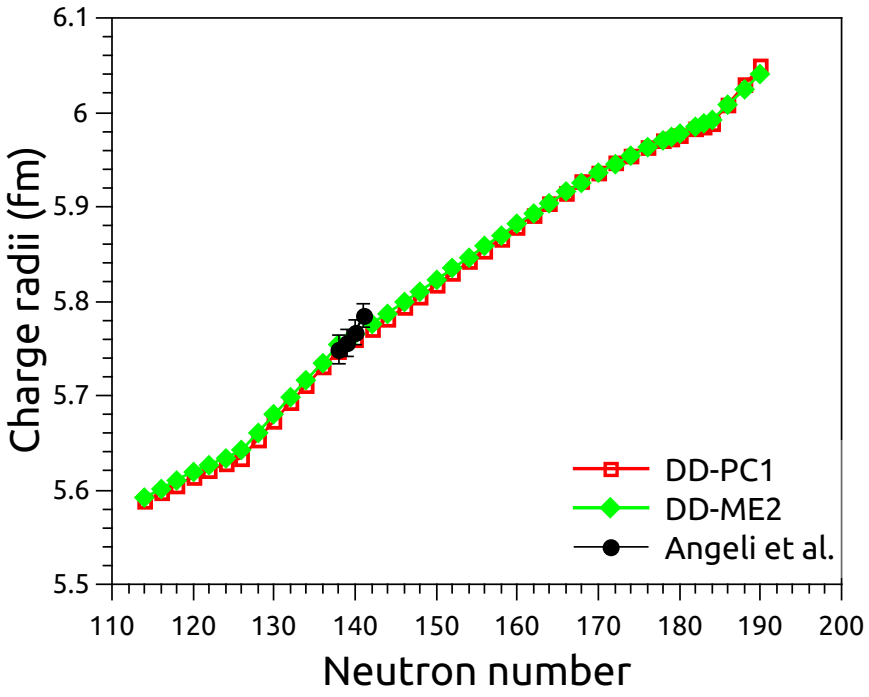

Figure 3.2: Variation of the nuclear charge radii of thorium nuclei lying on and in between the drip lines, estimated by using the density-dependent meson exchange interaction DD-ME2 and the density-dependent point-coupling interaction DD-PC1.

The charge radii increase as we move from the proton drip-line to neutron drip-line and broken linearity are observed at neutron number N=126, 138 and 184. This may be due to the shell closure or mid-shell closure at the neutron

number N=126, 138 and 184. The obtained data based on the relativistic meson-exchange and point-coupling model are in good agreement with the experimental data of Angeli et al. [60]. The deviation from the linearity is less at around N=138 when comparing the same at N=126 and 184. Hence, this nucleus with neutron number N=138 is not as stable as nuclei with neutron number N=126 and 184. So, neutron numbers N=126 and 184 are neutron magic numbers and N=138 may be a semi-magic number in the case of thorium nuclei. To confirm the stability or shell closure around these neutron numbers, we have explored other structure properties also.(see the following sections)

3.3.3 Two-neutron separation energy

The two-neutron separation energy (S_{2n}) give information on the structure of nuclei and the nature of shell closure or mid-shell closure. We had estimated the two-neutron separation energy (S_{2n}) of thorium nuclei using the relativistic mean-field theory with DD-ME2 and DD-PC1 interactions. If the binding energy (B.E) of a nucleus with neutron number N and proton number Z is B.E(N, Z), then the two-neutron separation energy (S_{2n}) is,

$$S_{2n} = B.E(N, Z) - B.E(N-2, Z) \tag{3.40}$$

The calculated results were compared with the experimental data of two-neutron separation energy [58]. Figure 3.3 shows the calculated results and compared data of two-neutron separation energy of thorium nuclei lying between the drip-lines. Two-neutron separation energy of thorium nuclei is slowly increasing from proton drip-line to neutron drip-line and sudden jumps are observed at N=126, 138 and 184. This broken linearity can be attributed to shell closure or mid-shell closure.

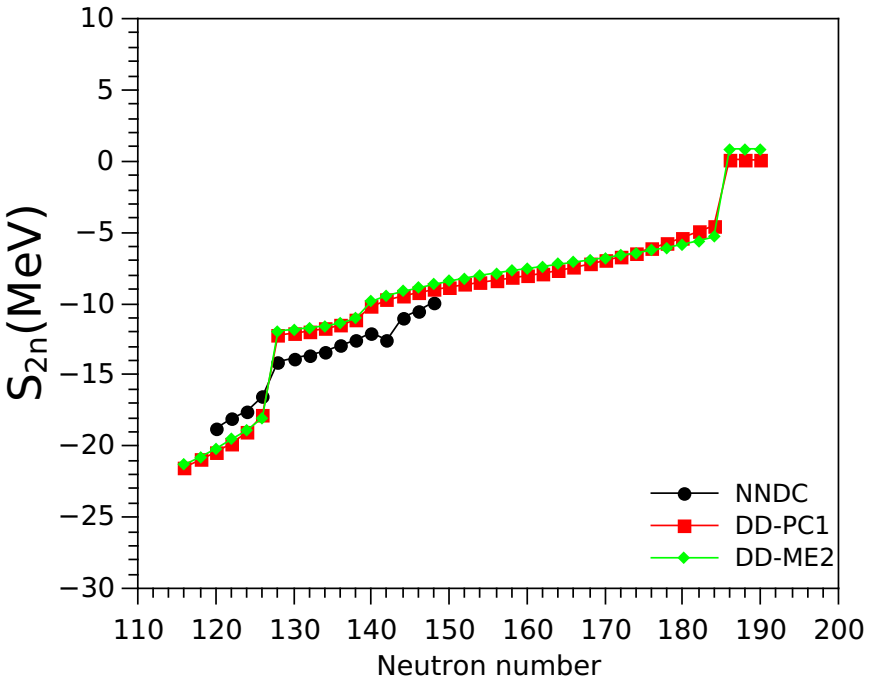

Figure 3.3: Two-neutron separation energy S_{2n} of thorium nuclei, lying on and in between the proton drip-line and neutron drip-line, estimated by using the DD-ME2 and DD-PC1 parameterizations.

3.3.4 Two-neutron shell gap

The two-neutron shell gap (δ_{2n}) also give information on the structure of nuclei and shell closure. Here, we calculated the two-neutron shell gap of thorium nuclei in between the drip-lines. The two-neutron shell gap (δ_{2n}) is,

$$\delta_{2n} = S_{2n}(N, Z) - S_{2n}(N-2, Z) \tag{3.41}$$

The two-neutron shell gap (δ_{2n}) of thorium nuclei were evaluated using the relativistic mean-field theory and the results are plotted in Figure 3.4. Large shell gaps were observed at around N=126 and 184 and a small rise at around N=138. This broken linearity confirm the shell closure or mid-shell closure at N=126, 138 and 184. The experimental data of nuclear binding energy, charge radii and neutron separation energy are available for certain isotopes of thorium. Hence,

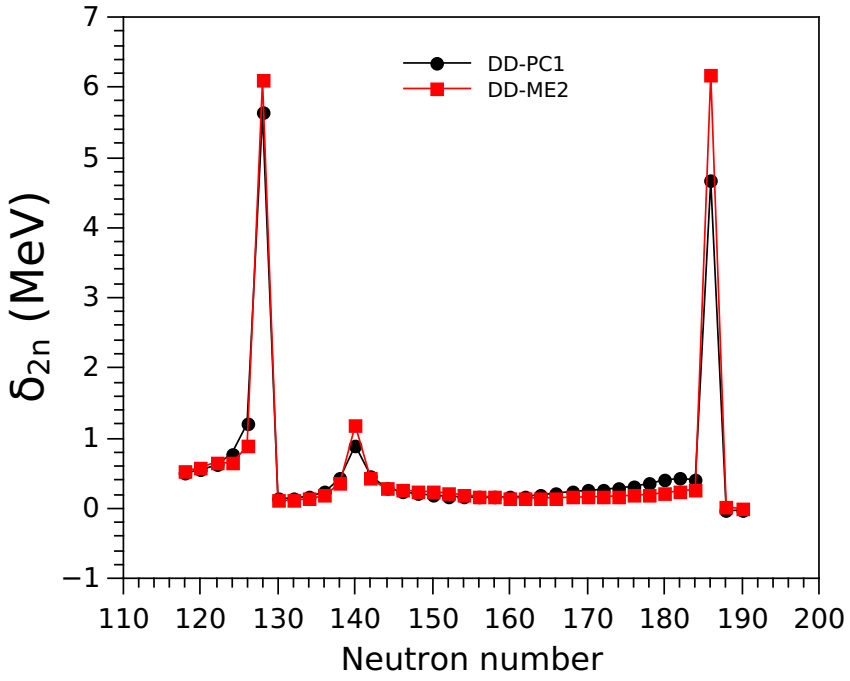

Figure 3.4: Two-neutron shell gap (δ_{2n}) of thorium nuclei, lying on and in between the proton drip-line and neutron drip-line, estimated by using the DD-ME2 and DD-PC1 parameterizations.

we compared our results with experimental data and extended the studies towards the region of drip-lines in estimating other structure properties such as the rms radii and its isotopic shift, neutron and proton chemical potential, deformation parameters, single particle energy level and charge density distribution. The evaluated data and the experimental data are in good agreement. From this study, we observed few evidences of neutron shell closure at N=126, 138 and 184 in the case of thorium nuclei.

3.3.5 Rms radii and isotopic shift

The rms radii of even-even thorium nuclei were estimated by applying the relativistic mean-field theory, with zero and finite range interactions DD-ME2 and DD-PC1. We have plotted the variation of rms radii with neutron number and is shown in Figure 3.5. The nuclear rms radii were found to be increasing

on adding neutrons (towards the neutron drip-line). On increasing the neutron number, the rms radii increases from 5.56 fm to 6.31 fm. The dependence of the rms radius on the neutron number may influence the nuclear shape. In the case of rms radii, slope variation is distinguished at N=126, 138 and 184.

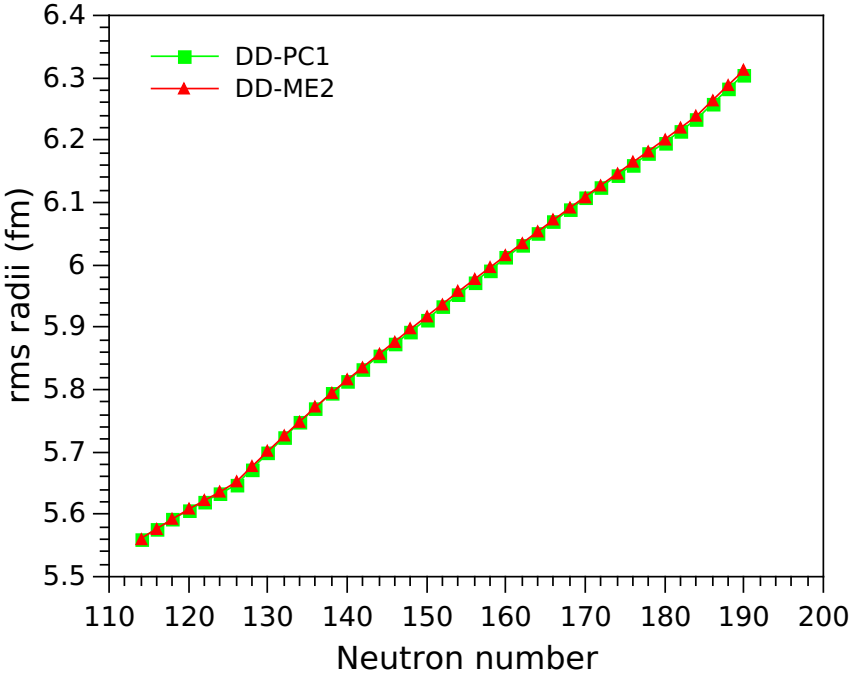

Figure 3.5: Variation of the nuclear rms radius with neutron number in thorium isotopes, estimated by using the density-dependent meson exchange interaction DD-ME2 and the density-dependent point-coupling interaction DD-PC1

To understand the behaviour of rms radii at the above mentioned magic or semi-magic neutron numbers, the isotopic shift of rms radii were evaluated using the three-point formula [27]. The three-point formula for the isotopic shift is given by,

$$\Delta R(Z,N) = \frac{1}{2}[R(Z,N+2) - 2R(Z,N) + R(Z,N-2)] \tag{3.42}$$

The variation in the isotopic shift of rms radii with neutron number, estimated by the three-point formula by using the rms radii obtained from the meson exchange interaction DD-ME2 and the point-coupling interaction DD-PC1 is

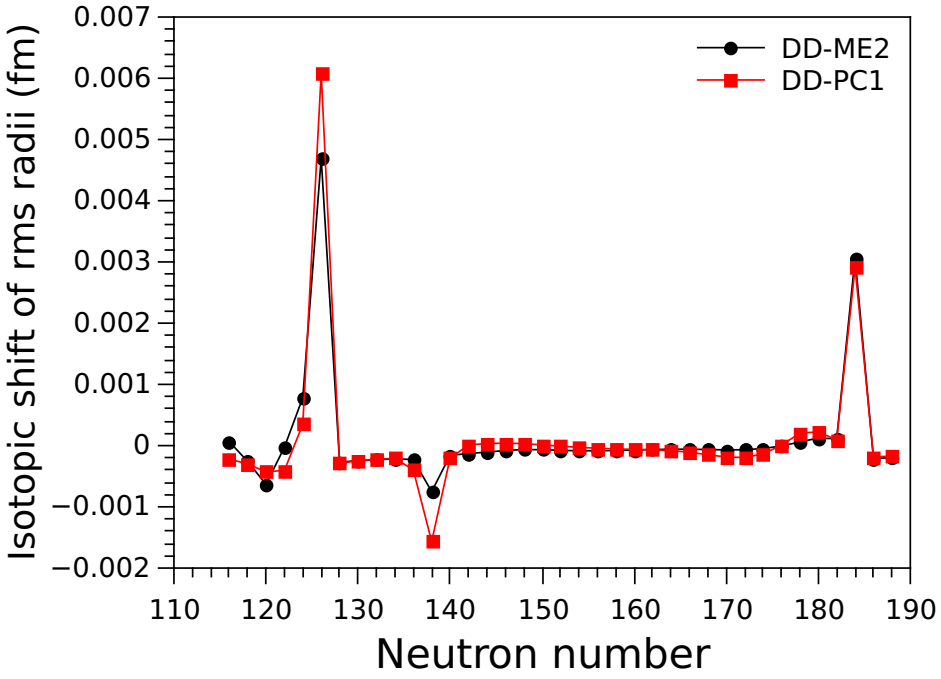

Figure 3.6: Isotopic shift in rms radii of thorium nuclei, lying on and in between the proton drip-line and neutron drip-line, estimated by using the DD-ME2 and DD-PC1 parameterizations.

shown in Figure 3.6. Three prominent peaks were identified at around N=126, 138 and 184. A positive shift is observed at around N=126 and 184 and a negative shift at N=138. So, these results also point to the possibility of having shell closure and extra stability of thorium nuclei at these neutron numbers.

3.3.6 Chemical potential

The chemical potential also plays an important role in determining the stability of a nucleus. It is the energy for adding a nucleon to the system. The possibility of shell closure can be predicted from the variation of the chemical potential. The neutron and proton chemical potential (λ_n and λ_p) of thorium nuclei were plotted by varying the neutron number and it is shown in Figure 3.7.

The proton chemical potential decreases on adding neutron to the system, whereas the neutron chemical potential increases. Broken linearity can be seen in

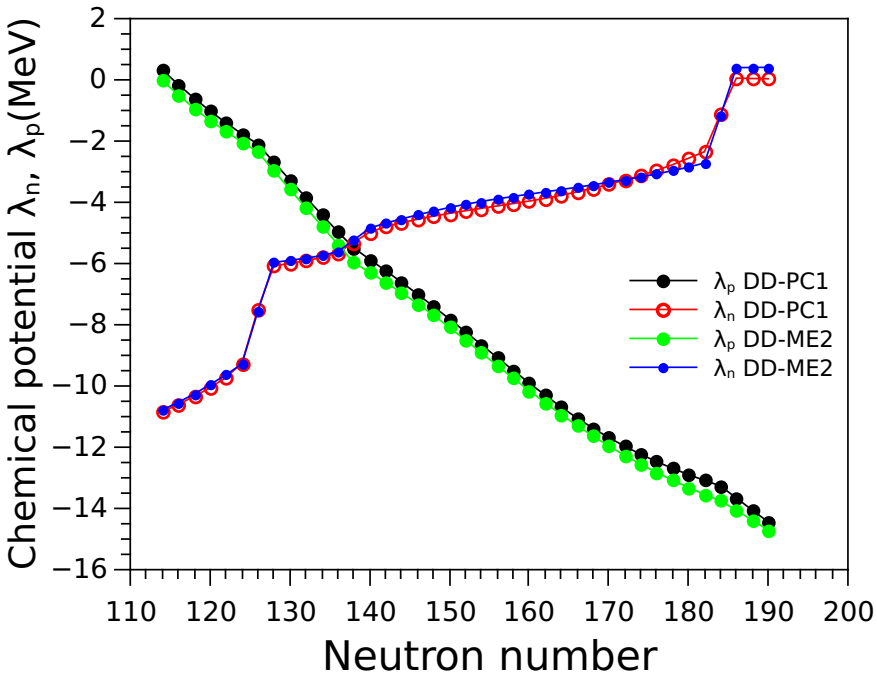

Figure 3.7: Variation of the proton and neutron chemical potential λ_n and λ_p (MeV) with neutron number of thorium nuclei, respectively for the density dependent meson exchange interaction DD-ME2 and the density-dependent point-coupling interaction DD-PC1.

the case of neutron chemical potential at N=126, 138 and 184. A sharp increase of neutron chemical potential is observed at N=126 and 184 and slow change at around N=138. The neutron chemical potential λ_n is zero for nuclei near the neutron drip-lines (^{204}Th) and proton chemical potential λ_p is zero for nuclei near the proton drip-line (^{280}Th). For $N \leq 140$, the system is proton bound and for $N \geq 140$ it is neutron bound, for thorium nuclei.

3.3.7 Quadrupole deformation

The nuclear quadrupole deformation parameters are significant, as they provide information on the nuclear shape, size and moments of nuclei. The deformation parameters of thorium isotopes were estimated by using the density-dependent meson exchange interaction DD-ME2 and the point-coupling interaction DD-

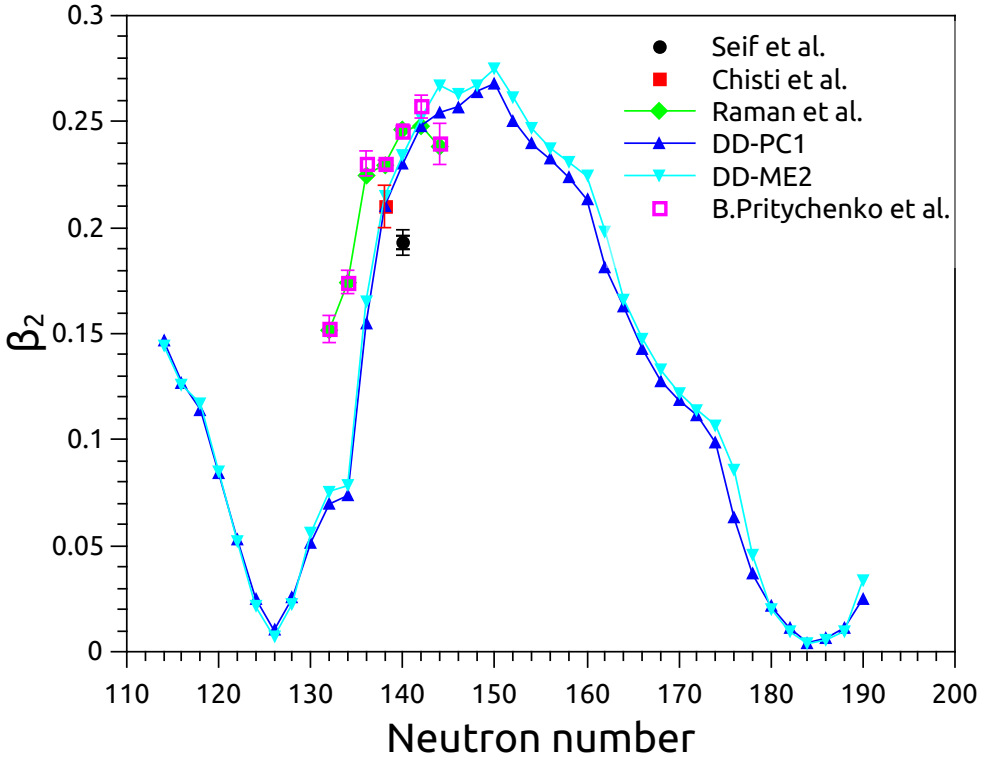

Figure 3.8: Comparison of nuclear quadrupole deformation parameter of thorium isotopes estimated by using the density-dependent meson exchange interaction DD-ME2 and the density-dependent point-coupling interaction DD-PC1, with the available data.

PC1. The deformations of quadrupole shapes can be described by the quadrupole moment Q_{20}

$$Q_{20} = 2z^2 - x^2 - y^2 \tag{3.43}$$

The deformation prameter β_2 which are connected to the quadrupole moments Q_{20}. as,

$$\beta_2 = \sqrt{\frac{5\pi}{9}} \frac{Q_{20}}{AR_0^2} \tag{3.44}$$

The calculated quadrupole deformation parameters of thorium nuclei are plotted in Figure 3.8.

The experimental data of quadrupole deformation parameter β_2 are available for certain thorium nuclei [61–63]. We compared our results with these values. The estimated values agree well with these.

Most of the thorium isotopes are having positive quadrupole deformation parameter and it indicates that they are of prolate shape. The quadrupole deformation parameter decrease and approache the minimum value near to zero at neutron number N=126 and 184. Hence these nuclei are nearly spherical. Accordingly, there is shape transition from prolate to spherical. Hence these nuclei are more stable and there is the possibility of having shell closure. A sharp increase of deformation parameter is observed at around the neutron number N=138.

3.3.8 The density distribution

From the above observations, we noticed some signature of shell closure at N=126 and 184 in the isotopic chain of thorium nuclei and also observed some evidence for mid-shell closure at N=138. To confirm these features we studied the density distribution of nucleons. Figure 3.9 shows the density distribution of thorium nuclei in the mass range 204-240 and 244-280.

The central part are less dense as compared with the peripheral part for nuclei near the drip-lines, as is evident from Figure 3.9 (dotted line). $^{204-212}Th$ and $^{268-280}Th$ (with an increase of 4 in mass number) are shown to have centrally dipped density distributions. The contour plots of the density distribution along the symmetry axis y and the coordinate axis x are illustrated in Figure 3.10.

In this plot we can see that the centrally dipped density distribution for nuclei towards the drip-lines. This reduced density at the interior is generally referred to as bubble structure [64]. The reduced density is observed in the isotopes ^{204}Th, ^{208}Th, ^{212}Th, ^{252}Th, ^{256}Th, ^{260}Th, ^{272}Th, ^{274}Th, ^{276}Th and ^{280}Th. This is

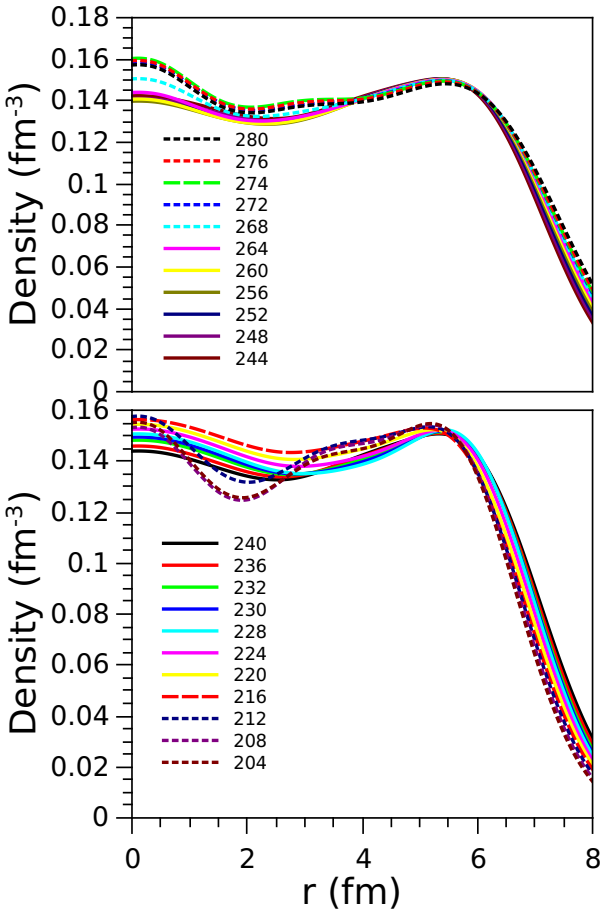

Figure 3.9: Density distribution of thorium isotopes generated by using DD-ME2 parameterization for the mass range 204-280.

due to the unoccupancy of the s-orbital near the Fermi level. The density is less at the interior and more at the surface of these nuclei.

3.3.9 Single-particle energy

The neutron single-particle energy levels of the selected thorium nuclei were plotted using the DD-ME2 parameterization and is shown in Figure 3.11.

The single-particle energy levels in thorium nuclei, corresponding to N=130, 140, 150, 160, 170, 180 and 190 are shown here. The Fermi energy level of nuclei are shown as red thick line. The gap between the levels are also marked here.

Large gaps are observed in between the levels $3p_{1/2}$ and $1i_{11/2}$, corresponding

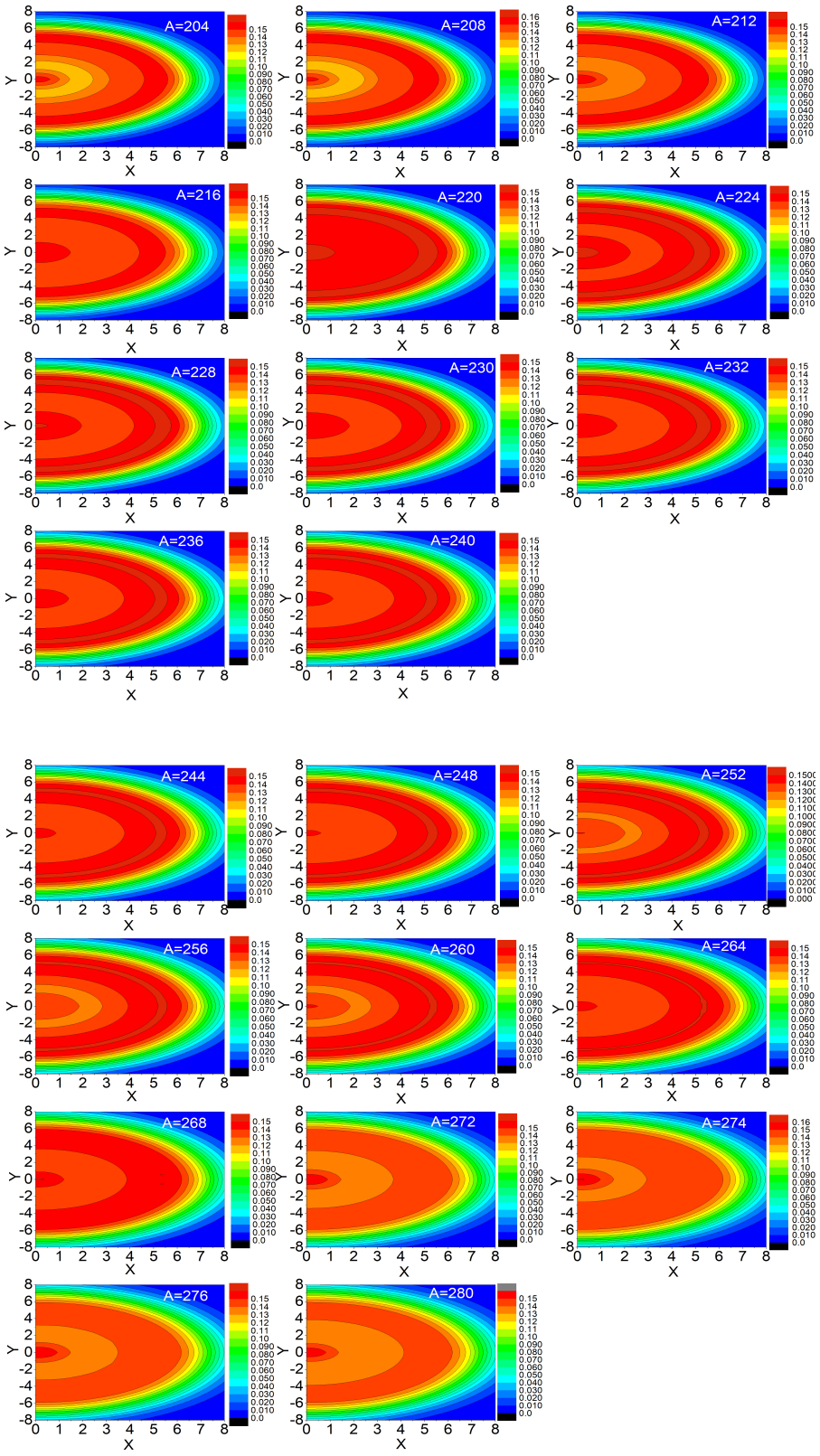

Figure 3.10: Contour plots of the density distribution of thorium nuclei along the symmetry axis y and the coordinate axis x, using DD-ME2 parameterization.

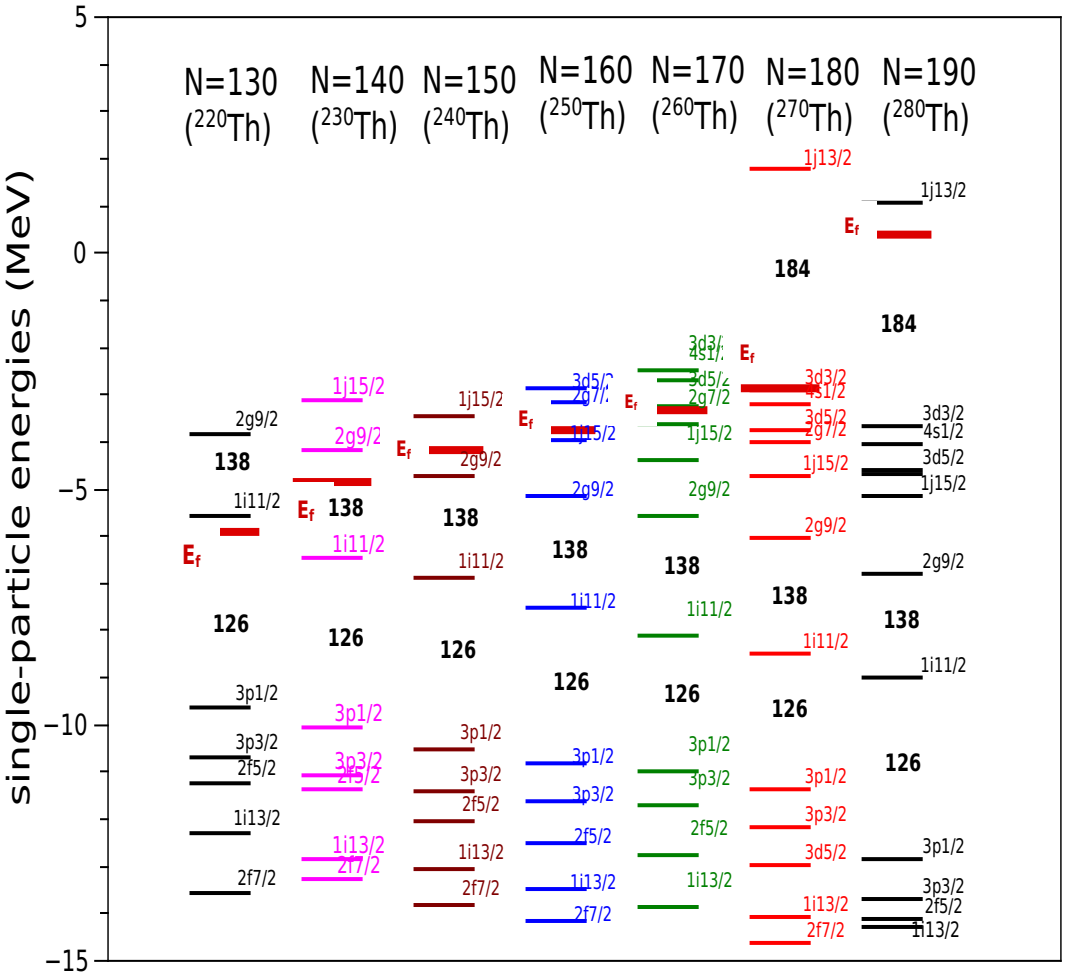

Figure 3.11: The single-particle energy levels of $^{220,230,240,250,260,270,280}Th$ isotopes by using the DD-ME2 parameteriztion.

to neutron number N=126 and also between $3d_{3/2}$ and $1j_{13/2}$, corresponding to neutron number N=184. A small gap is observed in between $1i_{11/2}$ and $2g_{9/2}$, corresponding to the neutron number N=138.

To confirm the gap between the energy levels, we have plotted the neutron single-particle energies of ^{280}Th as a function of the deformation parameter β_2 and is shown in Figure 3.12. These results also support our prediction of shell closure at N=126 and 184 and the mid-shell closure at N=138, in thorium isotopes.

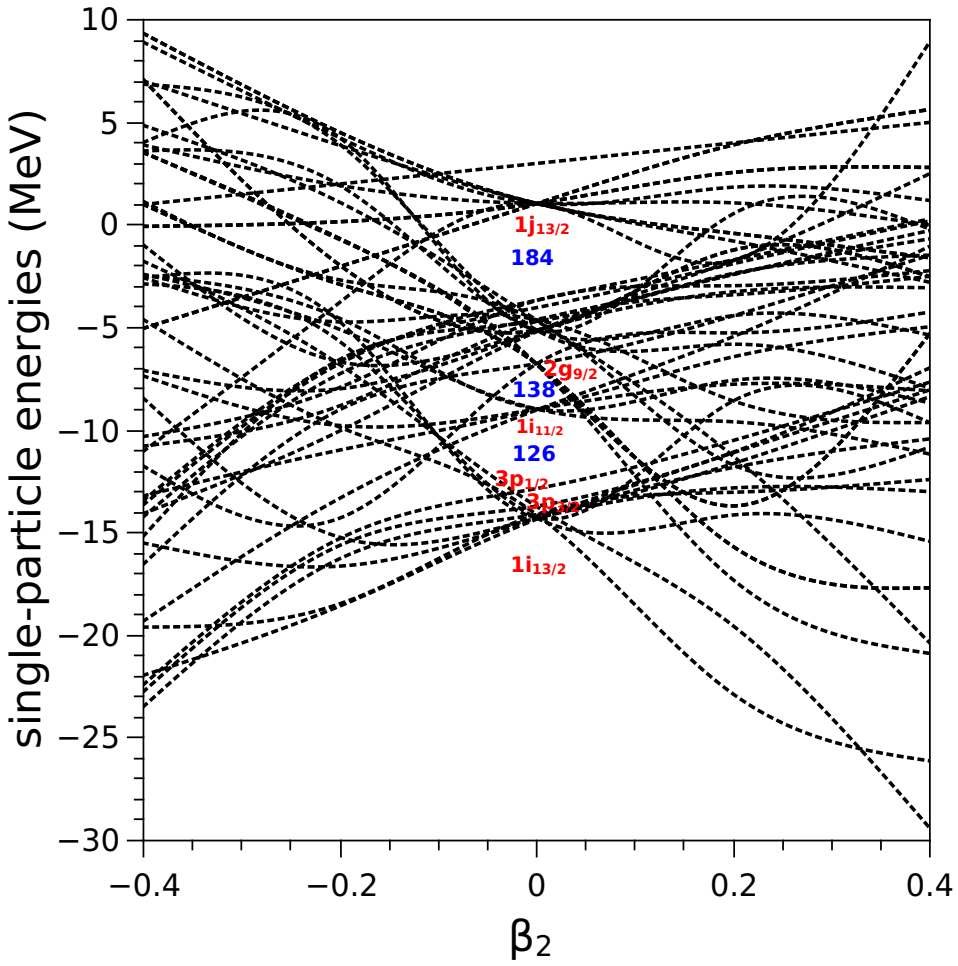

Figure 3.12: The single-particle energies of ^{280}Th, as a function of the deformation parameter β_2

Bhattacharya et al.[65] studied the interaction between alpha particles and the respective daughter nuclei formed in the double folding approach using density dependent NN interaction. They found a subshell closure at N=138 in Cm isotopes. In another study Zhang et al. [66] in 2005 searched the magic proton and neutron number in the superheavy region, with Z=100-140. They also found some significant gap at neutron number N=138 in two neutron separation energy and vanishing pairing energy. In yet another study Rong et al. [67] also observed an pronounced change in the nuclear charge radii with even Z=84-120. Their

results also support our observations.

3.4 Conclusion

The nuclear structure properties of thorium nuclei lying on and in between the drip-lines were investigated in the framework of the relativistic mean-field theory by applying the density-dependent meson exchange and point-coupling models. The ground state parameters like binding energy, charge radii, two-neutron separation energy and shell gap, rms radii and its isotopic shift, chemical potential, quadrupole deformation, density distribution and single-particle energy were estimated. These values were then compared with the available experimental and theoretical data and were found to be in good agreement. Broken linearities were observed at around the neutron numbers N=126, 138 and 184 in the plots of various evaluated values against neutron number and single-particle energy gaps were observed at around these neutron numbers. Large deviation and shell gaps were observed at around the neutron number N=126 and 184. Hence these numbers are neutron magic numbers and the corresponding thorium nuclei are more stable than their neighbours. A small deviation and shell gap were observed at around N=138, and hence we conclude that this neutron number is semi-magic and the associated nucleus is relatively stable. Most of the thorium nuclei are of prolate shape. However, they are spherical at N=126 and 184. The dipped density distriution is due to the unoccupancy of the s-orbital near the Fermi level. The density is less at the interior and more at the surface of these nuclei.

Bibliography

[1] C Samanta and S Adhikari. Extension of the bethe-weizsäcker mass formula to light nuclei and some new shell closures. *Physical Review C*, 65(3):037301, 2002.

[2] Peter Möller, JR Nix, WD Myers, and WJ Swiatecki. Nuclear ground-state masses and deformations. *arXiv preprint nucl-th/9308022*, 1993.

[3] THR Skyrme. Cvii. the nuclear surface. *Philosophical Magazine*, 1(11):1043–1054, 1956.

[4] J Dechargé and D Gogny. Hartree-fock-bogolyubov calculations with the d 1 effective interaction on spherical nuclei. *Physical Review C*, 21(4):1568, 1980.

[5] Y EL Bassem and Mustapha Oulne. Ground state properties of even–even and odd nd, ce and sm isotopes in hartree–fock–bogoliubov method. *International Journal of Modern Physics E*, 24(10):1550073, 2015.

[6] Y El Bassem and M Oulne. Hartree–fock–bogoliubov calculation of ground state properties of even–even and odd mo and ru isotopes. *Nuclear Physics A*, 957:22–32, 2017.

[7] Younes El Bassem and Mustapha Oulne. Nuclear structure investigation of even–even and odd pb isotopes by using the hartree–fock–bogoliubov method. *International Journal of Modern Physics E*, 26(12):1750084, 2017.

[8] John Dirk Walecka. A theory of highly condensed matter. *Annals of Physics*, 83(2):491–529, 1974.

[9] P-G Reinhard. The relativistic mean-field description of nuclei and nuclear dynamics. *Reports on Progress in Physics*, 52(4):439, 1989.

[10] J Meng and Peter Ring. Giant halo at the neutron drip line. *Physical review letters*, 80(3):460, 1998.

[11] J Meng, K Sugawara-Tanabe, S Yamaji, and A Arima. Pseudospin symmetry in zr and sn isotopes from the proton drip line to the neutron drip line. *Physical Review C*, 59(1):154, 1999.

[12] LS Geng, H Toki, and J Meng. A systematic study of zr and sn isotopes in the relativistic mean field theory. *Modern Physics Letters A*, 19(29):2171–2190, 2004.

[13] Peter Ring. Relativistic mean field theory in finite nuclei. *Progress in Particle and Nuclear Physics*, 37:193–263, 1996.

[14] J Meng and P Ring. Relativistic hartree-bogoliubov description of the neutron halo in 11 li. *Physical review letters*, 77(19):3963, 1996.

[15] Joseph N Ginocchio. Pseudospin as a relativistic symmetry. *Physical Review Letters*, 78(3):436, 1997.

[16] Paul Gerhard Reinhard, C Reiss, Michaël Bender, Thomas Bürvenich, T Cornelius, and Joachim Alexander Maruhn. Exotic nuclei–a challenge for nuclear mean field models. *Hyperfine Interactions*, 127:13–20, 2000.

[17] Léo Neufcourt, Yuchen Cao, Samuel Giuliani, Witold Nazarewicz, Erik Olsen, Oleg B Tarasov, et al. Beyond the proton drip line: Bayesian analysis of proton-emitting nuclei. *Physical Review C*, 101(1):014319, 2020.

[18] Michael Bender, Paul-Henri Heenen, and Paul-Gerhard Reinhard. Self-consistent mean-field models for nuclear structure. *Reviews of Modern Physics*, 75(1):121, 2003.

[19] B Pfeiffer, K-L Kratz, F-K Thielemann, and WB Walters. Nuclear structure studies for the astrophysical r-process. *Nuclear Physics A*, 693(1-2):282–324, 2001.

[20] Raj K Gupta, M Balasubramaniam, Sushil Kumar, SK Patra, G Munzenberg, and Walter Greiner. Magic numbers in exotic light nuclei near drip lines. *Journal of Physics G: Nuclear and Particle Physics*, 32(4):565, 2006.

[21] D Vretenar. Nuclear structure far from stability. *Nuclear Physics A*, 751:264–281, 2005.

[22] Chen He and Jian-You Guo. Structure and α decay for the neutron-deficient nuclei with $89 \leq z \leq 94$ in the density-dependent cluster model combined with a relativistic mean-field approach. *Physical Review C*, 106(6):064310, 2022.

[23] Bruce A Marsh, T Day Goodacre, Simon Sels, Y Tsunoda, B Andel, Andrei N Andreyev, NA Althubiti, Dinko Atanasov, AE Barzakh, J Billowes, et al. Characterization of the shape-staggering effect in mercury nuclei. *Nature Physics*, 14(12):1163–1167, 2018.

[24] XF Yang, C Wraith, Liang Xie, C Babcock, Jonathan Billowes, ML Bissell, Klaus Blaum, B Cheal, KT Flanagan, RF Garcia Ruiz, et al. Isomer shift and magnetic moment of the long-lived 1/2+ isomer in zn 49 30 79: Signature of shape coexistence near ni 78. *Physical review letters*, 116(18):182502, 2016.

[25] A Krasznahorkay, H Akimune, AM Van Den Berg, N Blasi, S Brandenburg, M Csatlo, M Fujiwara, J Gulya, MN Harakeh, M Hunyadi, et al. Neutron-skin thickness in neutron-rich isotopes. *Nuclear Physics A*, 731:224–234, 2004.

[26] Wilfried Nortershauser, Dirk Tiedemann, M Zakova, Zoran Andjelkovic, Klaus Blaum, Mark L Bissell, R Cazan, GWF Drake, Ch Geppert, Magdalena Kowalska, et al. Nuclear charge radii of be 7, 9, 10 and the one-neutron halo nucleus be 11. *Physical review letters*, 102(6):062503, 2009.

[27] C Gorges, LV Rodriguez, DL Balabanski, ML Bissell, Klaus Blaum, B Cheal, RF Garcia Ruiz, G Georgiev, W Gins, Hanne Heylen, et al. Laser spectroscopy of neutron-rich tin isotopes: a discontinuity in charge radii across the n= 82 shell closure. *Physical review letters*, 122(19):192502, 2019.

[28] B Bastin, S Grevy, D Sohler, O Sorlin, Zs Dombradi, NL Achouri, JC Angelique, F Azaiez, D Baiborodin, R Borcea, et al. Collapse of the n= 28 shell closure in si-42. *Physical Review Letters*, 99(2), 2007.

[29] F Sarazin, H Savajols, W Mittig, F Nowacki, NA Orr, Zhongzhou Ren, P Roussel-Chomaz, G Auger, D Baiborodin, AV Belozyorov, et al. Shape coexistence and the n= 28 shell closure far from stability. *Physical review letters*, 84(22):5062, 2000.

[30] T. Nikšić, D. Vretenar, and P. Ring. *Progress in Particle and Nuclear Physics*, 66(3):519–548, 2011.

[31] D. Vretenar, A.V. Afanasjev, G.A. Lalazissis, and P. Ring. *Physics Reports*, 409(3):101–259, 2005.

[32] Tamara Nikšić, Dario Vretenar, and Peter Ring. Relativistic nuclear energy density functionals: Adjusting parameters to binding energies. *Physical Review C*, 78(3):034318, 2008.

[33] Y. Tian, Z.Y. Ma, and P. Ring. *Physics Letters B*, 676(1):44–50, 2009.

[34] K Pomorski, P Ring, GA Lalazissis, A Baran, Z Lojewski, B Nerlo-Pomorska, and M Warda. Ground state properties of the β stable nuclei in various mean field theories. *Nuclear Physics A*, 624(3):349–369, 1997.

[35] A Ozawa, T Suzuki, and Isao Tanihata. Nuclear size and related topics. *Nuclear Physics A*, 693(1-2):32–62, 2001.

[36] B Cheal and KT Flanagan. Progress in laser spectroscopy at radioactive ion beam facilities. *Journal of Physics G: Nuclear and Particle Physics*, 37(11):113101, 2010.

[37] Klaus Blaum, Jens Dilling, and Wilfried Nortershauser. Precision atomic physics techniques for nuclear physics with radioactive beams. *Physica Scripta*, 2013(T152):014017, 2013.

[38] Ian U Roederer, Karl-Ludwig Kratz, Anna Frebel, Norbert Christlieb, Bernd Pfeiffer, John J Cowan, and Christopher Sneden. The end of nucleosynthesis: production of lead and thorium in the early galaxy. *The Astrophysical Journal*, 698(2):1963, 2009.

[39] Arthur Choplin, Stephane Goriely, and Lionel Siess. Synthesis of thorium and uranium in asymptotic giant branch stars. *Astronomy & Astrophysics*, 667:L13, 2022.

[40] T. Nikšić, N. Paar, D. Vretenar, and P. Ring. *Computer Physics Communications*, 185(6):1808–1821, 2014.

[41] J Boguta and AR Bodmer. Relativistic calculation of nuclear matter and the nuclear surface. *Nuclear Physics A*, 292(3):413–428, 1977.

[42] W Pannert, P Ring, and J Boguta. Relativistic mean-field theory and nuclear deformation. *Physical Review Letters*, 59(21):2420, 1987.

[43] R Brockmann and H Toki. Relativistic density-dependent hartree approach for finite nuclei. *Physical Review Letters*, 68(23):3408, 1992.

[44] Ferdinand Hofmann, CM Keil, and H Lenske. Density dependent hadron field theory for asymmetric nuclear matter and exotic nuclei. *Physical Review C*, 64(3):034314, 2001.

[45] S. Typel and H.H. Wolter. *Nuclear Physics A*, 656(3):331–364, 1999.

[46] Tamara Niksic, Dario Vretenar, P Finelli, and Peter Ring. Relativistic hartree-bogoliubov model with density-dependent meson-nucleon couplings. *Physical Review C*, 66(2):024306, 2002.

[47] F. de Jong and H. Lenske. *Phys. Rev. C*, 57:3099–3107, Jun 1998.

[48] P Manakos and T Mannel. Renormalized relativistic hartree fock models with skyrme type interactions. *Zeitschrift für Physik A Atomic Nuclei*, 334:481–489, 1989.

[49] John J. Rusnak and R.J. Furnstahl. *Nuclear Physics A*, 627(3):495, 1997.

[50] T. Bürvenich, D. G. Madland, J. A. Maruhn, and P.-G. Reinhard. *Phys. Rev. C*, 65:044308, Mar 2002.

[51] P. W. Zhao, Z. P. Li, J. M. Yao, and J. Meng. *Phys. Rev. C*, 82:054319, Nov 2010.

[52] Re Machleidt. The meson theory of nuclear forces and nuclear structure. *Springer*, pages 189–376, 1989.

[53] G. A. Lalazissis, T. Niksic, D. Vretenar, and P. Ring. *Phys. Rev. C*, 71:024312, Feb 2005.

[54] Tamara Niksic, Dario Vretenar, and Peter Ring. Relativistic nuclear energy density functionals: Adjusting parameters to binding energies. *Physical Review C*, 78(3):034318, 2008.

[55] Peter Ring and Peter Schuck. The nuclear many-body problem. *Springer Science & Business Media*, 2004.

[56] Bharat Kumar, S. K. Biswal, S. K. Singh, and S. K. Patra. *Phys. Rev. C*, 92:054314, Nov 2015.

[57] P. Möller, A.J. Sierk, T. Ichikawa, and H. Sagawa. *Atomic Data and Nuclear Data Tables*, 109-110:1–204, 2016.

[58] *https://www.nndc.bnl.gov/nudat3/.*

[59] GD Alkhazov, SL Belostotsky, OA Domchenkov, Yu V Dotsenko, NP Kuropatkin, MA Schuvaev, and AA Vorobyov. Nuclear sizes of 40, 48ca and 32, 34s isotopes determined from 1 gev proton elastic scattering. *Physics Letters B*, 57(1):47–50, 1975.

[60] I. Angeli and K.P. Marinova. *Atomic Data and Nuclear Data Tables*, 99(1):69, 2013.

[61] WM Seif and Hesham Mansour. Systematics of nucleon density distributions and neutron skin of nuclei. *International Journal of Modern Physics E*, 24(11):1550083, 2015.

[62] M. M. R. Chishti, D. O Donnell, G. Battaglia, M. Bowry, D. A. Jaroszynski, B. S. Nara Singh, M. Scheck, P. Spagnoletti, and J. F. Smith. *Nature Physics.*, 16:1853, 2020.

[63] Subramanyan Raman, CW Nestor Jr, and P Tikkanen. Transition proba-

bility from the ground to the first-excited 2+ state of even–even nuclides. *Atomic Data and Nuclear Data Tables*, 78(1):1–128, 2001.

[64] G. Saxena, M. Kumawat, M. Kaushik, S.K. Jain, and Mamta Aggarwal. *Physics Letters B*, 788:1–6, 2019.

[65] Madhubrata Bhattacharya, Subinit Roy, and G Gangopadhyay. Spectroscopic factors for alpha decay in the npnn scheme. *Physics Letters B*, 665(4):182–185, 2008.

[66] W Zhang, J Meng, SQ Zhang, LS Geng, and H Toki. Magic numbers for superheavy nuclei in relativistic continuum hartree–bogoliubov theory. *Nuclear Physics A*, 753(1-2):106–135, 2005.

[67] Rong An, Xiao-Xu Dong, Li-Gang Cao, and Feng-Shou Zhang. Local variations of charge radii for nuclei with even z from 84 to 120. *Communications in Theoretical Physics*, 75(3):035301, 2023.

Chapter 4

Shape Evolution in Thorium Isotopes

4.1 Introduction

An atomic nucleus is primarily characterized by its shape, with the most commonly encountered ones being spherical, prolate, and oblate. There is a direct correlation between the shell structure and the intrinsic shape of nuclei. The evolution of the shell structure is influenced by the residual interactions among nucleons, which in turn, can modify the shape of a nucleus. The ground state deformation of a nucleus is commonly described using two deformation parameters: the axially symmetric deformation parameter β_2 and the triaxial deformation parameter γ [1]. The quadrupole collectivity is a significant aspect of nuclei and is responsible for the structural phenomena like shape phase transition [2] and shape co-existence [3]. Shape phase transitions refer to abrupt transformations in the nuclear structure, where a nearly spherical, vibrational system can undergo a change into a well-deformed, rotational system upon the addition of nucleons. Additionally, shape coexistence can occur in a single nucleus, where two or more intrinsic shapes exist near the ground state. These coexisting equilibrium or

quasi-equilibrium shapes play a crucial role in dictating how the nucleus evolves in shape under the influence of specific forces.

Nuclei, characterized by specific count of protons and neutrons, are self-contained entities. Despite extensive research, the exact number of distinct nuclear species bound in the universe remains an unresolved question. Comprehensive investigations into the isotopic shifts of nuclei, spanning significant shell closures serve as stringent assessments for theoretical comprehension in nuclear physics. These studies reveal diverse shapes, including transitions from spherical to oblate or from prolate to triaxial configurations. The analysis of the fundamental characteristics of stable and unstable nuclei, incorporating axial deformation, using the relativistic mean-field (RMF) theory has been an area of interest. Nevertheless, it becomes imperative for us to introduce an additional degree of freedom and broaden the theory to encompass triaxial deformations. In numerous nuclei, axial symmetric computations yield an energy curve concerning the β_2 deformation, featuring minima on both the prolate and oblate sides with extremely close energy values. Consequently, it becomes challenging to definitively ascertain the ground state configuration shape of the nucleus or determine if it exhibits yet another form of deformation. The concept of quantum triaxiality holds significant curiosity in the field of nuclear structure physics. While the potential to achieve nuclear shapes with unequal lengths in all three axes has been a subject of discussion for an extended period, it still remains a compelling and fascinating topic.

Investigating nuclear rotations and the occurrence of shape phase transitions in nuclei has proven to be a highly sensitive approach for exploring nuclear structure. Atomic nuclei engage in collective motions such as rotation and vibration, and the interplay between these motions is crucial for comprehending both their intrinsic and extrinsic structures. The shapes exhibited by various

nuclei depend on the type and extent of deformations present. Generally, most identified nuclei display axial symmetry. Nevertheless, among axially deformed nuclei with even-Z and even-N, prolate deformations are more prevalent in their ground state compared to oblate deformations [4]. In the heavy mass region of the nuclide chart, typically around $A \approx 180$, there observed shape transitions [5–7] and deformed mass distributions. These phenomena lead to the disruption of spontaneous rotational axial symmetry, indicating the existence of non-axial or triaxial deformations [8]. This area of investigation holds significant interest as it contributes to a deeper understanding of the shell structure, elucidating the origins of deformation and the occurrence of triaxial ground states. Hence, the transitional nuclei situated in the heavy mass region provide a valuable foundation for the analysis and exploration of shape alterations, particularly concerning triaxial deformation.

Different theoretical models are available to explore the shape of nuclei [9–13]. Many of these give results which are comparable with available experimental data. The mean-field theory gives the best theoretical results for nuclei far away from the β-stability line, spherical and deformed nuclei as well as for neutron deficient and rich nuclei. Data related to the deformation are useful for experiments in future and will enable us to understand the behaviour of complex nuclei. The present theoretical study will also help to predict the shape evolution, especially, of thorium nuclei. The study of deformation is important in the field of nuclear fusion [14]. The degree of deformation is a critical factor in determining the height and shape of the fission barrier. Understanding quadrupole deformations is essential for predicting and analyzing the fission processes.

In the present study, we have incorporated both axial and triaxial degrees of freedom, to examine how the shape of thorium nuclei evolves within the boundaries of the drip-lines. In our earlier study, we investigated the nuclear level

density and the shapes of thorium nuclei located between the drip-lines [15]. In that work, we noticed a correlation between nuclear level density parameter and nuclear shapes. The calculations throughout the present study were carried out using the relativistic mean-field theory, with the incorperaion of density-dependent meson exchange functional. The nuclear deformation also affects the features of rotation of a nucleus.

4.2 Theoretical Formalism

The self-consistent mean-field theory is a powerful approach that allows us to trace the development of quadrupole shapes within nuclei. The energy density functional provides precise details of the structural characteristics of nuclei, ranging from light to heavy, extending from the proton drip-line to the neutron drip-line. In the framework of the nuclear self-consistent mean-field model, the complex many-body system of nuclei is simplified into a one-body problem. This simplification is achieved by approximating the energy density functional with a function that depends on neutron density and current density. These densities represent the distribution of nuclear matter, and those aspects like spin, momentum, and kinetic energy [9–11, 16].

The relativistic equation was addressed by solving it within the configurational space of harmonic oscillator wave functions, while the calculations of densities were carried out in coordinate space. This particular method was employed in the context of studying quadrupole deformation with axial symmetry, and it was assumed that both parity and the third component of isospin remained conserved throughout the analysis. The quadrupole moments $Q_{20}^{(n,p)}$ and $Q_{22}^{(n,p)}$ are,

$$Q_{20}^{(n,p)} = \sqrt{\frac{5}{16\pi}} \langle 3z^2 - r^2 \rangle_{(n,p)} \tag{4.1}$$

and

$$Q_{22}^{(n,p)} = \sqrt{\frac{5}{32\pi}}\langle x^2 - y^2\rangle_{(n,p)} \tag{4.2}$$

The quadrupole moments can be expressed in terms of the deformation parameters a_{20} and a_{22},

$$Q_{20}^{(n,p)} = \frac{3A}{4\pi}R_0^2 a_{20}^{(n,p)} \tag{4.3}$$

and

$$Q_{22}^{(n,p)} = \frac{3A}{4\pi}R_0^2 a_{22}^{(n,p)} \tag{4.4}$$

In the case of axial symmetry, the deformation parameter β_2 was determined from the quadrupole moment Q_{20} as,

$$Q_{20} = \sqrt{\frac{9}{5\pi}}AR_0^2\beta_2 \tag{4.5}$$

Positive values of β_2 correspond to the prolate shape and negative values correspond to the oblate shape.

The energy was determined as a function of the quadrupole deformation parameters β and γ by solving the relativistic Hartree-Bogoliubov equation while applying constraints on the triaxial quadrupole moment of the specified nucleus. This approach utilizes the quadratic technique, allowing for unrestricted variations of the function to find the desired energy values,

$$<H> + \sum_{\mu=0,2} C_{2\mu}(< Q_{2\mu} > - q_{2\mu}) \tag{4.6}$$

where $<H>$ is the total energy, $< Q_{2\mu} >$ is the expectation value of the mass

quadrupole operators and $q_{2\mu}$ is the constraint value of the multipole moment and $C_{2\mu}$ is the corresponding stiffness constant [17]. Also,

$$Q_{20} = 2z^2 - x^2 - y^2 \tag{4.7}$$

and

$$Q_{22} = x^2 - y^2 \tag{4.8}$$

Furthermore, the difference between $< Q_{2\mu} >$ and $q_{2\mu}$ depends on the stiffness constant, as smaller value of $C_{2\mu}$ lead to the diversion of the quadrupole moment from the constrained value. The large value of $C_{2\mu}$ may lead to distruction of convergence in the self-consistant procedure. The Augmented Lagrangian [18] method can solve this problem.

The deformations of quadrupole shapes can be described by using the polar coordinates β_2 and γ, which are connected to the quadrupole moments Q_{20} and Q_{22} as,

$$\beta_2 = \sqrt{\frac{5\pi}{9}} \frac{Q_{20}}{AR_0^2} \tag{4.9}$$

and

$$\gamma = arctan(\frac{Q_{22}}{Q_{20}}) \tag{4.10}$$

The axial prolate shape corresponds to the value of $\gamma = 0°$, while the oblate shape corresponds to $\gamma = 60°$. Intermediate values between 0 and 60 degrees ($0° < \gamma < 60°$) are indicative of triaxial shapes.

4.3 Results and Discussion

In literature, we can find several theoretical attempts on shape phase transition and shape coexistence in light and heavy stable nuclei [19–23]. In the current chapter, our focus is directed towards identifying the shape evolution of thorium isotopes, specifically considering the axial and triaxial quadrupole deformations. Our findings were systematically compared with the available data, enhancing our understanding of the intricate nuclear structure of thorium isotopes.

The solution of the relativistic Hartree-Bogoliubov equations with axial deformation provides information on the quadrupole shape of nuclei. The models are designed to calculate the mean-field solutions for deformed nuclei. To represent the wave function, it is expanded using an axially symmetric harmonic oscillator basis. In this study, 12 harmonic oscillator shells were employed for fermions, and 20 for bosons. The iterative diagonalization of the Hamiltonian was employed to determine the optimal solutions. This study focuses on examining the shape evolution of thorium nuclei located between the two drip-lines. The study identified the evolution of shapes in thorium isotopes spanning from ^{204}Th to ^{280}Th with an increment in mass number by 4.

4.3.1 Shape of thorium isotopes with axial deformation

We performed calculations to determine the total binding energy of thorium nuclei, varying with the deformation parameter β_2. The resulting binding energy curves are presented in Figure 4.1. These energies were scaled or normalized with respect to the binding energy of the lowest-energy state. The binding energy curve spans a range of β_2 values from -0.4 to 0.4. The minima observed in the binding energy curves for each isotope offer valuable insights into the shapes of the corresponding isotope.

From Figure 4.1, it is evident that the shapes of ^{204,208}Th are predomi-

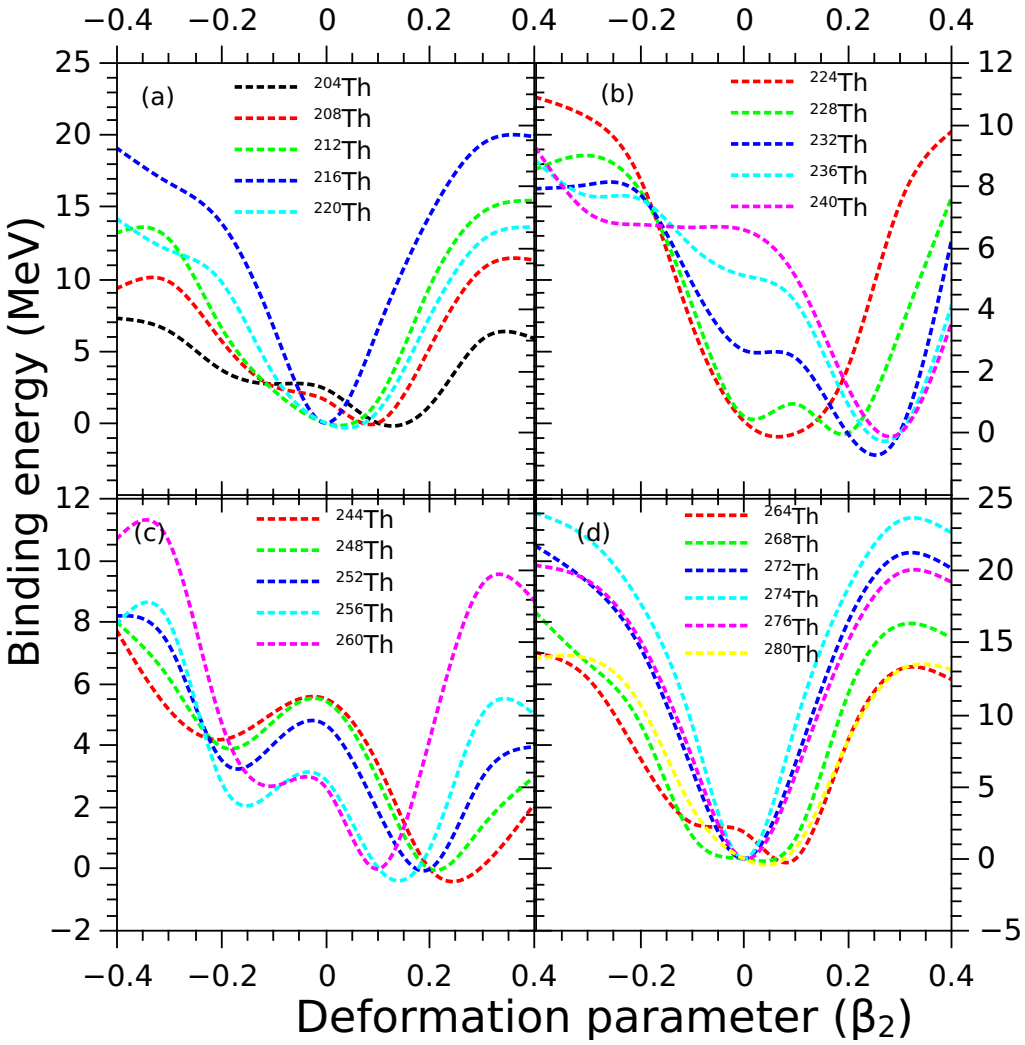

Figure 4.1: The binding energy of thorium isotopes as a function of deformation parameter β_2. Binding energy curves for isotopes ranging from ^{204}Th (N=114) to ^{220}Th (N=130) are displayed in the upper section (a) of the left panel, binding energy curves for isotopes ranging from ^{224}Th (N=134) to ^{240}Th (N=150) are displayed in the upper section (b) of the right panel, binding energy curves for isotopes ranging from ^{244}Th (N=154) to ^{260}Th (N=170) are displayed in the lower section (c) of the left panel and binding energy curves for isotopes ranging from ^{264}Th (N=174) to ^{280}Th (N=190) are displayed in the lower section (d) of the right panel.

nantly prolate, with their minima approaching positive β_2 values. Notably, ^{204}Th (N=114) exhibits higher deformation compared to ^{208}Th (N=118), as evidenced by the binding energy minimum being considerably away from zero. For ^{212}Th (N=122) and ^{220}Th (N=130), the binding energy curves show broad minima

around zero, suggesting a transitional shape that lies between prolate and spherical configurations. The distribution of binding energy for ^{216}Th (N=126) is centered around zero, indicating a shape closer to being spherical. Likewise, ^{224}Th (N=134) displays a wide minima around zero in its binding energy curve, suggesting a potential transitional shape. This observations imply that ^{224}Th (N=134) may be in a transitional state between different nuclear shapes. In the case of ^{228}Th (N=138), the presence of two minima near to $\beta_2 = 0$ and 0.2 suggests the possibility of shape coexistence between a spherical and a prolate configuration.

On the other hand, isotopes $^{232-264}$Th predominantly exhibit prolate shapes, as indicated by the minima being situated towards positive β_2 values. For ^{268}Th (N=178), a wide minimum is observed, signifying that this isotope falls within a transitional shape region. In contrast, isotopes ^{272,274,276}Th exhibit minima concentrated around zero, suggesting shapes that are closer to being spherical. Notably, ^{274}Th (N=184) specifically displays a binding energy minimum, indicative of a spherical shape. Majority of thorium isotopes exhibit prolate shapes while ^{216}Th (N=126) and ^{274}Th (N=184) are characterized by spherical shapes, contributing to the stability of the corresponding nucleus. The charge radius of thorium nuclei increases and a small variation is observed around a particular neutron number corresponding to the shell closure, and at that neutron number the nucleus is spherical in shape. The shape of a nucleus is correlated with the charge radii. In Chapter 3, we have considered the average charge radii of thorium nuclei. If we are estimating charge radii along three axes, we can predict the shape variation with charge radii.

4.3.2 Shape of thorium isotopes with triaxial deformation

In this part of the current study, we have extended our investigations to include the consideration of triaxial quadrupole deformation in thorium isotopes spanned between the drip-lines. When carrying out the calculations that impose constraints on the shape by fixing particular values for the deformation parameters, the augmented Lagrangian method was employed [18]. Figure 4.2 illustrates the self-consistent energy surfaces for triaxial quadrupole deformations in thorium isotopes. It shows the two-dimensional contour plots of the potential energy surfaces for isotopes of thorium, lying on and off the line of β-stability, in the $\beta_2 - \gamma$ plane. Here also, the energies were scaled relative to the binding energy of the lowest energy configuration. The contours on the surface connect points with identical energy values, and the separation between adjacent contours was set at 0.5 MeV. The β_2 parameter, representing the quadrupole deformation, is depicted along the radial axis (0-0.5), while γ, indicating the triaxial angle, is shown along the angular axis ($0 - 60^\circ$).

The energy surface related to the deformation exhibits energy minima with axial symmetry along the prolate axis for nuclei lying towards the proton drip-lines. The minima in ^{204}Th, (N=114) ^{208}Th (N=118), and ^{212}Th (N=122) are oriented towards the prolate axis. These isotopes show shifts from deformed to spherical shape. ^{216}Th (N=126) is observed to have a spherical shape. Furthermore, these spherical minima shows a shift in the direction of the deformed prolate axis. The prolate minimum progressively moves towards higher deformation and levels off at approximately $\beta_2 = 0.27$ in isotope ^{240}Th (N=150). Following that, the minima gradually diminishes and eventually approaches zero for ^{274}Th (N=184). These sequences of isotopes show shifts from deformed to spherical shapes. The isotopes ranging from ^{224}Th (N=134) to ^{264}Th (N=174) exhibit a higher level of deformation, while ^{216}Th with neutron number N=126

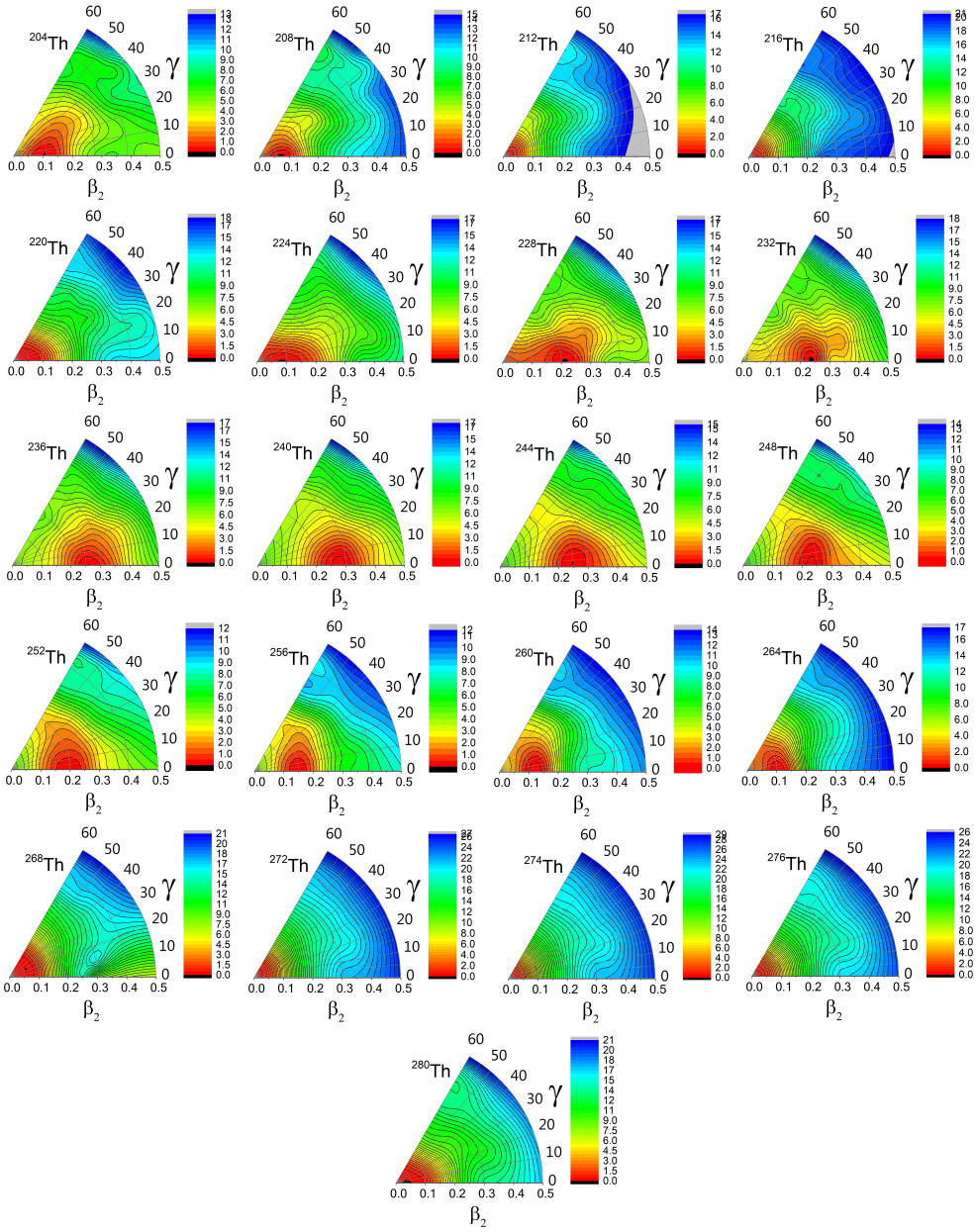

Figure 4.2: Self-consistent energy surfaces for isotopes of thorium lying on and off the line of β-stability in the $\beta_2 - \gamma$ plane, where β_2 represents the quadrupole deformation and γ represents the triaxial angle (ranging from 0 to 60°). In each case, the energies were scaled relative to the binding energy of the lowest energy configuration. The contours on the surface connect points with identical energy values, and the separation between adjacent contours was set at 0.5 MeV.

and ^{274}Th with N=184 are less deformed and tend to be more spherical in shape. Li et al.[20] estimated the quadrupole and octupole shape phase transitions in $^{220,224,228}Th$. Their calculation indicates a rapid shape transition between N =

Table 4.1: The comparison between β_2 values of thorium isotopes associated with the minimum energy from the self-consistent energy surfaces and other available data.

Isotopes	Estimated values	DRHBc [24]	Experimental data
^{204}Th	0.10	0.155	
^{208}Th	0.07	0.118	
^{212}Th	0.02	0.040	
^{216}Th	0	0	
^{220}Th	0.05	0.018	
^{224}Th	0.09	0.081	0.1744 ± 0.0055 [25]
^{228}Th	0.21	0.227	0.2299 ± 0.0019 [25],0.21 ± 0.01 [26]
^{232}Th	0.24	0.263	0.2571 ± 0.0054 [25]
^{236}Th	0.25	0.282	
^{240}Th	0.27	0.294	
^{244}Th	0.25	0.276	
^{248}Th	0.23	0.252	
^{252}Th	0.2	0.220	
^{256}Th	0.15	0.158	
^{260}Th	0.12	0.128	
^{264}Th	0.1	0.111	
^{268}Th	0.05	0.060	
^{272}Th	0	0	
^{274}Th	0	0	
^{276}Th	0	0	
^{280}Th	0.05	0	

130 and N = 138, from non-octupole to pronounced octupole deformations. An intriguing aspect of the isotopic progression is the presence of a flattened prolate minimum in the deformation of ^{224}Th (N=134). This flat minimum spans the range of axial deformation parameter values from 0 to 0.2. Potentials with flat-bottom shapes are distinguished by fluctuations in their deformation parameters, which could suggest the occurrence of a phase transition. A slight triaxial behaviour was observed in ^{220}Th (N=134) and ^{268}Th (N=178) for the values of $\beta_2 = 0.05$ and $\gamma = 10^{\circ}$. Due to their proximity to the origin, distinguishing the triaxial behavior becomes challenging. Additionally, the energy separation between adjacent contours is very small in this case. We estimated the binding energy of each thorium isotope for various β_2 values at a fixed γ deformation and

plotted the curves. Consequently, we observed minima occurring at $\beta_2 = 0.05$ and $\gamma = 10^0$. This triaxial behavior is observed within the region associated with shape phase transitions. The study on shape evolution with triaxial deformation also confirms that majority of thorium isotopes exhibit a prolate shape, while ^{216}Th (N=126) and ^{274}Th (N=184) are characterized by spherical shapes. The nuclear deformation of thorium isotopes were studied by using the deformed relativistic Hartree Bogolioubov theory in continuum (DRHBc) [24]. We have tabulated the β_2 values for thorium isotopes corresponding to the minimum energy from the self-consistent energy surfaces in $\beta_2 - \gamma$ plane in Table 4.1 along with the available experimental and theoretical data.

Figures 4.1 and 4.2 reveal the influence of axial and triaxial deformation on the nuclear ground state. In the case of ^{232}Th isotope, a comparison has been made between the deformations with and without triaxial degree of freedom, as shown in Figure 4.3. It is noted that the binding energy minima obtained from both curves are nearly the same, approximately around 0.24. The deformation obtained from the binding energy curve is supported by the deformation from the energy surface. This observation implies that for ^{232}Th, the inclusion or exclusion of triaxial deformation does not significantly affect the overall binding energy, as it is an axially deformed nucleus. However, it is important to note that the significance of triaxial deformation becomes more pronounced for nuclei with triaxial shapes, where the deviation from axial symmetry is more substantial. In such cases, the inclusion of triaxial degrees of freedom can lead to significant changes in binding energy and deformation properties. The transition between stable shapes within a series of isotopes are controlled by changes in the shell structure of individual nucleon orbitals. Specifically, under certain conditions, the potential energy minima can emerge due to the presence of gaps or areas with reduced density of single-particle energy levels around the Fermi surface when

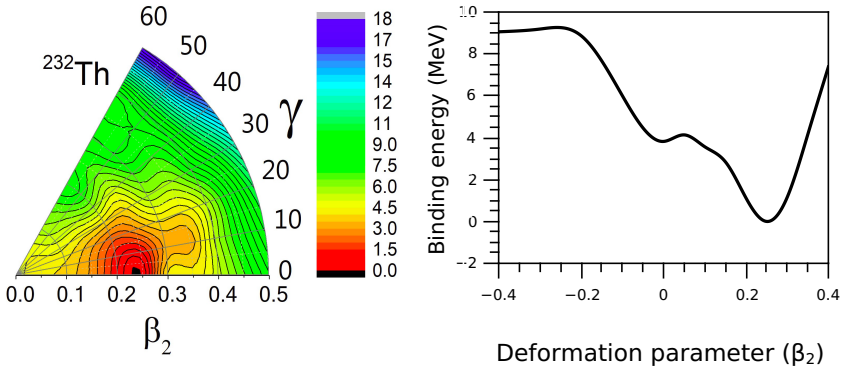

Figure 4.3: The comparison between the deformation of ^{232}Th isotope with and without the triaxial degree of freedom.

the nucleus is deformed. These sequences of isotopes show shifts from spherical to deformed shapes.

4.4 Conclusion

The ground state deformation of thorium nuclei lying in between the drip-lines were described in terms of the axially symmetric deformation parameter β_2 and the triaxial deformation parameter γ. The nuclear shape evolution of thorium isotopes ranging from ^{204}Th to ^{280}Th (with an increment of 4 in mass number) was investigated using the relativistic mean-field theory. The binding energy curves of thorium isotopes as a function of the deformation parameter β_2 were plotted and the minima were identified. ^{216}Th and ^{274}Th are spherical in shape and the nearby isotopes are less deformed and nearly spherical. Isotopes ranging from ^{220}Th to ^{264}Th (N=174) exhibit a higher level of deformation. The majority of thorium isotopes exhibit a prolate shape. The most deformed nucleus is ^{240}Th (N=150) and is prolate. We have also plotted the self-consistent energy surfaces for isotopes of thorium lying on and off the line of β-stability in the $\beta_2 - \gamma$ plane. The study on shape evolution with triaxial deformation also confirms that majority of thorium isotopes exhibit a prolate shape, while ^{216}Th (N=126) and

^{274}Th (N=184) are characterized by spherical shapes. A slight triaxial behaviour is observed in ^{220}Th (N=130) and ^{268}Th (N=178) for the values of $\beta_2 = 0.05$ and $\gamma = 10^{\circ}$. This triaxial behavior is observed within the region associated with shape phase transition.

Bibliography

[1] A. Bohr and B.R. Mottelson. *Nuclear Structure*. Number v. 1 in Nuclear Structure. World Scientific, 1998.

[2] Pavel Cejnar, Jan Jolie, and Richard F Casten. Quantum phase transitions in the shapes of atomic nuclei. *Reviews of Modern Physics*, 82(3):2155, 2010.

[3] Kris Heyde and John L Wood. Publisher's note: Shape coexistence in atomic nuclei. *Reviews of Modern Physics*, 83(4):1655, 2011.

[4] Ikuko Hamamoto and Ben R. Mottelson. Further examination of prolate-shape dominance in nuclear deformation. *Phys. Rev. C*, 79:034317, 2009.

[5] Ragnar Bengtsson, Tord Bengtsson, Jerzy Dudek, Georg Leander, Witold Nazarewicz, and Jing-Ye Zhang. Shape coexistence and shape transitions in even-even pt and hg isotopes. *Physics Letters B*, 183(1):1–6, 1987.

[6] W Nazarewicz, MA Riley, and JD Garrett. Equilibrium deformations and excitation energies of single-quasiproton band heads of rare-earth nuclei. *Nuclear Physics A*, 512(1):61–96, 1990.

[7] JL Wood, Kristiaan Heyde, W Nazarewicz, Marc Huyse, and Piet Van Duppen. Coexistence in even-mass nuclei. *Physics reports*, 215(3-4):101–201, 1992.

[8] JA Sheikh, GH Bhat, Y Sun, GB Vakil, and R Palit. Triaxial projected shell model study of γ-vibrational bands in even-even er isotopes. *Physical Review C*, 77(3):034313, 2008.

[9] Dario Vretenar, AV Afanasjev, GA Lalazissis, and P Ring. Relativistic hartree–bogoliubov theory: static and dynamic aspects of exotic nuclear structure. *Physics reports*, 409(3-4):101–259, 2005.

[10] Michael Bender, Paul-Henri Heenen, and Paul-Gerhard Reinhard. Self-consistent mean-field models for nuclear structure. *Reviews of Modern Physics*, 75(1):121, 2003.

[11] T Niksic, Dario Vretenar, and Peter Ring. Relativistic nuclear energy density functionals: Mean-field and beyond. *Progress in Particle and Nuclear Physics*, 66(3):519–548, 2011.

[12] Tamara Niksic, Dario Vretenar, and Peter Ring. Relativistic nuclear energy density functionals: Adjusting parameters to binding energies. *Physical Review C*, 78(3):034318, 2008.

[13] Yuan Tian, Zhong-yu Ma, and P Ring. A finite range pairing force for density functional theory in superfluid nuclei. *Physics Letters B*, 676(1-3):44–50, 2009.

[14] M Dasgupta, DJ Hinde, N Rowley, and AM Stefanini. Measuring barriers to fusion. *Annual Review of Nuclear and Particle Science*, 48(1):401–461, 1998.

[15] E Ummukulsu and Antony Joseph. Nuclear collective level density and shape of thorium isotopes. *Indian Journal of Physics*, 97:1–6, 2023.

[16] J Rikovska Stone and P-G Reinhard. The skyrme interaction in finite nuclei

and nuclear matter. *Progress in Particle and Nuclear Physics*, 58(2):587–657, 2007.

[17] P. Schuck P. Ring. *The Nuclear Many-Body Problem.* Springer-Verlag, Berlin, 1980.

[18] Andrzej Staszczak, Mario Stoitsov, Andrzej Baran, and Witold Nazarewicz. Augmented lagrangian method for constrained nuclear density functional theory. *The European Physical Journal A*, 46:85–90, 2010.

[19] Andrius Juodagalvis, Ingemar Ragnarsson, and Sven Åberg. Triaxiality in 48cr. *Physics Letters B*, 477(1-3):66–72, 2000.

[20] ZP Li, BY Song, JM Yao, D Vretenar, and J Meng. Simultaneous quadrupole and octupole shape phase transitions in thorium. *Physics Letters B*, 726(4-5):866–869, 2013.

[21] S Hellgartner, D Mucher, K Wimmer, V Bildstein, JL Egido, R Gernhauser, R Krucken, AK Nowak, M Zielinska, C Bauer, et al. Axial and triaxial degrees of freedom in 72zn. *Physics Letters B*, 841:137933, 2023.

[22] Rajat Gupta, Amit Kumar, Suram Singh, Arun Bharti, GH Bhat, and JA Sheikh. Systematic investigation of γ-band structure of triaxial even-even neutron-deficient os nuclei. *Chinese Journal of Physics*, 72:191–206, 2021.

[23] K Nomura, D Vretenar, ZP Li, and J Xiang. Interplay between pairing and triaxial shape degrees of freedom in os and pt nuclei. *Physical Review C*, 104(2):024323, 2021.

[24] Kaiyuan Zhang, Myung-Ki Cheoun, Yong-Beom Choi, Pooi Seong Chong, Jianmin Dong, Zihao Dong, Xiaokai Du, Lisheng Geng, Eunja Ha, Xiao-Tao

He, et al. Nuclear mass table in deformed relativistic hartree–bogoliubov theory in continuum, i: Even–even nuclei. *Atomic Data and Nuclear Data Tables*, 144:101488, 2022.

[25] B Pritychenko, M Birch, B Singh, and M Horoi. Tables of e2 transition probabilities from the first 2+ states in even–even nuclei. *Atomic Data and Nuclear Data Tables*, 107:1–139, 2016.

[26] MMR Chishti, D O'Donnell, G Battaglia, M Bowry, DA Jaroszynski, BS Nara Singh, M Scheck, P Spagnoletti, and JF Smith. Direct measurement of the intrinsic electric dipole moment in pear-shaped thorium-228. *Nature Physics*, 16(8):853–856, 2020.

Chapter 5

Collective Behaviour:Isovector Giant Dipole Response

5.1 Introduction

The excitation of atomic nuclei offers valuable information into their structure. The Random Phase Approximation (RPA) stands as the foremost theory for investigating the dynamics of nuclei. Collective excitation within the nucleus entails the coordinated motion of individual protons and neutrons, rather than the independent motion of nucleons. The collective motion of nucleons leads to various phenomena, including nuclear deformation, rotational and vibrational motions, giant resonances etc. It yields extensive information on nuclear structure, nuclear reactions and features of nuclear matter.

Giant resonance is the prime example of collective oscillation of nucleons. There are different types of giant resonances like Isoscalar Giant Monopole Resonance (ISGMR), Isoscalar Giant Dipole Resonance (ISGDR), Isoscalar Giant Quadrupole Resonance (ISGQR), Isovector Giant Monopole Resonance (IVGMR), Isovetor Giant Dipole Resonance (IVGDR), Isovector Giant Quadrupole Resonance (IVGQR) etc. If protons and neutrons are oscillating in

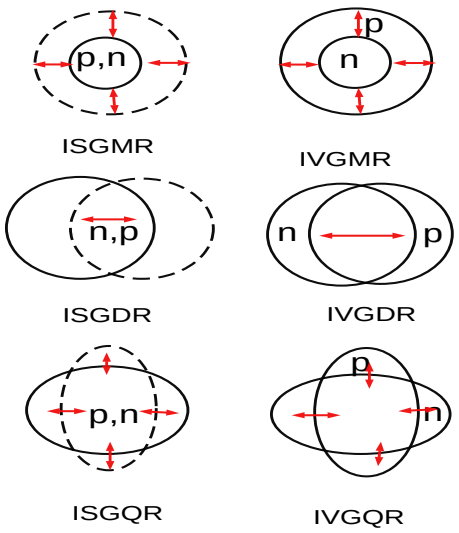

Figure 5.1: The schematic representation of Isoscalar Giant Monopole Resonance (ISGMR), Isoscalar Giant dipole Resonance (ISGDR), Isoscalar Giant Quadrupole Resonance (ISGQR), Isovector Giant Monopole Resonance (IVGMR), Isovetor Giant dipole Resonance (IVGDR), Isovector Giant Quadrupole Resonance (IVGQR).

phase, it is termed as the isoscalar mode and if protons and neutrons are oscillating out of phase it is termed as the isovector mode. Giant monopole resonance is the compression and expansion of nucleus, similar to the breathing mode. In Giant dipole resonance, the collective oscillation of protons is relative to the oscilation of neutrons and creates the dipole mode. In the case of giant quadrupole resonance, the motion of protons and neutron creates the quadrupole mode.

The schematic representation of giant resonances is shown in Figure 5.1.

The giant dipole resonance (GDR) is the primary collective oscillation mode within a nucleus. The study of GDRs give information on structure of atomic nuclei, particularly in revealing the deformations present in nuclei. Mastery of GDR dynamics is essential not only for advancing the structural studies but also for its wide-ranging applications, in fields such as astrophysics, nuclear engineering etc. Furthermore, the information gained from GDR research serves as vital resource for developing both theoretical frameworks and experimental endeavors

in nuclear physics.

The prediction of GDR includes two theoretical approaches, the microscopic approach and the phenomenological approach. Among the microscopic approaches, the most commonly used one is the quasiparticle random phase approximation (QRPA), which implements the self-consistent density functionals like Gogny functional [1–3], Skyrme functional [4, 5] and relativistic functional like DD-ME [6, 7]. In phenomenological approach, GDR is obtained from the Lorentzian transformations of the experimental photo-absorption cross-section, such as Standared Lorentzian model (SLM) [8, 9], modified Lorentzian approach (MLO) [10] and simplified version of the modified Lorentzian approach (SMLO)[11].

The Energy Density Functionals (EDF) offer a precise depiction of the ground state properties and collective behaviour of nuclei, spanning from proton drip line to neutron drip line and from light to heavy nuclei [12–15]. One of the fascinating areas of research in this field involves the multipole response of nuclei far away from the line of β-stability. Theoretical investigations of the collective behaviour within nuclei is commonly performed with quasiparticle random phase approximation. The dimension of QRPA matrices increases very rapidly for deformed heavy systems and the calculations become complex. In such situations an alternative method, the Finite Amplitude Method (FAM) is used to compute the multipole response function. It has been effectively applied in various studies conducted in harmonic oscillator basis and coordinate space [16–25]. In the present study, we have investigated the multipole response of even-even thorium isotopes, lying in between the drip lines, following the framework of the relativistic self-consistent mean-field model. This is achieved through the implementation of the finite amplitude method for relativistic quasiparticle random phase approximation. One category of the self-consistent mean-field models, which

specifically utilizes the relativistic (covariant) energy density functionals with zero-range interactions, have been proven effective in studying various nuclear structure phenomena. These models have been demonstrated to have successful application in analyzing and understanding the diverse aspects of nuclear structure.

5.2 Theoretical Formalism

5.2.1 Random Phase Approximation

The relativistic Hartree-Bogoliubov (RHB) model integrates the nuclear particle-hole (ph) and particle-particle (pp) correlations at a mean-field level. It accomplishes this by combining two average potentials: the self-consistent nuclear mean-field (h), encompassing long-range ph correlations, and a pairing field (Δ), accounting for the pp correlations. In the RHB framework, the nuclear single-reference state is represented by a generalized Slater determinant ($|\phi>$), symbolizing a vacuum concerning independent quasiparticles. These quasiparticles are defined through a unitary Bogoliubov transformation and the associated Hartree-Bogoliubov wave functions (U and V) are determined by solving the RHB equation [26],

$$\begin{pmatrix} h_D - m - \lambda & \Delta \\ -\Delta^* & -h_D^* + m + \lambda \end{pmatrix} \begin{pmatrix} U_\mu \\ V_\mu \end{pmatrix} = E_\mu \begin{pmatrix} U_\mu \\ V_\mu \end{pmatrix} \tag{5.1}$$

Under the relativistic case, the self-consistent mean-field is incorporated into the single-nucleon Dirac Hamiltonian (h_D). Here U and V are used to represent the Dirac spinors. The nucleon mass is denoted by m and the chemical potential λ is established as a Lagrange multiplier. U_μ and V_μ are particle wave functions and E_μ represents the quasiparticle energies.

Here, the generalized density $\mathcal{R}$ is,

$$\mathcal{R} = \mathcal{W}^{+} \begin{pmatrix} \rho & \kappa \\ -\kappa^{*} & 1-\rho^{*} \end{pmatrix} \mathcal{W} \tag{5.2}$$

where ρ is the density matrix and κ is the pairing tensor. The Bogoliubov unitary transformation matrix $\mathcal{W}$ is,

$$\mathcal{W} = \begin{pmatrix} U & V^{*} \\ V & U^{*} \end{pmatrix} \tag{5.3}$$

The relativistic Hartree-Bogoliubov Hamiltonian which is the derivative of the energy density functional with respect to the generalized density R is,

$$\mathcal{H} = \frac{\delta E[R]}{\delta R} = \mathcal{W}^{+} \begin{pmatrix} h & \Delta \\ -\Delta^{*} & -h* \end{pmatrix} \mathcal{W} \tag{5.4}$$

If the quasiparticle operator $\alpha_{\mu}(t)$ is subjected to a time-dependent external perturbation $F(t)$, then the evolution of $\alpha_{\mu}(t)$ is determined by the equation of motion,

$$i\partial_{t}\alpha_{\mu}(t) = [H(t) + F(t), \alpha_{\mu}(t)] \tag{5.5}$$

For weak harmonic field,

$$F(t) = \eta[F(\omega)e^{-i\omega t} + F^{+}(\omega)e^{i\omega t}] \tag{5.6}$$

where η is a small real parameter and the operator $F(\omega)$ is,

$$F(\omega) = \frac{1}{2}\sum_{\mu\nu} F^{20}_{\mu\nu}\alpha^{+}_{\mu}\alpha^{+}_{\nu} + F^{02}_{\mu\nu}\alpha_{\nu}\alpha_{\mu} \tag{5.7}$$

The term containing $F^{11}_{\mu\nu}$ do not contribute in linear response, since the single particle operator,

$$F = \frac{1}{2}\begin{pmatrix}\alpha^+ & \alpha\end{pmatrix}\mathcal{F}\begin{pmatrix}\alpha \\ \alpha^+\end{pmatrix} + constant \tag{5.8}$$

with

$$\mathcal{F} = \begin{pmatrix}F^{11} & F^{20} \\ -F^{02} & -F^{11^+}\end{pmatrix} \tag{5.9}$$

The external perturbation induces small-amplitude oscillations in the quasi-particle operator $\alpha_\mu(t)$ around the ground-state solution with same energy. Hence,

$$\alpha_\mu(t) = [\alpha_\mu + \delta\alpha_\mu(t)]e^{iE_\mu t} \tag{5.10}$$

where E_μ stands for the quasiparticle energies and $\delta\alpha_\mu(t)$ is the oscillating part of $\alpha_\mu(t)$. It is obtained from the expansion of the quasiparticle creation operator α^+. That is,

$$\delta\alpha_\mu(t) = \eta\sum_\nu \alpha^+_\nu[X_{\nu\mu}(\omega)e^{-i\omega t} + Y^*_{\nu\mu}(\omega)e^{+i\omega t}] \tag{5.11}$$

where $X_{\nu\mu}(\omega)$ and $Y_{\nu\mu}(\omega)$ are the amplitudes of the oscillations. Consequent to the oscillations in the density matrix and pairing tensor, an oscillating field is induced in the single-particle Hamiltonian as,

$$h(t) = h_0 + \delta h(t) \tag{5.12}$$

and in the pairing field as,

$$\Delta(t) = \Delta_0 + \delta\Delta(t) \tag{5.13}$$

with h_0 and Δ_0 denoting the corresponding ground state values.

As a result, the Hamiltonian $H(t)$ can also be split into,

$$H(t) = H_0 + \delta H(t) = H_0 + \eta[\delta H(\omega)e^{-i\omega t} + \delta H^{+}(\omega)^{+}e^{+i\omega t}] \tag{5.14}$$

$\delta H(\omega)$ can be decompossed in the quasiparticle basis as,

$$\delta H(\omega) = \frac{1}{2}\sum_{\mu\nu} \delta H^{20}_{\mu\nu}(\omega)\alpha^{+}_{\mu}\alpha^{+}_{\nu} + \delta H^{02}_{\mu\nu}(\omega)\alpha_{\nu}\alpha_{\mu} \tag{5.15}$$

Substituting these equations in the equation of motion the linear term is obtained as quasiparticle random phase approximation method (QFAM) equations, as given below,

$$(E_\mu + E_\nu - \omega)X_{\mu\nu}(\omega) + \delta H^{20}_{\mu\nu}(\omega) = -F^{20}_{\mu\nu} \tag{5.16}$$

$$(E_\mu + E_\nu + \omega)Y_{\mu\nu}(\omega) + \delta H^{02}_{\mu\nu}(\omega) = -F^{02}_{\mu\nu} \tag{5.17}$$

These equations 5.16 and 5.17 are nonlinear and can be solved self-consistently. $\delta H^{20}_{\mu\nu}(\omega)$ and $\delta H^{02}_{\mu\nu}(\omega)$ are expanded in terms of $X_{\mu\nu}(\omega)$ and $Y_{\mu\nu}(\omega)$ upto linear order and obtained as QRPA equations.

The transition strength function $S(f,\omega)$ is defined as [26],

$$S(f,\omega) = \sum_{\mu<\nu} F^{20*}_{\mu\nu}(\omega)X_{\mu\nu}(\omega) + F^{02*}_{\mu\nu}(\omega)Y_{\mu\nu}(\omega) \tag{5.18}$$

and the response function is,

$$\frac{dB}{d\omega} = -\frac{1}{\pi} ImS(f,\omega) \tag{5.19}$$

where B is strength distribution.

5.3 Results and Discussion

The multipole response of thorium nuclei lying far away from the line of β-stability are of interest here. The collective degree of freedom of nuclei is a commonly explored aspect in nuclear structure physics. The quasiparticle random phase approximation technique is used here to study the collective vibrations of thorium nuclei. In the present investigation, we have studied the isovector dipole strength distribution of thorium isotopes, spanning from proton drip line to neutron drip line. Here, the finite amplitude method for the relativistic quasiparticle random phase approximation is incorporated into the stationary relativistic Hartree-Bogoliubov equation. The computational code solves the single-nucleon Hartree-Bogoliubov equation by utilizing an expansion of the Dirac spinors based on the eigenfunctions derived from an axially symmetric harmonic oscillator potential.

In the present calculation, we have employed the relativistic density dependent point-coupling (DD-PC1) functional [27]. The simplified form of the pairing force has been implemented into the RHB calculations for spherical and deformed nuclei [28–30]. This force separable in momentum space, and is depends on two parameters G and a, which appears in the equations to be followed. The parameters are accurately tuned to produce the pairing gap predicted by Gogny force.

The pairing force is,

$$V^{pp}(\mathbf{r}1,\mathbf{r}2,\mathbf{r}1',\mathbf{r}2') = -\frac{G}{2}(1-P_\sigma)\delta^3(\mathbf{R}-\mathbf{R}')P(\mathbf{r})P(\mathbf{r}') \tag{5.20}$$

where $P(r)$ is the Fourier transform of the sigle Guassian ansatz $p(k) = e^{a^2k^2}$

$$P(\mathbf{r}) = \frac{1}{(4\pi a^2)^{\frac{3}{2}}} e^{\frac{-r^2}{2a^2}} \tag{5.21}$$

Here G and a are the two parameters, which are determined as $G = 728$ MeVfm^3 and $a = 0.644$fm. The isovector multipole operator is [26],

$$f^{IV}_{JK} = \sum_{i=1}^{Z} f_{JK}(\mathbf{r}_i) - \sum_{i=1}^{N} f_{JK}(\mathbf{r}_i) \tag{5.22}$$

The operator $f_{JK}(\mathbf{r})$ is generally defined as,

$$f_{JK}(\mathbf{r}) = r^J Y_{JK}(\theta,\phi) \tag{5.23}$$

Using these operators, the nuclear giant resonance can be reliably explained [7, 31, 32]. In the case of dipole excitation, the isovector operator is defined as [26] $D_K = rY_{1K}$, $K = 0, 1$.

Also,

$$D_K = e\frac{NZ}{A}\left[\frac{1}{Z}\sum_{i=1}^{Z} D_K(\mathbf{r}_i) - \frac{1}{N}\sum_{i=1}^{N} D_K(\mathbf{r}_i)\right] \tag{5.24}$$

To avoid the divergence of the QFAM solutions near the QRPA state, a minor imaginary component is introduced to the energy, transforming ω into $\omega + i\gamma$. This approach is similar to folding the QRPA strength function with a Lorentzian distribution characterized by a width of $\Gamma = 2\gamma$ [22], where the smearing width

γ in MeV is taken as $\gamma \approx 0.01 - 1MeV$. The solution is achieved when the maximum variance between collective amplitudes of consecutive iterations falls below a predetermined threshold ($\epsilon = 10^{-6}$). To guarantee the stability and swift convergence of the FAM iteration process, the modified Broyden's method was employed [33, 34].

The isovector giant dipole resonance is widely studied in heavy and superheavy nuclei [35–39]. Here we have performed the calculation for $J = 1$ (K=0,1) response of thorium isotopes. Figure 5.2 gives the strength distribution of

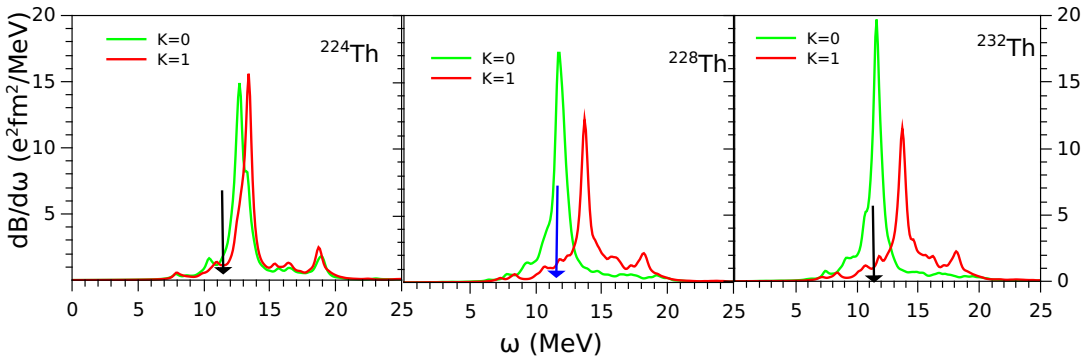

Figure 5.2: Isovector giant dipole response of $^{224-232}Th$ isotopes obtained from the RPA calculation for K=0 and K=1 modes of excitation. The black arrow represents the centroid energy from experimental data and the blue arrow represents the centroid energy from other theoretical data [40].

$^{224,228,232}Th$ isotopes obtained from the RPA calculations and the results were compared with the available data. The centroid energy obtained from the experimental data are available for ^{224}Th and ^{232}Th [41–43]. Bai et al. [40] described the giant dipole resonance based on the multitask learning approach, in which they had calculated the GDR parameter of ^{228}Th. We compared our results with that of them. The centroid energy obtained from the available data are indicated by arrows in Figure 5.2. The results are agreeing reasonably well with the available data.

The Isovector giant dipole response of thorium isotopes $^{204-280}Th$ with an increment of 4 in mass number were estimated with RPA. The black and red curves

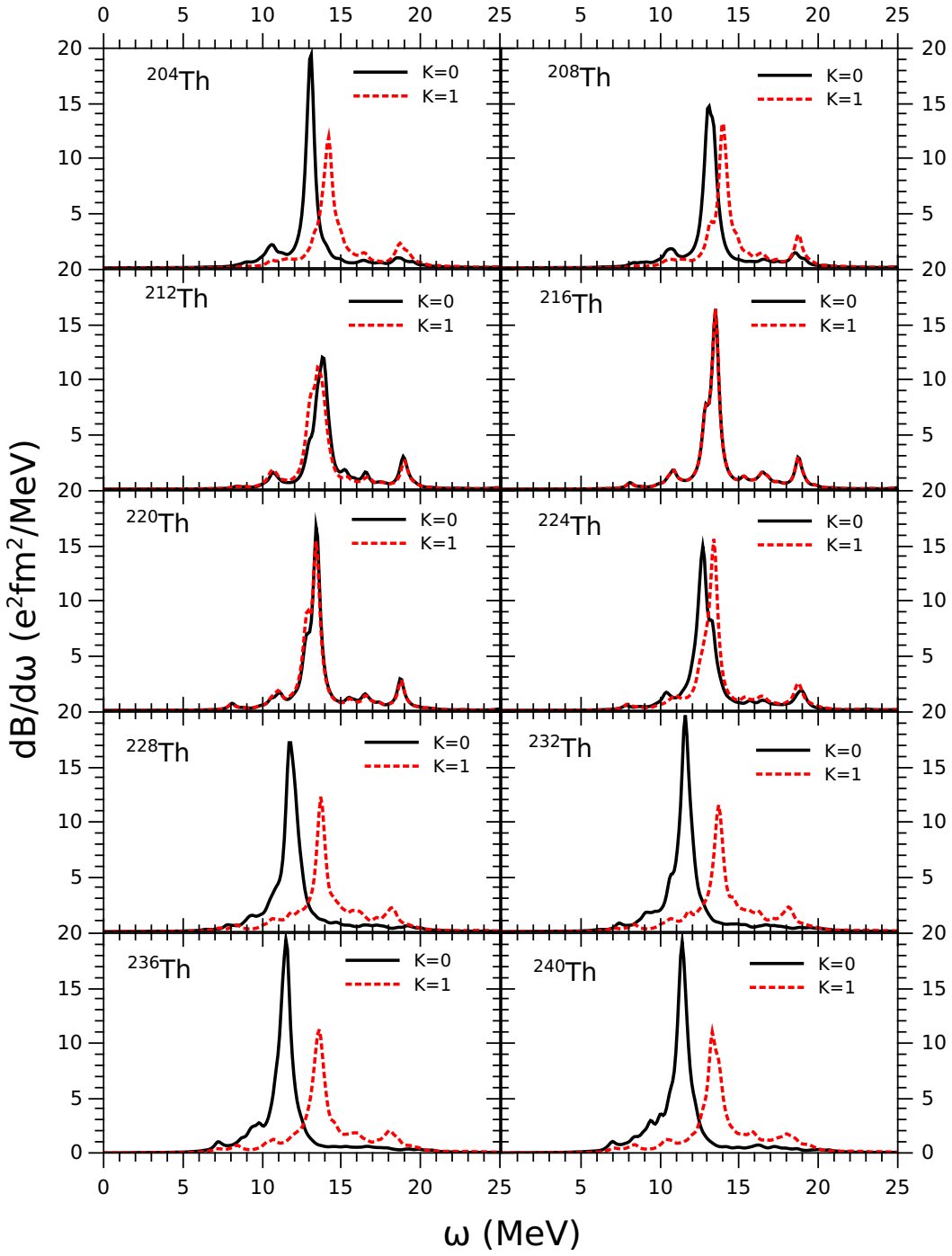

Figure 5.3: Isovector giant dipole response of $^{204-240}Th$ isotopes obtained from the relativistic quasiparticle random phase approximation. The black and red curves, respectively correspond to K=0 and K=1 modes of excitation.

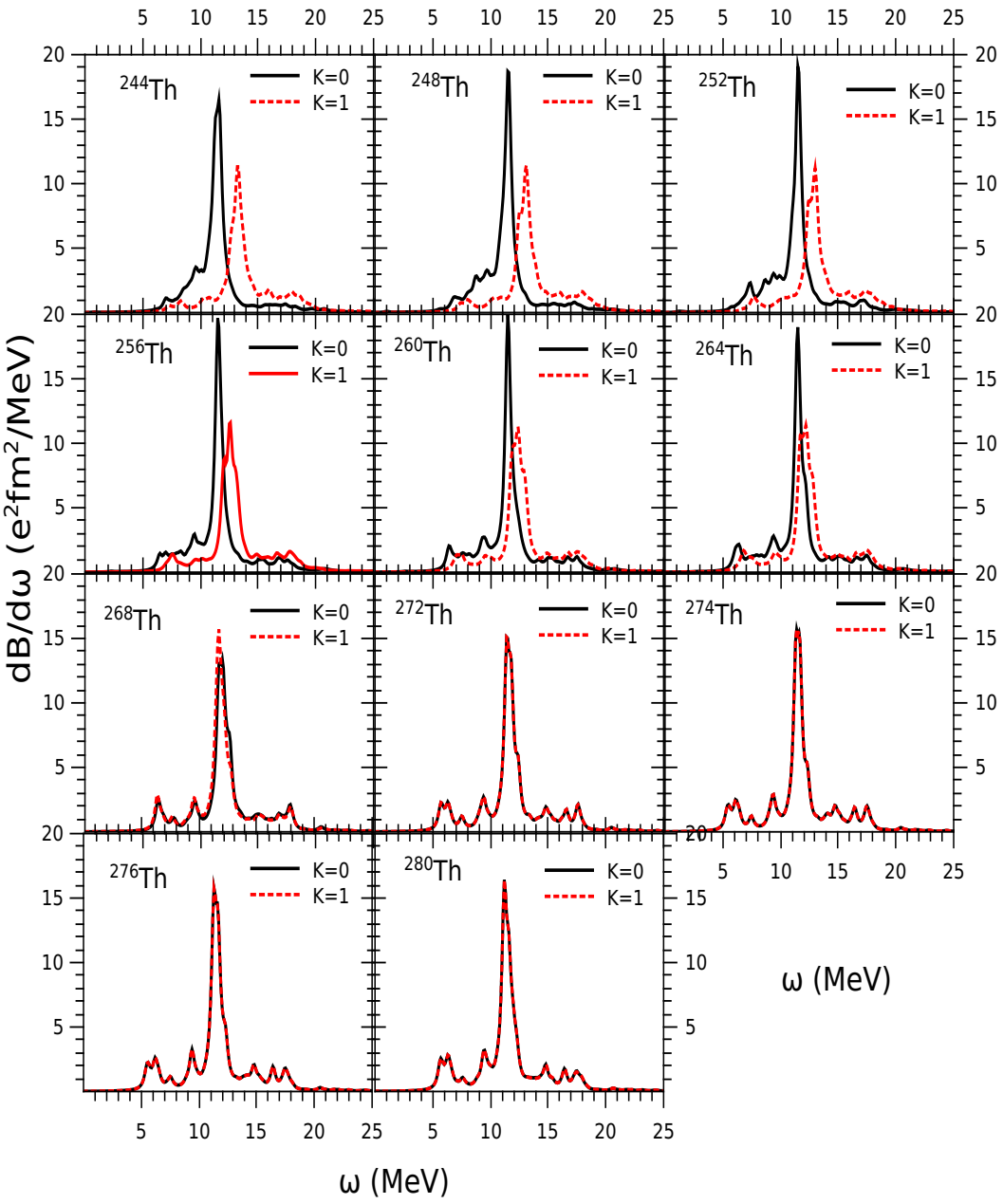

Figure 5.4: Isovector giant dipole response of $^{244-280}Th$ isotopes obtained from the relativistic quasiparticle random phase approximation. The black and red curves, respectively correspond to K=0 and K=1 mode of excitation.

Table 5.1: Centroid energy obtained from the relativistic quasiparticle random phase approximation and its comparison with the available experimental data.

Isotopes	Estimated values (MeV)	Experimental data (MeV)
^{204}Th	13.1	
^{208}Th	13.1	
^{212}Th	13.8	
^{216}Th	13.5	
^{220}Th	13.4	
^{224}Th	12.7	10.3 ± 0.3[42], 11.0 [44]
^{228}Th	11.8	
^{232}Th	11.6	11.08 ± 0.12[43], 11.03 ± 0.04[45]
^{236}Th	11.5	
^{240}Th	11.4	
^{244}Th	11.6	
^{248}Th	11.5	
^{252}Th	11.5	
^{256}Th	11.5	
^{260}Th	11.5	
^{264}Th	11.5	
^{268}Th	11.9	
^{272}Th	11.4	
^{274}Th	11.4	
^{276}Th	11.3	
^{280}Th	11.2	

corresponds to K=0 and K=1 modes of excitation and are plotted in Figure 5.3 and Figure 5.4. In GDR, a dual component structure is observed in deformed nuclei, and this splitting arises from the distinct frequencies of oscillation along the major and the minor axes of deformation. In axially deformed thorium nuclei, the isovector giant dipole resonance displays two components with K=0,1, where K represents the projection of the total angular momentum J=1 along the symmetry axis.

The nuclear potential is more extended along the symmetry axis, making it more energetically favourable for nucleons to oscillate in that direction compared to the perpendicular direction where the potential is narrower. The energy separates corresponding to the two modes of oscillation in deformed nuclei and peaks for both excitation modes. In spherical nuclei the peaks appear at the same

energy level.

In the case of thorium, the peaks of strength distribution for K=0 mode lie at lower energy as compared to that for K=1 mode. The splitting of the response is observed in deformed nuclei due to the broken spherical symmetry. The microscopic approach reveals strong correlation between neutron excess and the enhancement of the low lying dipole strength. As neutron number increases, the peaks of the strength distribution moves to lower energies. The isospin splitting, neutron excess and deformation can affect the splitting of GDR. There is no energy separation between the two modes of oscillation in ^{216}Th and ^{274}Th, due to their spherical symmetry. This study also confirms the possibility of extra stability of ^{216}Th (N=126) and ^{274}Th (N=184) in the isotopic chain of thorium.

The centroid energy values obtained from relativistic quasiparticle random phase approximation with relativistic Hartree-Bogoliubov approach are tabulated in Table 5.1.

5.4 Conclusion

The giant dipole resonance (GDR) is the primary collective oscillation mode within a nucleus, characterized by the oscillation of protons relative to neutrons, resulting in an electric dipole moment. The study of GDRs offers deeper and significant insights into the understanding of the structure of atomic nuclei, particularly in revealing the deformations present in their ground states. The Isovector giant dipole response of thorium isotopes are estimated with RPA and are plotted. In GDR, a dual component structure is observed in deformed nuclei, and this splitting arise from the distinct frequencies of oscillation along the major and minor axes of deformation. In axially deformed thorium nuclei, the isovector giant dipole resonance display two components with K=0,1, where K represents the projection of the total angular momentum J=1 along the symmetry axis.

There is no energy separation between the two modes of oscillation in ^{216}Th and ^{274}Th, due to their spherical symmetry. This study also confirms the possibility of extra stability of ^{216}Th (N=126) and ^{274}Th (N=184) in the isotopic chain of thorium nuclides.

Bibliography

[1] S Péru, H Goutte, and JF Berger. Giant and pygmy resonances within axial-deformed qrpa with the gogny force. *Nuclear Physics A*, 788(1-4):44–49, 2007.

[2] Stéphane Goriely, Stéphane Hilaire, S Péru, and K Sieja. Gogny-hfb+ qrpa dipole strength function and its application to radiative nucleon capture cross section. *Physical Review C*, 98(1):014327, 2018.

[3] M Martini, S Péru, and M Dupuis. Low-energy dipole excitations in neon isotopes and n= 16 isotones within the quasiparticle random-phase approximation and the gogny force. *Physical Review C*, 83(3):034309, 2011.

[4] Stéphane Goriely and Elias Khan. Large-scale qrpa calculation of e1-strength and its impact on the neutron capture cross section. *Nuclear Physics A*, 706(1-2):217–232, 2002.

[5] Stéphane Goriely, Elias Khan, and Mathieu Samyn. Microscopic hfb+ qrpa predictions of dipole strength for astrophysics applications. *Nuclear Physics A*, 739(3-4):331–352, 2004.

[6] Nils Paar, Peter Ring, Tamara Nikšić, and Dario Vretenar. Quasiparticle random phase approximation based on the relativistic hartree-bogoliubov model. *Physical Review C*, 67(3):034312, 2003.

[7] Nils Paar, Dario Vretenar, Elias Khan, and Gianluca Colo. Exotic modes of excitation in atomic nuclei far from stability. *Reports on Progress in Physics*, 70(5):R02, 2007.

[8] DM Brink. Ph. d. thesis, university of oxford, 1955.

[9] Peter Axel. Electric dipole ground-state transition width strength function and 7 MeV photon interactions. *Physical Review*, 126(2):671, 1962.

[10] Vladimir A Plujko, SN Ezhov, MO Kavatsyuk, AA Grebenyuk, and RV Yermolenko. Testing and improvements of gamma-ray strength functions for nuclear model calculations. *Journal of Nuclear Science and Technology*, 39(sup2):811–814, 2002.

[11] VA Plujko, IM Kadenko, OM Gorbachenko, and EV Kulich. The simplified description of dipole radiative strength function. *International Journal of Modern Physics E*, 17(01):240–244, 2008.

[12] Michael Bender, Paul-Henri Heenen, and Paul-Gerhard Reinhard. Self-consistent mean-field models for nuclear structure. *Reviews of Modern Physics*, 75(1):121, 2003.

[13] Dario Vretenar, AV Afanasjev, GA Lalazissis, and P Ring. Relativistic hartree–bogoliubov theory: static and dynamic aspects of exotic nuclear structure. *Physics reports*, 409(3-4):101–259, 2005.

[14] J Rikovska Stone and P-G Reinhard. The skyrme interaction in finite nuclei and nuclear matter. *Progress in Particle and Nuclear Physics*, 58(2):587–657, 2007.

[15] T Nikšić, Dario Vretenar, and Peter Ring. Relativistic nuclear energy density functionals: Mean-field and beyond. *Progress in Particle and Nuclear Physics*, 66(3):519–548, 2011.

[16] Xuwei Sun and Dinghui Lu. Implementation of a finite-amplitude method in a relativistic meson-exchange model. *Physical Review C*, 96(2):024614, 2017.

[17] M Kortelainen, Nobuo Hinohara, and W Nazarewicz. Multipole modes in deformed nuclei within the finite amplitude method. *Physical review C*, 92(5):051302, 2015.

[18] Tamara Nikšić, Nenad Kralj, Tea Tutiš, Dario Vretenar, and Peter Ring. Implementation of the finite amplitude method for the relativistic quasiparticle random-phase approximation. *Physical Review C*, 88(4):044327, 2013.

[19] Haozhao Liang, Takashi Nakatsukasa, Zhongming Niu, Jie Meng, et al. Feasibility of the finite-amplitude method in covariant density functional theory. *Physical Review C*, 87(5):054310, 2013.

[20] Nobuo Hinohara, Markus Kortelainen, and Witold Nazarewicz. Low-energy collective modes of deformed superfluid nuclei within the finite-amplitude method. *Physical Review C*, 87(6):064309, 2013.

[21] M Stoitsov, M Kortelainen, T Nakatsukasa, C Losa, and Witold Nazarewicz. Monopole strength function of deformed superfluid nuclei. *Physical Review C*, 84(4):041305, 2011.

[22] Paolo Avogadro and Takashi Nakatsukasa. Finite amplitude method for the quasiparticle random-phase approximation. *Physical Review C*, 84(1):014314, 2011.

[23] Tsunenori Inakura, Takashi Nakatsukasa, and Kazuhiro Yabana. Emergence of pygmy dipole resonances: Magic numbers and neutron skins. *Physical Review C*, 84(2):021302, 2011.

[24] Tsunenori Inakura, Takashi Nakatsukasa, and Kazuhiro Yabana. Self-consistent calculation of nuclear photoabsorption cross sections: Finite amplitude method with skyrme functionals in the three-dimensional real space. *Physical Review C*, 80(4):044301, 2009.

[25] Takashi Nakatsukasa, Tsunenori Inakura, and Kazuhiro Yabana. Finite amplitude method for the solution of the random-phase approximation. *Physical Review C*, 76(2):024318, 2007.

[26] A Bjelčić and T Nikšić. Implementation of the quasiparticle finite amplitude method within the relativistic self-consistent mean-field framework: The program dirqfam. *Computer Physics Communications*, 253:107184, 2020.

[27] Tamara Nikšić, Dario Vretenar, and Peter Ring. Relativistic nuclear energy density functionals: Adjusting parameters to binding energies. *Physical Review C*, 78(3):034318, 2008.

[28] Yuan Tian, Zhong-yu Ma, and Peter Ring. Axially deformed relativistic hartree bogoliubov theory with a separable pairing force. *Physical Review C*, 80(2):024313, 2009.

[29] Yuan Tian, Zhong-yu Ma, and Peter Ring. Separable pairing force for relativistic quasiparticle random-phase approximation. *Physical Review C*, 79(6):064301, 2009.

[30] Yuan Tian, Zhong-yu Ma, and P Ring. A finite range pairing force for density functional theory in superfluid nuclei. *Physics Letters B*, 676(1-3):44–50, 2009.

[31] Muhsin N Harakeh and Adriaan Woude. *Giant Resonances: fundamental high-frequency modes of nuclear excitation*, volume 24. Oxford Studies in Nuclear Phys, 2001.

[32] Pier Francesco Bortignon, Angela Bracco, and Ricardo A Broglia. *Giant Resonances: Nuclear structure at finite temperature*. CRC Press, 2019.

[33] Duane D Johnson. Modified broyden's method for accelerating convergence in self-consistent calculations. *Physical Review B*, 38(18):12807, 1988.

[34] Andrzej Baran, Aurel Bulgac, Michael McNeil Forbes, Gaute Hagen, Witold Nazarewicz, Nicolas Schunck, and Mario V Stoitsov. Broyden's method in nuclear structure calculations. *Physical Review C*, 78(1):014318, 2008.

[35] W Kleinig, VO Nesterenko, J Kvasil, P-G Reinhard, and P Vesely. Description of the dipole giant resonance in heavy and superheavy nuclei within skyrme random-phase approximation. *Physical Review C*, 78(4):044313, 2008.

[36] B Lo Berman and SoCo Fultz. Measurements of the giant dipole resonance with monoenergetic photons. *Reviews of Modern Physics*, 47(3):713, 1975.

[37] A Van der Woude. Giant resonances. *Progress in particle and nuclear physics*, 18:217–293, 1987.

[38] Q Wu, BS Hu, FR Xu, YZ Ma, SJ Dai, ZH Sun, and Gustav R Jansen. Chiral nnlo sat descriptions of nuclear multipole resonances within the random-phase approximation. *Physical Review C*, 97(5):054306, 2018.

[39] T Aumann and T Nakamura. The electric dipole response of exotic nuclei. *Physica Scripta*, 2013(T152):014012, 2013.

[40] JH Bai, ZM Niu, BY Sun, and YF Niu. The description of giant dipole resonance key parameters with multitask neural networks. *Physics Letters B*, 815:136147, 2021.

[41] I Diószegi, NP Shaw, I Mazumdar, A Hatzikoutelis, and P Paul. Nuclear viscosity of hot rotating 224 th. *Physical Review C*, 61(2):024613, 2000.

[42] M Thoennessen, DR Chakrabarty, MG Herman, R Butsch, and P Paul. Giant dipole resonance in highly excited thorium: Evidence for strong fission hindrance. *Physical review letters*, 59(25):2860, 1987.

[43] A Veyssiere, H Beil, R Bergere, P Carlos, A Lepretre, and K Kernbath. A study of the photofission and photoneutron processes in the giant dipole resonance of 232th, 238u and 237np. *Nuclear Physics A*, 199(1):45–64, 1973.

[44] I Dioszegi, DJ Hofman, CP Montoya, S Schadmand, and P Paul. Giant dipole resonance decay from fusion-fission and quasifission of hot thorium nuclei. *Physical Review C*, 46(2):627, 1992.

[45] JT Caldwell, EJ Dowdy, BL Berman, RA Alvarez, and P Meyer. Giant resonance for the actinide nuclei: Photoneutron and photofission cross sections for u 235, u 236, u 238, and th 232. *Physical Review C*, 21(4):1215, 1980.

Chapter 6

Summary and Future Perspectives

A nucleus is a quantum many-body system, where single-particle and collective motions give rise to the fundamental modes of excitation. This thesis work is a theoretical investigation on the structure properties of thorium nuclei lying on and off the line of β-stability. Here, we have broadly divided the investigations into two parts related to ground state properties and the dynamic properies. In the studies on the ground state properties, we have included-the effective and collective level density parameter of thorium isotopes, charge radii, binding energy, rms radii, ground state deformation and single particle energies etc. As part of the dynamical aspects we have studied the shape evolution of thorium isotopes and the collective behavior-the giant dipole response.

The level density of nuclei give important information on its structure. We have calculated the effective and collective level density parameters of even-even thorium nuclei in the mass range 204-280 with an increment of 4 in mass number, for nuclei lying on the β-stability line and the drip lines. The level density parameter was found to decrease towards the neutron numbers N=126 and 184. The variation of both the effective and collective level density parameters of

thorium nuclei shows similar behaviour. The collective level density parameter is smaller than the effective level density parameter. The collective enhancement factor of thorium isotopes around neutron number N=126 (^{216}Th) and 184 (^{274}Th) were also evaluated. The collective enhancement factor for ^{216}Th and ^{274}Th are less when compared to those for the nearby isotopes. This may be due to the shell closure at neutron number N=126 and 184. As an extension of this study, we have estimated the collective level density parameter for few selected even-even actinides, having neutron number lying around N=184. Accordingly, the level density parameters have been systematically evaluated for the isotopes of U, Pu, Cm, Cf, Fm and No. The calculations were performed on the basis of the phenomenological models such as the Gilbert Cameron (GCM) and the Back-Shifted Fermi Gas (BFGM).

The nuclear structure properties of thorium nuclei lying on and in between the drip-lines were investigated in the framework of the relativistic mean-field theory by applying the density dependent meson exchange and point-coupling models. The ground state parameters like binding energy, charge radii, two-neutron separation energy and shell gap, rms radii and its isotopic shift, chemical potential, quadrupole deformation, density distribution and single-particle energy were estimated. These values were then compared with the available experimental and other theoretical data and were found to be in good agreement. Broken linearities were observed at around the neutron numbers N=126, 138 and 184 in the plots of various evaluated values against neutron number. Single-particle energy gaps were also determined corresponding to neutron numbers. Large deviation and shell gaps were observed at around the neutron number N=126 and 184. Hence, these numbers are neutron magic numbers and the corresponding thorium nuclei are more stable than their neighbours. A small deviation and shell gap were observed at N=138, and hence we conclude that this neutron number

is semi-magic and the associated nucleus is relatively stable.

An atomic nucleus is also characterized by its shape, with the most commonly encountered ones being spherical, prolate, and oblate. There is a direct correlation between the shell structure and the intrinsic shapes of nuclei. The evolution of the shell structure is influenced by the residual interactions among the nucleons, which in turn, can modify the shape of a nucleus. The ground state deformation of thorium nuclei lying in between the drip lines were identified in terms of the axially symmetric deformation parameter β_2 and triaxial deformation parameter γ. The nuclear shape evolution of thorium isotopes, ranging from ^{204}Th to ^{280}Th, was investigated using the relativistic mean-field theory. The binding energy curves of thorium isotopes as a function of the deformation parameter β_2 were plotted and the minima were located. ^{216}Th and ^{274}Th are spherical in shape and the nearby isotopes are moderately deformed and nearly spherical. Isotopes ranging from ^{220}Th to ^{264}Th exhibit a higher level of deformation. Majority of thorium isotopes we have studied exhibit a prolate shape. The most deformed nucleus is ^{240}Th and is prolate. We have also plotted the self-consistent energy surfaces for isotopes of thorium lying on and off the line of β-stability in the $\beta_2 - \gamma$ plane. This study on shape evolution with triaxial deformation confirms that majority of thorium isotopes exhibit a prolate shape, while ^{216}Th and ^{274}Th are characterized by spherical shapes. A slight triaxial behaviour was observed in ^{220}Th and ^{268}Th for the values of $\beta_2 = 0.05$ and $\gamma = 10^\circ$. This triaxial behavior was observed within the region associated with shape phase transition.

The excitation of atomic nuclei also offers valuable insights into their structure. The Random Phase Approximation (RPA) stands as the foremost theory for investigating the dynamics of nuclei. Collective excitation within the nucleus entails the coordinated motion of individual protons and neutrons, rather than

the independent motion of nucleons. The collective motion of nucleons leads to various phenomena, including nuclear deformation, rotational and vibrational motions and giant resonances. It yields extensive information on nuclear structure, nuclear reactions and features of nuclear matter. The giant dipole resonance (GDR) is the primary collective oscillation mode within a nucleus, characterized by the oscillation of protons relative to neutrons and resulting in an electric dipole moment. The study of GDRs offers deeper and significant insights into the understanding of the structure of atomic nuclei, particularly in revealing the deformations present in their ground states. The Isovector giant dipole response of thorium isotopes were estimated with RPA and are plotted. In GDR, a dual component structure is observed in deformed nuclei, and this splitting arise from the distinct frequencies of oscillation along the major and minor axes of deformation. In axially deformed thorium nuclei, the isovector giant dipole resonance display two components with K=0,1, where K represents the projection of the total angular momentum J=1 along the symmetry axis. There was no energy separation between the two modes of oscillation in ^{216}Th and ^{274}Th, due to their spherical symmetry. This study also confirms the possibility of extra stability of ^{216}Th (N=126) and ^{274}Th (N=184) in the isotopic chain of thorium.

6.1 Future perspectives

In this thesis work, we have estimated the structure properties of even-even thorium isotopes, lying on and off the line of β-stability, with relativistic mean-field theory. Further investigations which can be carried out as continuation to this work can be listed as follows.

- Nuclear structure properties of thorium can be investigated with other parametrizations.

- Estimate the effects of higher level deformations like hexadecapole and octupole deformations.
- Check whether this behaviour is observed in other nearby isotopic chains.
- Here we have estimated structure properties only for even-even thorium nuclei. We can extend these studies by including even-odd thorium nuclei also.
- Isoscalar and isovector multipole response of thorium isotopes can also be investigated.

Recommentations

The study of atomic nuclei is important because of many reasons, especially, due to the wide, variety of its applications, including those in nuclear energy, nuclear medicine, in maintaining health in living organisms, including human beings by keeping the trace level of essential elements, etc. More over, it is important in astrophysical scenarios such as stellar evolution, nucleosynthesis and also in understanding nuclear reactions. The structure properties of nuclei are of considerable attention in nuclear physics. Over the last several decades, many developments had taken place in nuclear structure studies, both on its theoretical and experimental aspects. Even after attaining considerable progress in this direction, many information on the structure of nuclei are still unknown.

The present thesis work is a theoretical investigation on the structural properties of thorium (Z=90) isotopes lying on and off the line of β-stability. Thorium nuclei are of special interest, because of their various practical applications. They have use in various stages of nuclear fuel reactors. The isotope ^{232}Th is relatively stable and other isotopes decay very slowly through alpha and other decay modes. ^{232}Th is not fissile by itself and so it is not directly usable in thermal neutron reactors. However, it can be transmuted inside a reactor into the fissile isotope ^{233}U. ^{232}Th is placed within and around the reactor core, where it absorbs neutrons and becomes ^{233}Th. Following two subsequent β-decays, it becomes ^{233}U. which is an excellent fissile material. An important observation is the possibility of the production of medical isotopes from thorium by irradi-

ating thorium targets with light charged particles like protons and deuterons. Radioisotopes usually used for both the diagnostic and the therapeutic purposes depend on the radiation emitted by them. Radioisotopes of medical interest ^{99}Mo, ^{115}Cd and ^{111}I are obtained from the fission of thorium, by using protons and deuterons as the projectiles.

The present study can be broadly classified into two, aiming to understand the ground state and the dynamic properties of thorium isotopes. As the first part of the present study, we have calculated nuclear level density and other related parameters of selected thorium isotopes. The nuclear level density (LD) holds a significant position in the realm of nuclear physics. The task of forecasting the array of excited levels within a nucleus poses a substantial challenge, underscoring the complexity of this quantum system. Concurrently, LDs play a crucial role in the statistical model computations of nuclear reaction cross sections. These calculations find applications in diverse fields including in astrophysical studies. These applications range from determining thermonuclear rate in nucleosynthesis. The determination of nuclear level density (LDs) through experimental study is not so feasible, particularly in applications like nucleosynthesis calculations. In such cases, the reliance is on the level density values obtained from theoretical models or extrapolated experimental data. Hence, understanding nuclear level density is crucial in various domains including basic nuclear physics research, nuclear medicine, nuclear reactor design, and nuclear astrophysics etc. and it provides the essential insight into the nuclear thermodynamics.

The nuclear structure properties like binding energy, charge radii, rms radii and its isotopic shift, two-neutron separation energy and shell gap, chemical potential, quadrupole deformation, density distribution and single-particle energy of thorium nuclei, lying on and off the line of β-stability were estimated. This study will help us understand the variation of nuclear properties with neutron

number (towards the drip-lines) and to predict the shell closure and nuclear stability. Data related to the structure properties are useful for experiments in future and will be helpful in understanding the behaviour of complex nuclei. Broken linearities were observed at around neutron numbers N=126, 138 and 184 in the plots of various evaluated values against neutron number. Single-particle energy gaps were evaluated at around these neutron numbers. Large deviation and shell gaps were observed at around the neutron number N=126 and 184. Hence these numbers are neutron magic numbers and the corresponding thorium nuclei are more stable than their neighbours. A small deviation and shell gap were also observed at around N=138, and hence we conclude that this neutron number is semi-magic and the associated thorium nucleus ^{228}Th is relatively stable. Most of the thorium nuclei are of prolate shape However, they are spherical at N=126 and 184.

Investigating nuclear rotations and the occurrence of shape phase transitions in nuclei has proven to be a highly sensitive approach for exploring the nuclear structure. Atomic nuclei engage in collective motions such as rotation and vibration, and the interplay between these motions is crucial for comprehending both their intrinsic and extrinsic structures. The shapes exhibited by various nuclei depend on the type and extent of deformation present. This area of investigation holds significant interest as it contributes to a deeper understanding of the shell structure, elucidating the origins of deformation and the occurrence of triaxial ground states. Hence, the transitional nuclei situated in the heavy mass region provide a valuable foundation for the analysis and exploration of shape alterations, particularly concerning triaxial deformation. ^{216}Th and ^{274}Th are spherical in shape and the nearby isotopes are relatively less deformed and are nearly spherical. Isotopes ranging from ^{220}Th to ^{264}Th exhibit a higher level of deformation. Majority of thorium isotopes exhibit a prolate shape. The most

deformed nucleus is ^{240}Th and is prolate. The study on shape evolution with triaxial deformation reconfirms our earlier observation that majority of thorium isotopes exhibit a prolate shape, while ^{216}Th and ^{274}Th are characterized by spherical shapes. A slight triaxial behaviour is observed in ^{220}Th and ^{268}Th for the values of $\beta_2 = 0.05$ and $\gamma = 10^{\circ}$. This triaxial behavior is observed within the region associated with shape phase transition.

The excitation of atomic nuclei also offers valuable insights into their structure. The collective motion of nucleons leads to various phenomena, including rotational motion, vibrational motion, nuclear deformation, giant resonances and more. Here, as the last part of the thesis work, we have investigated the giant dipole resonances (GDR) in the series of thorium nuclei selected. In GDR, a dual component structure is observed in deformed nuclei, and this splitting arise from the distinct frequencies of oscillation along the major and minor axes of deformation. In axially deformed thorium nuclei, the isovector giant dipole resonance display two components with K=0,1, where K is the projection of total angular momentum J=1 on the symmetry axis. There is no energy separation between the two modes of oscillation in ^{216}Th and ^{274}Th, due to their spherical symmetry. This study also confirms the possibility of extra stability of ^{216}Th (N=126) and ^{274}Th (N=184) in the selected isotopic chain of thorium.